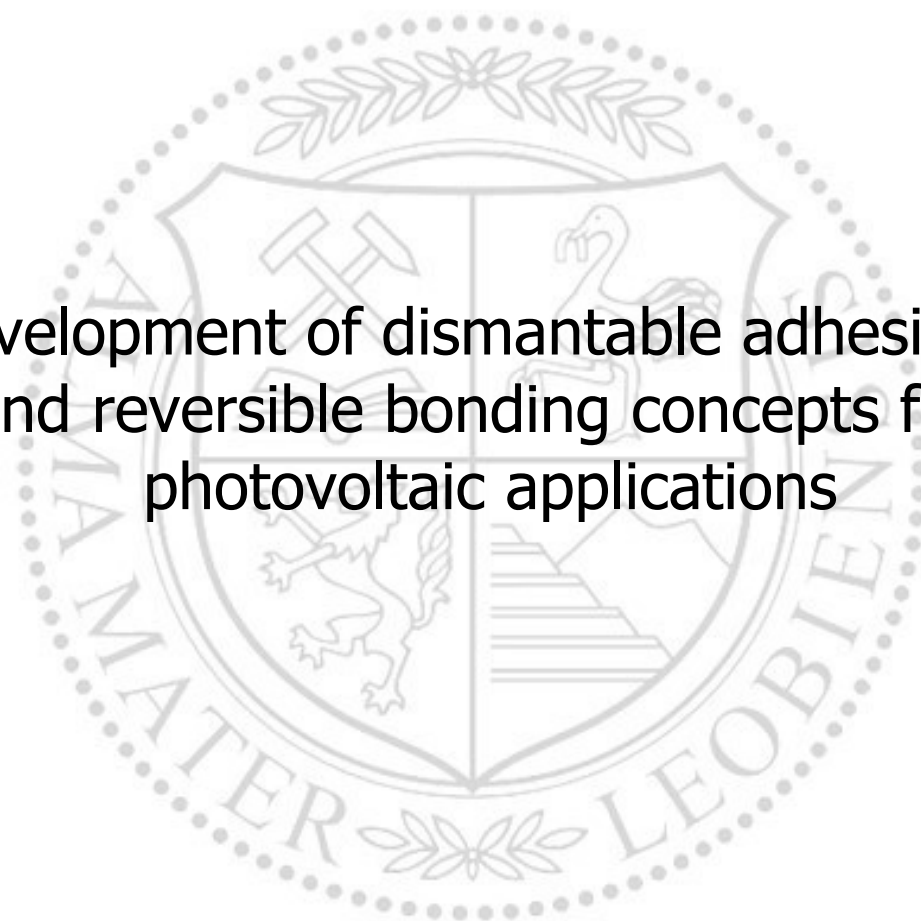Chair of Chemistry of Polymeric Materials

Master's Thesis

Development of dismantable adhesives and reversible bonding concepts for photovoltaic applications

Florian Wanghofer, BSc

Leoben, February 2020

AFFIDAVIT

I declare on oath that I wrote this thesis independently, did not use other than the specified sources and aids, and did not otherwise use any unauthorized aids.

I declare that I have read, understood, and complied with the guidelines of the senate of the Montanuniversitaet Leoben for "Good Scientific Practice".

Furthermore, I declare that the electronic and printed version of the submitted thesis are identical, both, formally and with regard to content.

Date 15.02.2020

Signature Author
Florian, Wanghofer

ACKNOWLEDGEMENTS

ABSTRACT

The present thesis aims at the development of disbonding concepts for adhesive connections used in photovoltaic (PV) modules to enable improved recyclability and reworkability of such modules.

To achieve reversible adhesive connections, thermally expandable fillers were implemented in a condensation-curing alkoxy-based silicone adhesive. 10-50 wt.% of expandable graphite (EG) as well as 10-50 wt.% of thermally expandable microspheres (TEM) were incorporated to obtain a thermally triggered expansion of the adhesive. The expansion ratio in dependence on time and temperature was examined. Furthermore, nanoscale magnetite (Fe_3O_4) passivated with a layer of SiO_2 was added to the formulation to trigger the expansion of TEMs and therefore separation of adhesive bonds by inductive heating. In this approach an efficient heating and expansion of the adhesive layers was feasible by applying an external alternating magnetic field with a ring coil. Aging stability, influence of filler content and expansion were further evaluated by lap shear tests. The addition of functional fillers decreased the bond strength by approximately 50 % for 50 wt.% EG and increased it by 10 % for 50 wt.% TEM. Expansion separated the bond with 30 and 50 wt.% EG and weakened it by up to 20 and 50 % for 30 and 50 wt.% TEM. Temperature cycling tests had no influence on the filled and unfilled adhesive's strength. After damp heat tests all samples exhibited similar strengths, less than 40 % of the unaged and unfilled reference samples.

In a further approach to achieve reversible and reworkable adhesive connections, vitrimeric elastomers based on functionalized poly(dimethylsiloxane) (PDMS) were realized. By exploiting reactions of epoxide functional groups with anhydrides and carboxylic acids, covalent adaptive networks (CAN) are formed in the presence of suitable catalysts. A reprocessable elastomeric CAN was successfully established by curing epoxidized PDMS with a multifunctional fatty acid and *n*-butylamine (BA) as a covalently bonded catalyst. In tensile tests the system showed a remaining strength of more than 85 % after reprocessing the grinded material in a hot-press for 5 h at 160°C. Lap shear tests were done to evaluate bond strength, rejoining, aging stability

and the ability to weaken the adhesive bond. The elastomeric CAN achieved approximately 20 % of the reference silicone adhesive's strength. Tests at 160°C decreased the bond strength by 60%, compared to a reduction of 40% for the reference sample. Temperature cycle tests did not influence the material strength, storage at 120°C for 930 h decreased the bond strength by approximately 20 % and in damp heat tests the material suffered from hydrolytic bond cleavage. Rejoining the lap shear samples resulted in a remaining bond strength of more than 70 %.

KURZFASSUNG

Das Ziel der vorliegenden Arbeit liegt darin, Klebeverbindungen in Photovoltaikmodulen zu lösen, um eine erhöhte Rezyklierbarkeit und Reparierbarkeit zu erreichen.

Reversible Klebeverbindungen wurden erzielt, indem thermisch expandierende Füllstoffe in einen kondensationsvernetzenden Silikonklebstoff auf Alkoxybasis implementiert wurden. 10-50 Gew.% Blähgraphit (EG) sowie 10-50 Gew.% thermisch expandierbare Mikrosphären (TEM) wurden eingearbeitet, um eine thermische Ausdehnung des Klebstoffs auszulösen. Das Expansionsverhältnis in Abhängigkeit von Zeit und Temperatur wurde untersucht und darüber hinaus wurde die Ausdehnung von TEMs und damit die Trennung von Klebeverbindungen durch Zugabe von nanoskaliertem Magnetit (Fe_3O_4), das mit einer Schicht aus SiO_2 passiviert ist, durch induktive Erwärmung ausgelöst. Dabei war eine effiziente Erwärmung und Ausdehnung der Klebstoffschichten durch Anlegen eines externen magnetischen Wechselfeldes mit einer Ringspule möglich. Die Alterungsstabilität, der Einfluss des Füllstoffgehalts und die Ausdehnung wurden durch Scherzugversuche weiter untersucht. Die Zugabe von funktionellen Füllstoffen verringerte die Festigkeit der Klebeverbindung um etwa 50 % mit 50 Gew.% EG und erhöhte sie um etwa 10 % mit 50 Gew.% TEM. Die Expansion erlaubte eine Trennung der Verbindung mit 30 und 50 Gew.% EG und schwächte sie um bis zu 20 und 50 % mit 30 und 50 Gew.% TEM. Klimawechseltests hatten keinen Einfluss auf die Festigkeit des gefüllten und ungefüllten Klebstoffs. Nach Alterungstests unter feuchter Hitze wiesen alle Proben eine ähnliche Festigkeit auf, die im Vergleich zu ungealterten und ungefüllten Referenzproben um 40 % geringer war.

In einem weiteren Ansatz zur Entwicklung reversibler und reparabler Klebeverbindungen wurden vitrimerartige Elastomere auf Basis von funktionalisiertem Poly(dimethylsiloxan) (PDMS) realisiert. Durch die Reaktion von Epoxiden mit Anhydriden und Carbonsäuren wurden in Gegenwart geeigneter Katalysatoren kovalent adaptierbare Netzwerke (CAN) gebildet. Ein wieder verarbeitbares elastomeres CAN wurde erfolgreich durch die Vernetzung von epoxidiertem PDMS mit einer multifunktionellen Fettsäure und *n*-Butylamin (BA) als kovalent gebundenem

Katalysator hergestellt. In Zugversuchen erreichte das System eine Restfestigkeit von mehr als 85 % nach der Wiederverarbeitung des zermahlenen Materials für 5 h bei 160°C in einer Heißpresse. Scherzugversuche wurden ebenfalls durchgeführt, um Festigkeit, erneutes Fügen, Alterungsstabilität und Fähigkeit zur Schwächung der Klebeverbindung zu untersuchen. Das elastomere CAN erreichte etwa 20 % der Festigkeit des Referenz-Silikonklebstoffs. Tests bei 160°C zeigten eine Abnahme der Festigkeit von 60 %, im Vergleich zu 40 % bei der Referenzprobe. Klimawechseltests hatten keinen Einfluss auf die Festigkeit und eine Lagerung bei 120°C für 930 h verminderte die Festigkeit um ca. 20 %. In Alterungstests unter feuchter Hitze trat hydrolytischer Abbau auf. Das erneute Fügen der Scherzugversuchsproben ergab eine Restfestigkeit von mehr als 70 %.

TABLE OF CONTENTS

1 INTRODUCTION

The demand for energy obtained from renewable and sustainable resources, including solar energy is currently rising, considering the EU target of at least 32 % share of renewable energy of the final energy consumption by 2030 in order to reduce CO_2 emissions, and to conserve resources. [1] In 2018, 18 % of the energy consumption in the EU was produced from renewable sources, compared to only 4 % in 2004. [2]

Photovoltaic (PV) modules provide renewable energy through the conversion of light into electricity by using the photovoltaic effect on semiconductors. [3] A module consists of multiple cells, sandwiched between layers of different materials, listed from front to back: a highly transparent front glass to protect the PV module, without absorbing the sunlight; the PV cells, embedded in an encapsulant, which bonds the multiple components and protects the PV cells; an insulating back sheet, providing electrical isolation and protection from moisture and weather; and the junction box, as electrical connection of the PV module. [4–6]

The production of PV devices has grown with a compound annual growth rate of over 40 % since 2000, cumulating to a worldwide installed PV power of 518 GW at the end of 2018. [7] Consequently, a significant increase in PV module waste is expected, estimations state a rise from less than 300.000 t in 2016 to values between 60 and 78 million t in 2050. [8] As of now, no dedicated PV module recycling process is available due to the currently low amount of waste.

The present thesis, which is part of the project "PVRe^2 – sustainable photovoltaics" (FFG Energy Research 4th call) targets the development of concepts for reversible adhesive bonds, to improve the recyclability of photovoltaic modules with the overall aim to increase sustainability of electricity generation from photovoltaics.

In a high number of PV modules, silicone-based adhesives are implemented to connect the surfaces of e.g. backsheet and photovoltaic cell or backsheet and junction box. For an application in photovoltaic modules, the adhesive system has several requirements to fulfil. Due to a long-term exposure of PV modules to external factors such as ultraviolet radiation, moisture and temperature cycles the adhesive is prone to

weathering induced degradation over the target lifetime of 20 to 30 years. Temperatures in service-life range from -40°C to possible local maxima of up to 80°C depending on the place of instalment. Additionally, the adhesive has to be flexible enough to compensate for differences in thermal expansion of the substrate materials. Furthermore, the adhesive has to carry a load for the target lifetime of 20 to 30 years, making creep highly undesirable.

The downside of highly reliable adhesive connections is that the separation of the connected parts to perform repair works or at the end of life of the module proves to be difficult. The joined components have to be shredded into smaller fragments before further processing. A separation before shredding would allow a greater yield of high purity material during the recycling process. There is a number of existing solutions for releasable and reusable adhesive systems with different advantages and drawbacks in terms of effectiveness and influence on the adhesive connection during service-life. However, a universal solution to achieve reversible adhesive bonds has yet to be found. [9]

Within the present work, different possible solutions to separate the adhesive bonds with external triggers have been examined. The chosen approaches can be divided into two concepts:

The first approach is based on modifying the connection with functional fillers that expand at elevated temperatures and weaken or destroy the adhesive connection mechanically. The expansion has to be strong enough to exceed the material strength and is achieved by blowing agents implemented into the filler particles. The functional fillers are incorporated into the adhesive and should allow a separation of the connection at any desired time. Therefore, the temperatures of expansion have to be in a range that is not reached during use and the functional fillers have to exhibit the same weathering resistance as the adhesive itself to ensure their functionality at the end of life of the PV module.

The second approach focuses on substituting the irreversibly crosslinked adhesive with a material that forms a covalent adaptable network (CAN) during crosslinking. CANs contain functional groups that can dynamically exchange their bond partners under stimuli such as light or temperature, which allow a topology rearrangement within the

material. Therefore, the material can be healed, reshaped or recycled at elevated temperatures, while behaving like a thermoset or elastomer at service temperatures. [10,11] As a response to external stimuli, the bond exchange reactions should facilitate a decrease in strength of the adhesive connection and allow an easier separation, and therefore improve recyclability and reworkability.

2 THEORETICAL BACKGROUND

2.1 Adhesive connections

An adhesive connection is a bonding technique that connects two parts of the same or different materials by applying a non-metallic intermediate layer, the adhesive. [12] Adhesion is achieved via mechanical interlocking and/or chemical or physical bonding effects. The proposed main mechanisms used as theoretical models of adhesion are mechanical interlocking, diffusion theory, electronic theory, adsorption theory, theory of boundary layers and interphases, and chemical bonding theory. The models are based on mechanical and specific adhesion, which includes all types of bonds that can be formed between two solids, e.g. electrostatic or chemical bonds. [13,14] An adhesive connection provides various advantages over mechanical fasteners such as rivets: The bonding provides a more uniform stress distribution without individual stress peaks and the joint is usually lighter. Furthermore, adhesives can provide functions additional to bonding the components, such as sealing of the surfaces, decreasing the sensitivity to fatigue crack propagation, and they can provide a stiffening effect to the connection area. [15]

Adhesives can be classified by various parameters, e.g. by origin (synthetic or natural source), by material (inorganic or organic), by curing method (one-part systems or two-part systems) or by load and application case (structural, semi-structural and non-structural). [9,16] Modern polymer chemistry allows to create synthetic adhesives with tailored properties to suit many different applications, which can be further classified by their chemical structure: In thermoplastics, thermosets and elastomers. Thermoplastic adhesives generally consist of long chain macromolecules and melt at elevated temperatures. They can be applied as hot melt and become rigid upon cooling. Thermoset and elastomers are applied as prepolymer or resin and irreversibly crosslink upon curing. The crosslinked networks cannot melt and usually exhibit higher weathering, chemical and temperature resistance, compared to thermoplastics. Furthermore, their mechanical properties commonly show less dependence on temperature. Thermosets form strong and rigid connections resulting from their high

crosslink density. Elastomeric adhesives form flexible connections that can tolerate high deformations before failure but possess only limited strength due to their low crosslink density. [17]

Silicone adhesives are synthetic elastomeric materials with a poly(siloxane) backbone, commonly with organic groups bonded to the silicon atoms. Therefore, they form their own class, in between inorganic and organic adhesives. Silicones exhibit high flexibility, very good temperature resistance ranging from -115°C to 265°C, good resistance against UV and IR radiation, as well as against oxidation. Furthermore, they generally possess a good weathering and chemical resistance. One-part silicone adhesive systems usually crosslink via the exposure to atmospheric moisture, and two-part systems cure by the addition of a hardener. The combination of those properties makes silicones suitable adhesive materials for the application in construction, marine and vehicle assembly industries, as well as for PV applications. [18]

2.2 Expandable additives/fillers

Additives are used in almost every polymer material to tailor the properties for each respective application. Commonly, additives are added to aid processing by e.g. decreasing viscosity or friction, or to improve the material behaviour during use, and e.g. provide increased aging resistance. [19] Additives that improve the recyclability of a material are very rare and rather uncommon. However, during the recycling process, a certain amount of process aiding additives and stabilizers are often added again to come closer to or even regain the properties of the virgin material.

Additives that aid the recycling process need to be able to withstand all conditions during use and maintain their functionality until the end of use of the product. Furthermore, it must be ensured that the additive does not migrate out of the polymer and that it is not consumed by conditions that might occur during the lifetime of the material.

Blowing agents are additives that expand due to physical effects or chemical reaction when triggered, which is usually done thermally. Chemical blowing agents consist of components such as azodicarbonamide and sodium bicarbonate [20] that are usually

implemented in solid or liquid form. They chemically dissociate into smaller molecules under gas release when triggered. Physical blowing agents (e.g. liquid CO_2) or hydrocarbons (e.g. pentane) [20] gain their expansion effect from physical effects such as the transition of a material from liquid to gaseous or the expansion of gas by heating. Physical effects such as phase transition are reversible and expansion effects are usually weaker than for chemical blowing agents. [21]

Fillers are usually used in a higher quantity, compared to additives, and are mostly used to improve specific material properties such as material strength or toughness or heat resistance, or to reduce the material costs. The effect of fillers on a material is determined by a variety of parameters including filler material, but also the geometry and filler size are important factors. [22]

Expandable fillers are fillers with implemented blowing agents, combining properties of fillers and additives, and will therefore be referenced as functional fillers. These functional fillers can be easily implemented into an adhesive formulation and weaken or separate an adhesive bond upon expansion. [23] The advantage of functional fillers over conventional blowing agents is that leaching or migration out of the matrix material is less likely due to their larger particle size. In the following chapters, two types of functional fillers are introduced.

2.2.1 Thermally expandable microspheres

Thermally expandable microspheres (TEM) are fillers used in bulk materials to decrease weight or improve their insulation behaviour. Furthermore, they are commonly used for coatings to produce an embossed effect or an anti-fingerprint surface. [24] They generally consist of solid or liquid blowing agents such as hydrocarbons with a suitable boiling point, encapsulated in a thermoplastic shell. At elevated temperatures the shell softens while a gas is formed, which stretches the spheres (see Figure 1). During cooling, the polymer shell stiffens in the expanded state and the volume is retained. These microspheres are produced via suspension polymerization, where the hydrocarbon is encapsulated during polymerization. The expansion ratio and temperature depend on the encapsulated hydrocarbon as well as on the softening temperature and flexibility of the thermoplastic shell. [25]
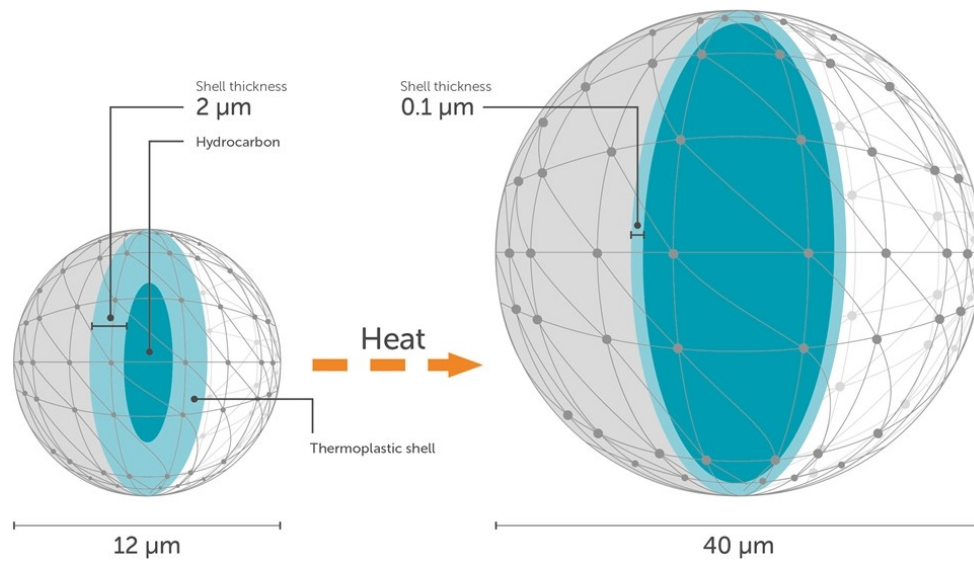
Figure 1: Schematic representation of thermally expandable microspheres before (left) and after expansion (right). Figure reprinted from [26].

2.2.2 Expandable graphite

Expandable graphite (EG) or intumescent flake graphite is a filler material that is mainly used for fire protection (e.g. in pipe or cable shielding or in flame retardant textiles). The material consists of graphite flake layers with intercalated blowing agents between the layers. The intercalant usually is a strong acid such as sulfuric acid or nitric acid, [27] which either decomposes or boils at higher temperatures, and therefore separates the graphite layers resulting in an increase of volume. Figure 2 illustrates an adhesive containing EG before (left) and after (right) expansion. The expansion temperature and expansion ratio depend on the type as well as the amount of intercalated blowing agent. Commercially available grades usually exhibit starting temperatures for expansion above 200°C due to the intended use as a flame retardant. Expandable graphite is produced by pre-oxidizing graphite flakes with e.g. hydrogen peroxide, followed by deep oxidization and intercalation with an alkali-salt and acid. [28]

Figure 2: Adhesive connection containing expandable graphite before (left) and after (right) expansion.

2.3 Inductive heating

Inductive heating allows heating of electrically conductive or ferromagnetic materials. The materials are exposed to an alternating electromagnetic field created by alternating current (AC) running through a coil. The inductive heating relies on two different effects: Eddy currents and hysteresis losses. Eddy currents are currents within a conductor that are induced by a changing external magnetic field. The induced currents form their own magnetic fields, which form and collapse with the alternating external magnetic field. This leads to losses in thermal energy, called Joule effect, and therefore heating of the material. Hysteresis losses result from polarizing magnetic domains in the material. Magnetic domains are regions in a material, where the magnetization is in a uniform direction. The application of an external magnetic field causes these domains to align with the magnetic field, consequently creating a magnetic dipole. Due to the alternation of the external magnetic field, the dipole direction alternates as well, and hysteresis losses occur. The main mechanism for heating of particles is reported to be hysteresis losses. [29–31]

Inductive heating is used in polymers to cure adhesives or composites as well as for thermoplastic fusion bonding. The majority of unfilled organic polymers cannot be heated inductively due to a lack of ferromagnetic and electrical properties. To this end, particulate susceptors are admixed to the matrix in form of metallic particles and their oxides as well as e.g. carbon nanotubes. To provide a well distributed heating, it must be made sure that the particles are dispersed evenly and do not agglomerate. This

method provides many advantages. High heating rates can be achieved because the material is heated throughout its volume, and therefore the distance for conductive heat transfer is reduced. Energy losses to surroundings can be minimized as inductive heating provides the possibility of selectively heating the targeted regions. Furthermore, the heating can be controlled more precisely, compared to a convection oven. [32–34]

2.3.1 Nanoferrites

Nanoferrites are nanoscale ferromagnetic particles, which can be added to organic polymer formulation as susceptor particles for inductive heating. In the present work, nanoferrites, consisting of a magnetite (Fe_3O_4) core and a silica shell, were used. The silica reduces agglomeration and protects the matrix from possible degradation by the oxide. Moreover, the silica shell can be functionalized to improve the embedding of the particles in the matrix and improve mechanical properties. [35] The silica coated particles are produced by adding a silica precursor to a mixture of water, ethanol and a catalyst with iron oxide particles. The precursor forms the silica layer via hydrolysis and condensation reaction. [36]

2.4 Dynamic reactions

A further approach to achieve reversible and reworkable adhesives is to use a crosslinked material that forms a covalent adaptable network (CAN) during the curing reaction. Materials based on covalent adaptable networks can be reshaped, healed and recycled due to the intrinsic property of the polymeric network to undergo dynamic bond exchange reactions, which allow for topology rearrangements. At service temperatures, CANs perform like thermosets or elastomers, however, by increasing the temperature, the rate of bond exchange reactions increases, and the material gains the ability to flow. The combination of the properties of a crosslinked material with the reprocessability of thermoplastic materials, forms a new material class of polymers, called vitrimers. [37]

A wide range of dynamic networks have been investigated in literature, which can be divided into associative and dissociative bond exchange mechanisms. Dissociative CANs contain crosslinks that can be reverted at elevated temperatures and reform at a different location upon cooling (see Figure 3 (a)). Dissociation of the network generally leads to a reduction of the average molecular mass, crosslink density and viscosity. In associative bond exchange reaction, crosslinks are broken only when a new bond is formed (see Figure 3 (b)). Due to the simultaneous bond breaking and forming the material remains a crosslinked system with a constant crosslink density throughout reprocessing. The exchange reaction rate rises with increasing temperature, enabling topology rearrangement, and therefore reprocessing. [38,39]
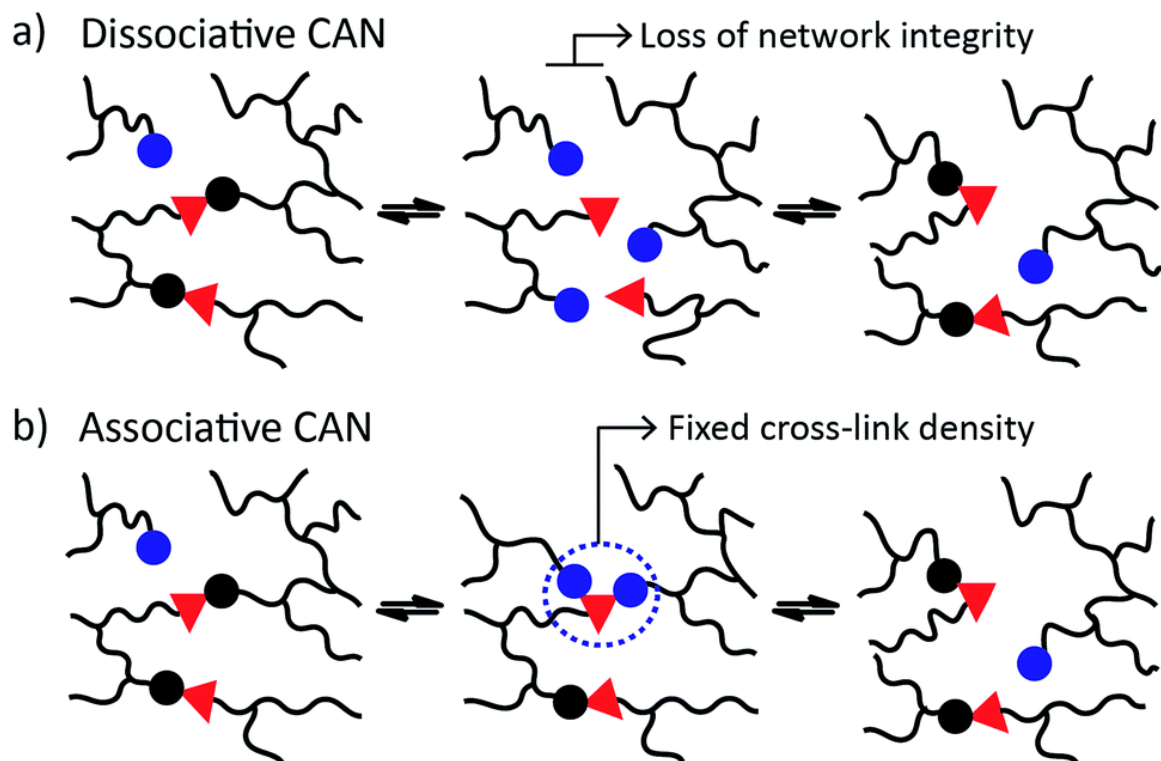

Figure 3: Schematic representation of bond exchanges in associative (a) and dissociative covalent adaptable networks. Figure reprinted from [39].

Dynamic bond exchange reactions have been reported in a number of material systems, with an ongoing strong interest for utilizing other chemical reactions to realize CANs. [40] In the following chapters, a small excerpt of selected dynamic reactions that are reported in literature for their use in crosslinked polymer networks, is described.

2.4.1 Diels-Alder reaction

The Diels-Alder reaction is a thermally reversible reaction between a conjugated diene and a dienophile, forming the Diels-Alder adduct, a six-membered aromatic ring. At elevated temperatures, the Diels-Alder adduct can revert to its initial components, which allows to achieve a controlled cleavage of the functional group. The dienophile contains double or triple bonds, whose reactivity is increased by additional unsaturation in the α- and β-position. Other unsaturated groups further increase the reactivity of the bonds. The dienophile is added to the 1,4 position of the conjugated diene. In literature the use of furane and maleimide derivatives in polymers is reported and schematically illustrated in Figure 4 (i). By using epoxy functionalized furanes and dimaleimide, their adduct (see Figure 4 (ii)) can be crosslinked with amines like a classical epoxy network, resulting in a dissociative CAN. The adduct separates at approximately 90°C and re-establishes its crosslinks at 60°C for the reported systems, but the decomposing reaction starts only slightly above 60°C, which is generally too low for a potential application in photovoltaics. [39,41,42]
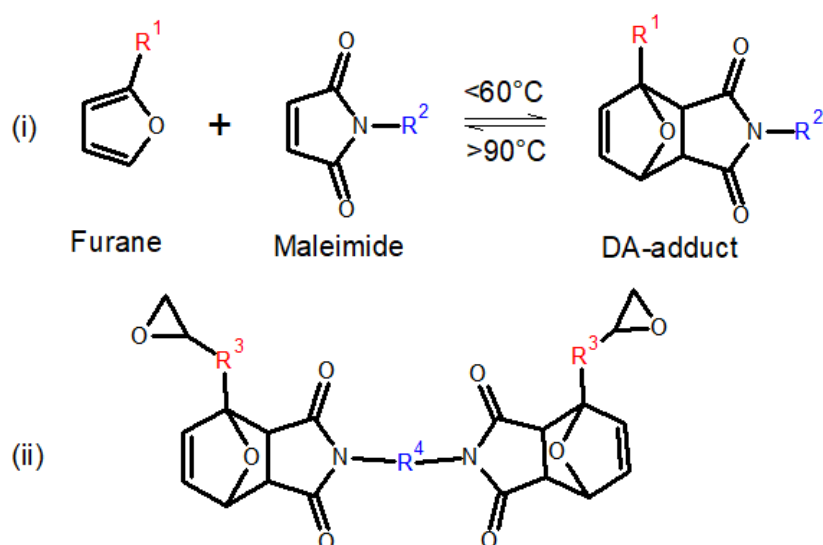

Figure 4: Schematic illustration of the reversible Diels-Alder reaction of furane and maleimide (i) and an epoxy functionalized Diels-Alder-adduct (ii).

2.4.2 Amine-based CANs

A number of dynamic reactions based on exchange reactions with amine functional groups have been reported, including transamination of vinylogous urethanes, transamidation and amine-imine exchange reaction, as schematically illustrated in Figure 5. All three systems belong to the group of associative CANs in the absence of water. Networks based on amine-imine exchange follow a dissociative mechanism in the presence of water, due to reversible imine hydrolysis. [43] In a dry state it can be reprocessed at elevated temperatures just like for transamination and transamidation networks. These exchange reactions generally achieve high rates and do not require catalysts. With transamidation being the slowest reaction, a catalyst is often employed. While the materials based on transamination and transamidation are expected to be stable against hydrolysis, water can catalyse the exchange reaction. [44] This can influence the necessary temperature for reprocessing and therefore seems unsuitable for an application in photovoltaic modules. Furthermore, the excess amine groups in the network are prone to oxidative degradation in long-term use. [39,44–47]
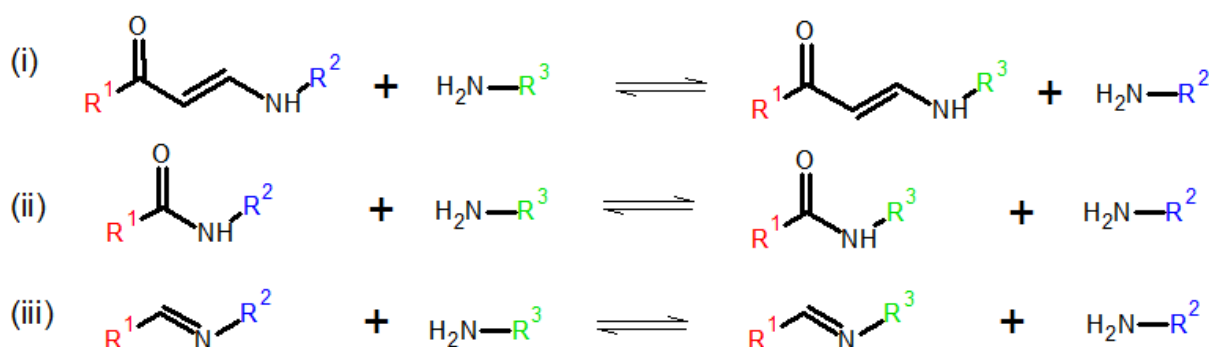

Figure 5: Schematic illustration of transamination of vinylogous urethanes (i), transamidation (ii), imine-amine exchange reaction (iii).

2.4.3 Siloxane exchange reaction

The possibility of reprocessing poly(dimethylsiloxane) (PDMS) was already postulated in 1954 by Osthoff et al. [48] The dynamic character of the siloxane exchange reaction (see Figure 6) originates from the anionic curing of PDMS, which results in living ends in the form of a negative charge on the terminal oxygen atom. The cationic rest of the

initiator serves as a catalyst of the reaction. The associative system can be reprocessed at starting temperatures of approximately 90°C, however, above temperatures of approximately 150°C the living ends are deactivated by thermal decomposition. [49,50]
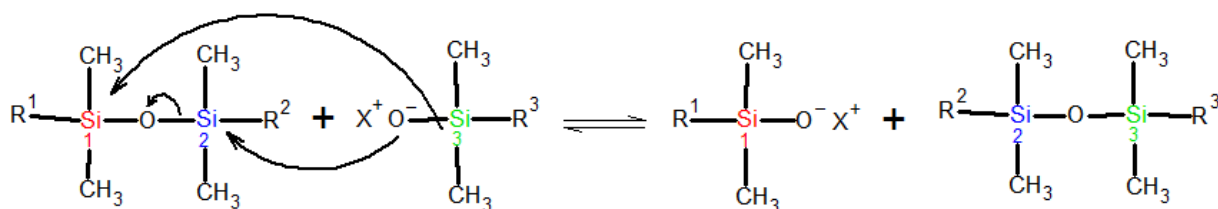

Figure 6: Schematic representation of the siloxane exchange reaction.

2.4.4 Transcarbamoylation

CANs based on transcarbamoylation reactions are associative networks with carbamate links in their backbone. Transcarbamoylation reactions are generally slow and require a catalyst. However, by incorporating free hydroxyl groups in the network e.g. with hydroxyl urethane moieties, the reaction speed can be increased without the need for adding a catalyst. Depending on the presence of hydroxyl groups in the material system, the transcarbamoylation follows different reaction mechanisms, as depicted in Figure 7. [50,51]
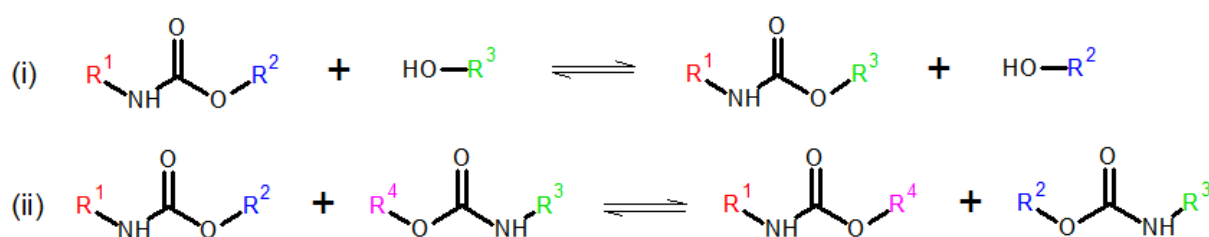

Figure 7: Schematic illustration of the hydroxyl mediated (i) and non-hydroxyl mediated (ii) transcarbamoylation reaction.

2.4.5 Transesterification

Associative CANs based on transesterification reaction, were first described by Leibler and co-workers in 2011. These vitrimeric systems were established by curing epoxy resins with carboxylic acids or anhydrides in suitable ratios in the presence of a catalyst to produce a network with beta hydroxyl ester linkages. [52] The realization of CANs from other starting compounds is possible as well, as long as the established network has ester and hydroxyl groups in its backbone. [53] The crosslinked material can rearrange its topology via transesterification reaction, an exchange reaction of an ester group with a hydroxyl group producing a new ester and hydroxyl by swapping their ligands, illustrated in Figure 8. The exchange reaction rates are generally low and to achieve higher rates, a catalyst and elevated temperatures are required. [52]
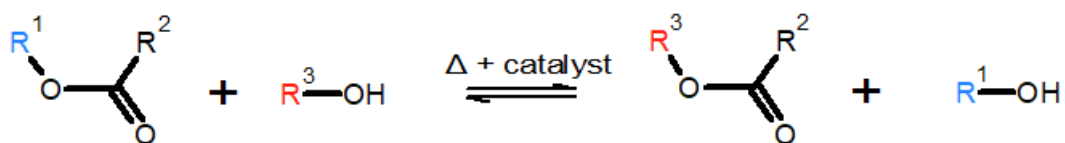

Figure 8: Schematic representation of the transesterification reaction.

Associative CAN networks based on transesterification reactions are seen as most suitable for the application in this work, especially in terms of long-term stability, due to their flexibility, vast amount of possible formulations and the relatively simple establishment of the systems, which is possible with conventional epoxy resins and hardeners. After the discovery by Leibler et al., immense amounts of research were done on vitrimers, which can be seen in the increasing number of publications since their discovery.

Curing reactions of epoxy-acid and epoxy-anhydride systems

Carboxylic acid and especially anhydride curing agents provide various advantages over amine curing agents for epoxy systems. Amine curing agents are often harmful before the crosslinking reaction takes place. [54] For technical applications, anhydride curing is often preferred, due to higher thermal stability, less water absorption, lower exothermic heat during reaction and lower shrinkage of the cured resins. [55,56] The

curing reaction requires elevated temperatures and catalysts such as tertiary amines allow curing at temperatures below 200°C. Reactions between epoxy groups and carboxylic acids lead to step growth polymerisation, while epoxy-anhydride systems undergo chain-wise polymerisation. [57] Figure 9 schematically illustrates the main reactions of epoxides with carboxylic acid as curing agents, which are addition-esterification of acids on epoxide rings (i), etherification by homopolymerization (ii) and Fischer esterification of acids on hydroxyl groups (iii). The alternating ring-opening polymerization with anhydrides and epoxides is illustrated in Figure 10: The anhydride ring opens via reaction with a hydroxyl group (i) or a catalyst resulting in a new hydroxyl group that reacts with an epoxide ring (ii). [58] With an excess of epoxide, homopolymerization takes place after the anhydride is used. [59,60]

To ensure that hydroxyl and ester groups are present after curing and, subsequently, a transesterification can take place, the molar ratio of epoxide groups to carboxyl groups must be 1:1. Respectively, the molar ratio of epoxide rings to anhydride rings must be 2:1. Therefore, every epoxide group reacts with one carboxyl group and full crosslinking is achieved mainly by addition-esterification (see Figure 9 (i) for carboxylic acids and Figure 10 (ii) for anhydrides). [58]
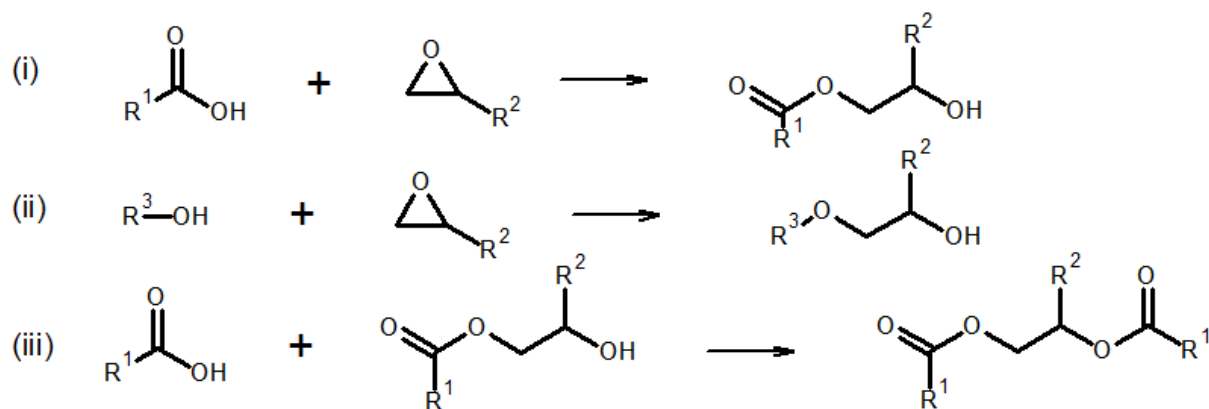

Figure 9: Schematic illustrations of the main reactions during epoxy-acid curing.
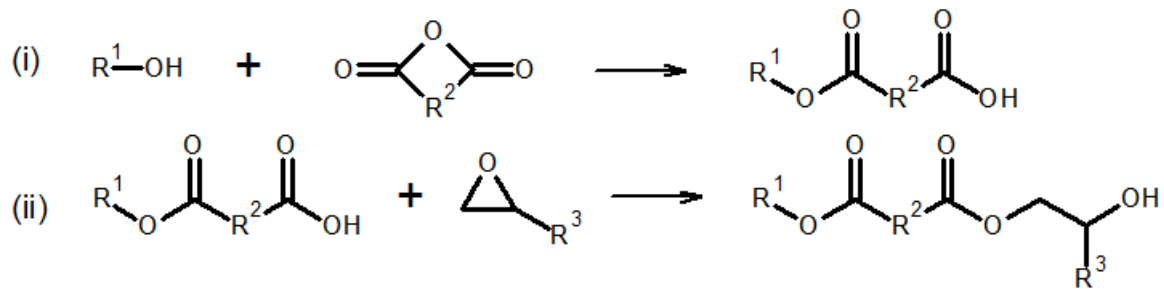
Figure 10: Schematic illustration of the alternating ring opening polymerisation of epoxy resins with anhydrides.

Vitrification temperature

At lower temperatures the network topology is frozen due to a low rate of bond exchange reactions, and the material behaves like a thermoset. The transition from elastic solid to viscoelastic liquid at the vitrification temperature (T_v) is similar to the glass transition of strong glass formers like silica. The viscosity gradually decreases, following the Arrhenius law, unlike thermoplastic organic polymers such as poly(methyl methacrylate) (PMMA) or poly(styrene) (PS) with a more rapid viscosity change, therefore called fragile liquids. [58] In Figure 11, the viscosity change of a vitrimer when approaching the vitrification temperature (T_v) is compared to silica and thermoplastics for their respective glass transition temperature (T_g) in an Angell plot. The abrupt viscosity drop of the thermoplastics PMMA, PS and poly(vinylchloride) (PVC) can be clearly seen in contrast to the gradual decrease for silica and vitrimer systems. [40]
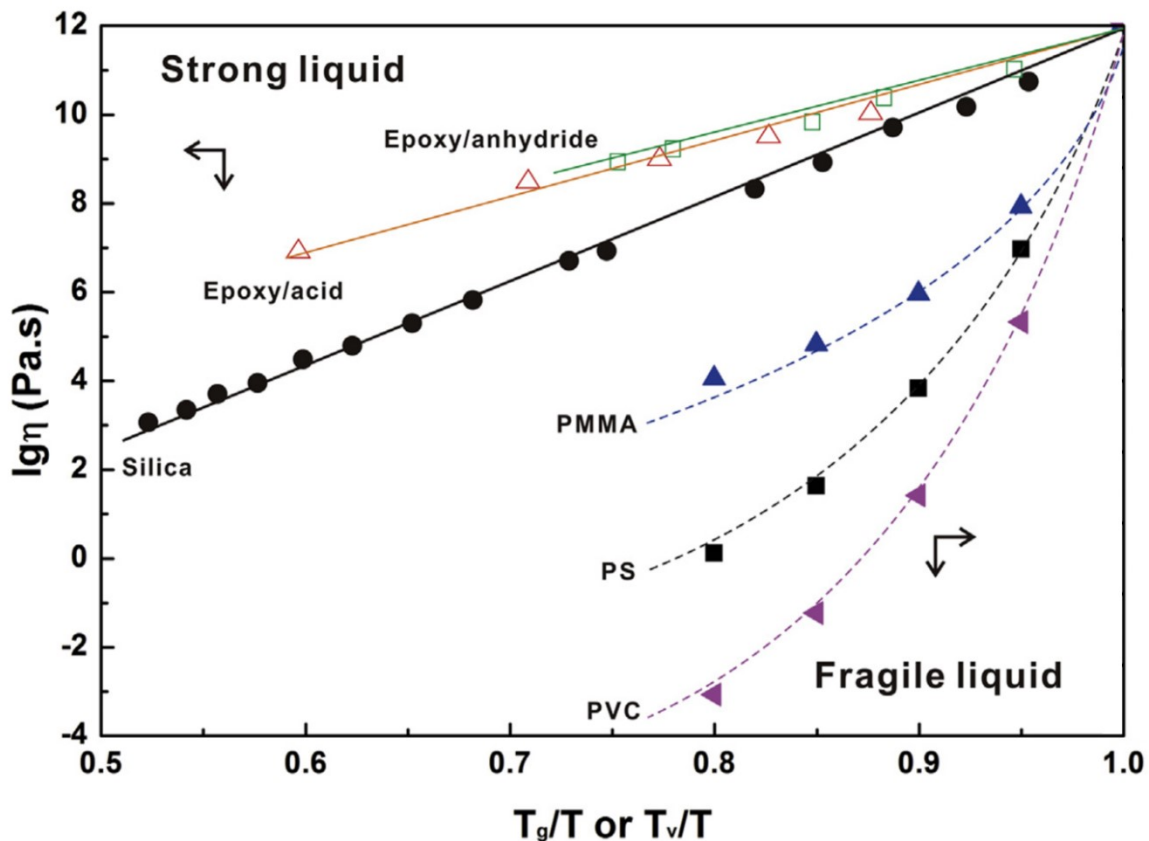
Figure 11: Angell plot of fragility describing the change in viscosity (η) for epoxy-anhydride and epoxy-acid vitrimers, silica, PMMA, PS and PVC. Figure modified from [40]

After transitioning it is possible to weld or reprocess the material or to heal cracks or other damages, as the vitrimer system behaves like a viscoelastic liquid. Nevertheless, it differs from a thermoplastic melt. The rheological properties of a thermoplastic polymer melt are controlled by friction of the macromolecules, while the transesterification reaction can still require a significant amount of time to rearrange, even if the temperature is above T_v. This means that the material properties are dependent on thermal history. [52] During heating, the vitrimer undergoes both a glass transition of polymers, following the Williams-Landel-Ferry equation, as well as the transition to a viscoelastic liquid at T_v. The vitrification temperature was originally set to the temperature, at which the viscosity of the material reaches values lower than 10^{12} Pa s, which is, by convention, the glass to liquid transition. [61] This allows determination of T_v via rheological measurements of stress relaxation, with a viscosity

of 10^{12} Pa s corresponding to a relaxation time of 10^6 s, and even calculated T_v values can be obtained by extrapolation from the Arrhenius plot. An efficient topology rearrangement requires increased mobility of polymer (side)chains, which occurs above the glass transition region. Therefore, if T_g is higher than T_v, the vitrification temperature cannot be measured directly but can only be assumed by extrapolation. [62] Another way of measuring the T_v are dilatometric tests, due to the fact that a vitrimer network exhibits an increased thermal expansion coefficient above its vitrification temperature.[39] The tests are done with a static tensile load applied to the sample, essentially making it a creep test with ramping temperature. Using those measurements, Capelot et al. postulated that the T_v can be controlled via catalyst loading, suggesting that T_v decreases with increasing catalyst content due to accelerated exchange reactions. [63] However, more recent studies provide new methods to detect the transition temperature, which propose that T_v is independent of catalyst concentration. [52,64]

Catalysts

While there are approaches that realize transesterification-based vitrimer systems without the need for catalysts by increasing the amount of hydroxyl groups in the network, [65,66] most epoxy vitrimer systems implement them to accelerate the dynamic bond exchange reaction. Catalysts used for curing, as well as to accelerate the transesterification reaction are, amongst others, tertiary amines or metal complexes. Their catalytic effects are achieved either by creating alkoxy-ions, which exhibit increased nucleophilicity; or by increasing the reactivity of covalent bonds, via the formation of hydrogen bonds between the functional group and the catalyst. Furthermore, they can have a coordinating effect by bringing the reactive centres closer to each other. [67,68]

Metal complex catalysts

Along with amines, metal complexes are the most used catalysts in vitrimers. In fact, the first described vitrimers used a combination of epoxy-carboxylic acid networks with zinc acetate ($Zn(OAc)_2$) and epoxy-anhydride networks with zinc acetylacetonate

(Zn(AcAc)₂) as catalysts. [52] Figure 12 contains the chemical structure of the catalysts Zn(AcAc)₂ and Zn(OAc)₂ (i). Zinc complexes are often present in hydrated form, increasing the coordination of Zn^{2+}. The metal complexes are commonly dissolved in the component containing the carboxylic acid for epoxy-acid systems, or in the epoxy component in the case of anhydride cured epoxy systems. [52] During solvation in a carboxylic acid, their ligands are substituted by carboxyl groups, creating carboxylate-ions (see Figure 12 (ii)). The propagation then occurs ionically (see Figure 12 (iii)). For anhydride curing of epoxies, the metal complex is dissolved in the epoxy component, creating ions by substituting the ligands with the oxygen of the epoxide ring. In the process, the epoxide ring is opened and after mixing with the anhydride carboxylate-ions are formed again, similar to reaction (ii) in Figure 13. The ligands evaporate during solvation, usually without requiring vacuum assistance. Zn^{2+} stays in the cured network, attached to either the carbonyl group or by replacing the hydrogen in the beta hydroxyl group. When attached to a carbonyl group, the bond is activated and increased transesterification occurs. [67,69]
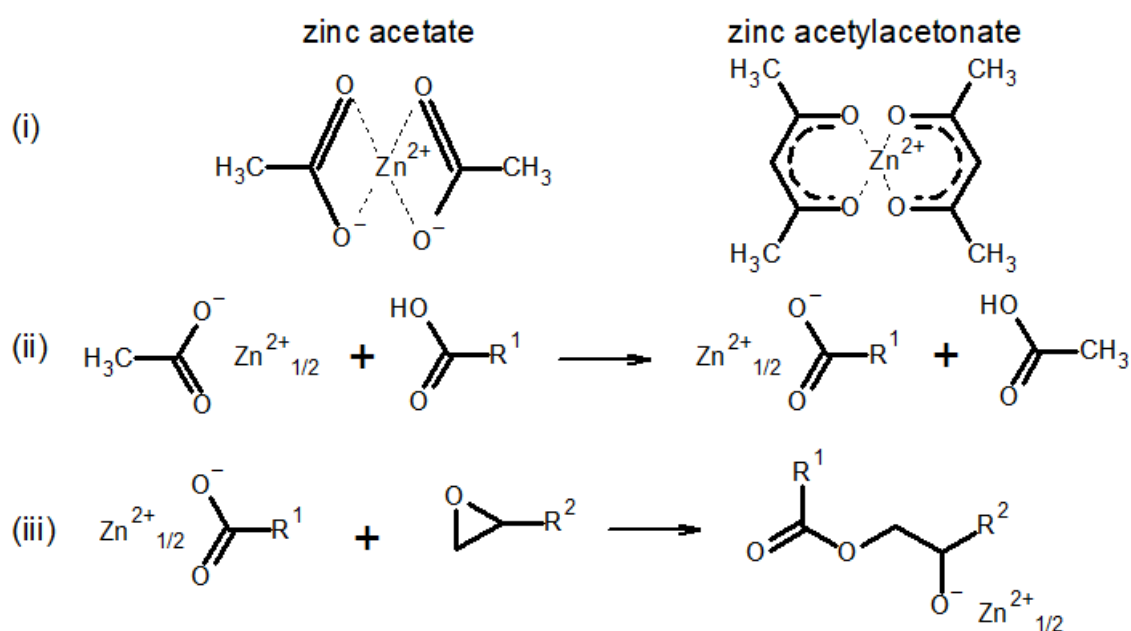

Figure 12: Zinc catalysts (i) and their effect on the curing reaction of epoxy-acid (ii) and epoxy-anhydride (iii) systems.

Amine catalysts

Figure 13 illustrates the most commonly used amine catalysts in vitrimers, namely, 1,5,7-triazabicyclo[4.4.0]dec-5-ene (TBD) and 1,5-diazabicyclo[4.3.0]non-5-ene (DBN) (i) and the initiation reaction of curing (ii,iii). Matějka et al. suggested that the catalyst attaches to the carbon atom of the epoxide rings to open the ring and create a zwitterion with a positively loaded catalyst end, and a negatively loaded oxygen atom. This zwitterion then reacts with an anhydride ring and forms a carboxyl-ion, which initiates the polymerization (see Figure 13 (ii)). [70] Pham proposed that the amine attaches to a carbon atom of the anhydride and the anhydride simultaneously reacts with the epoxide ring, resulting in the transition state in Figure 13 (iii). [68] For carboxylic acids, the amine either reacts with the hydrogen of the hydroxyl group by forming a quaternary ammonium salt [71] or attaches via hydrogen bonds and therefore reduces the bond strength of hydrogen to oxygen. [68] Both cases allow the reaction of the carboxylate/carboxyl with an epoxide ring. The transesterification reaction is catalysed in a similar manner to the catalysis of the acid curing. The difference is that the amine reacts with the hydrogen of a free hydroxyl group as the carboxyl groups have already been reacted to esters after curing. [72] The reaction is illustrated in Figure 14.
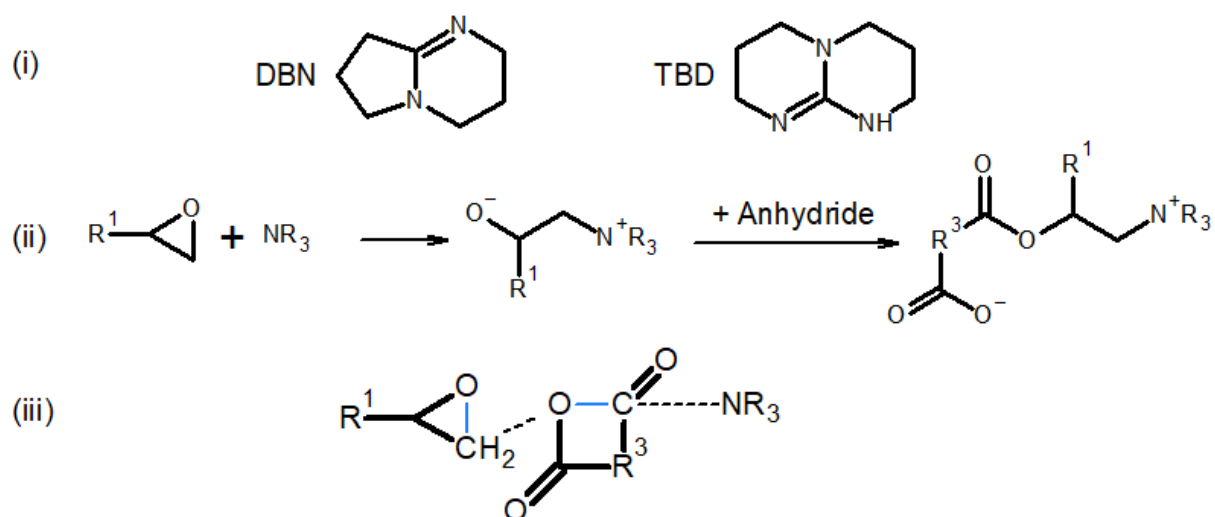

Figure 13: Structures of amine catalysts DBN and TBD (i), possible initiation reactions of epoxy-anhydride curing: ionically [70] (ii) or via hydrogen bond formation [68] (iii).
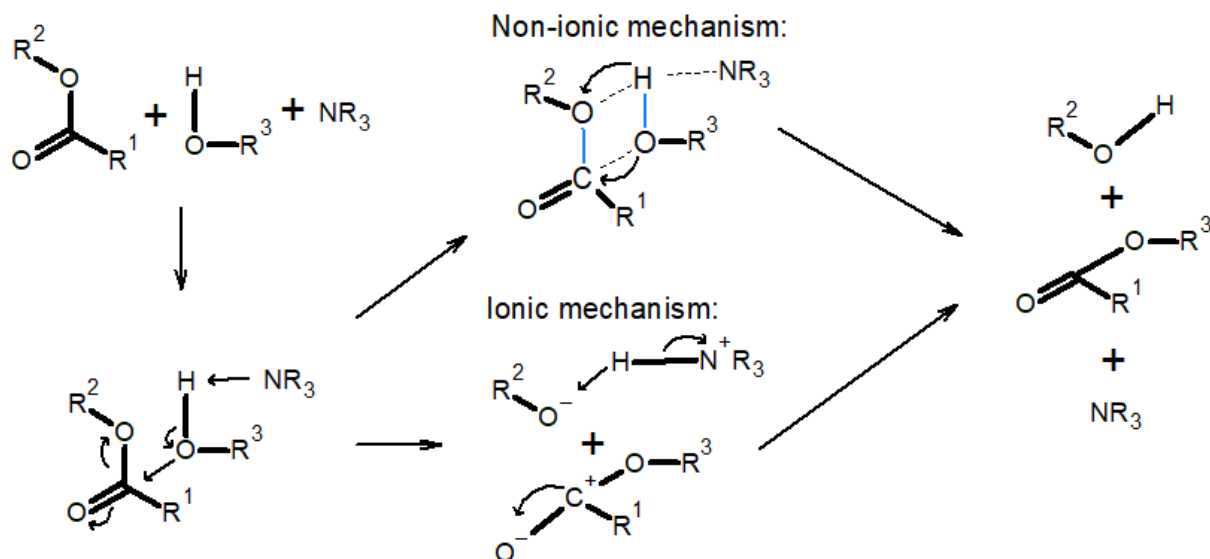
Figure 14: Proposed mechanism for amine catalysis of transesterification. [72]

Altuna et al. postulated that covalently bonded tertiary amines have similar capabilities of catalysing the curing and transesterification reactions compared to common catalysts used in vitrimers. The authors demonstrated this concept by reacting the primary amine *n*-butylamine (BA) and the secondary amine dibutylamine (DBA) with an excess of epoxide groups and then curing the epoxy with a stoichiometric amount of carboxylic acid to achieve a catalysis of the transesterification. The reaction of an epoxide ring with a primary or secondary amine is illustrated in Figure 15. The free hydroxyl groups, generated by the bonding reaction, additionally increase the effectiveness of the transesterification reaction. [66] The resulting network exhibits similar properties to conventional vitrimers in stress relaxation tests and the authors suggest that many other amines might be suitable as catalysts. [73] A covalently bonded catalyst would be favourable for long-term use and possible multiple recycling cycles in the process because the catalyst is directly bonded to the macromolecule and therefore cannot migrate to the sample surface or be leached from the bulk of the samples. Both amines described in the publication do not lead to a crosslinked network during the reaction. DBA is a secondary amine, and therefore has only one reactive hydrogen atom, and BA has two reactive hydrogen atoms, leading to a step-growth of the polymeric chains without network formation. [74]

In order to reduce the creep of elastomeric vitrimers, Li et al. demonstrated that a fraction of permanent crosslinks in a dynamic polymer network can lead to strongly supressed creep and excellent reproducibility. [53] This opens the possibility to introduce covalently bonded multifunctional amines for partial curing of epoxy-based resins, which additionally act as a catalyst for anhydride curing. At the time of writing, no other studies which exploit these concepts are known.
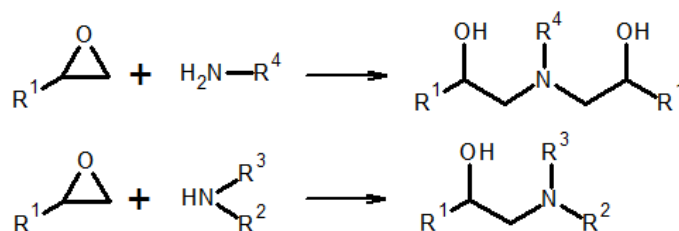

Figure 15: Covalent bonding of amine catalyst to epoxide functional groups.

2.5 Characterisation methods

In the following section, characterisation methods, which have been implemented during the research work, are described.

2.5.1 Fourier-transform infrared spectroscopy

Fourier-transform infrared (FTIR) spectroscopy allows to obtain a spectrum of absorption or emission of solids, liquids or gases in the infrared (IR) spectral region. This enables to draw conclusion on the chemical structure or specific functional groups of a sample. A light source produces IR light, which passes through an interferometer. The interferometer modulates the beam by varying the distance of the dynamic mirror, causing constructive and destructive interference for specific wavelengths. The beam then either passes through the sample (transmission mode) or is reflected on the sample surface (attenuated total reflection (ATR) mode). The sample absorbs specific wavelengths, which are characteristic for different types of bonds or functional groups. A detector measures all wavelengths simultaneously to obtain the interferogram. The

spectrum is produced by Fourier-transformation of the interferogram and is plotted as absorbance/transmittance versus wave number, which is the reciprocal wavelength with the unit cm^{-1}. [75,76]

The absorbance of specific wavelengths is based on the interaction of molecules with electromagnetic radiation. A molecule can absorb radiation if the radiation can induce or change the dipole moment of the molecule by stimulating the molecule vibration. The possible vibrations are characteristic for each molecule and depend on bonds and structure. The approximate regions of different bonds for a typical IR spectrum are illustrated in Figure 16 at the example of cellulose. If a vibration does not change the dipole moment or induce one, it cannot be detected in infrared spectroscopy. Additionally, the radiation stimulates vibration of the whole molecule, in the so-called fingerprint region of the spectra, ranging from approximately 1500 cm^{-1} to 650 cm^{-1}. [75,76]
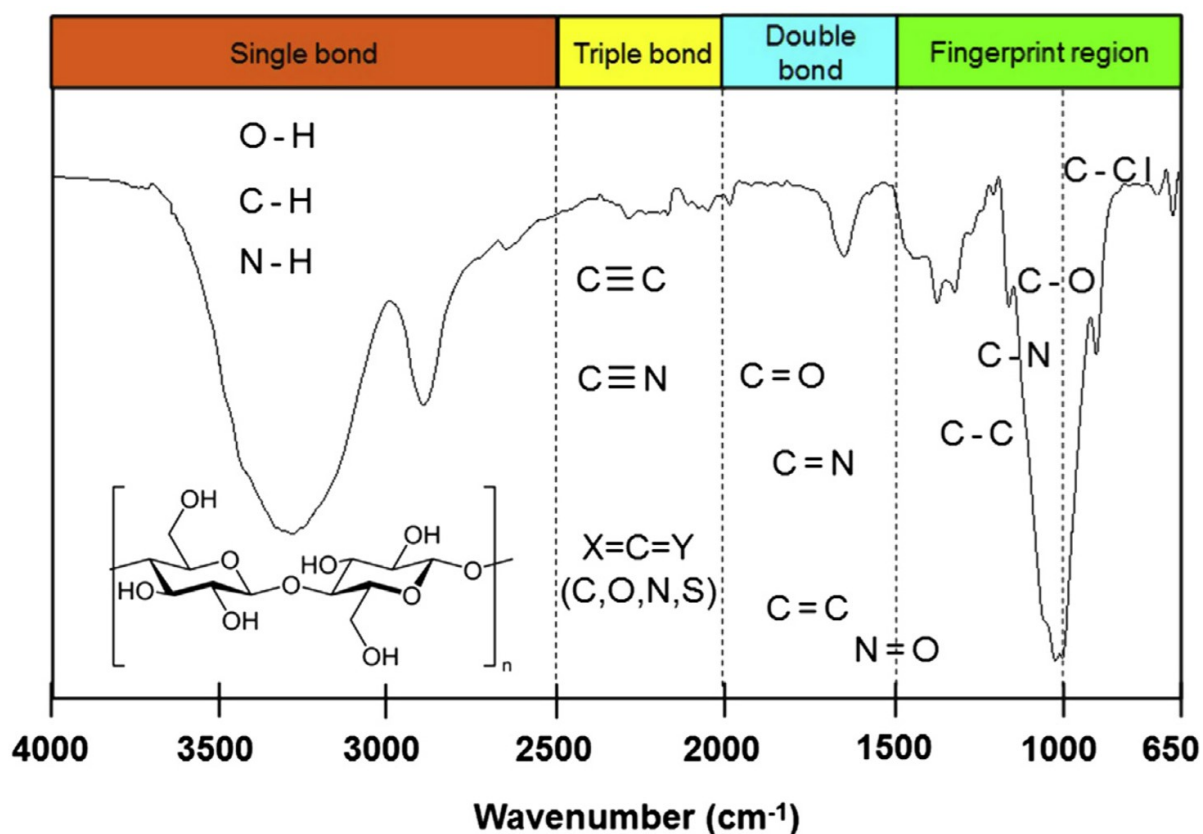

Figure 16: Approximate regions of absorbance bands for different bond types in a FTIR spectrum at the example of cellulose. Figure reprinted from [75].

2.5.2 Nuclear magnetic resonance spectroscopy

Nuclear magnetic resonance (NMR) spectroscopy uses radio frequencies to determine the molecular structure of a sample. For atoms to be NMR-active, they must have an odd number of protons and/or an odd number of neutrons, resulting in them possessing a spin, and therefore a magnetic moment. The most commonly used atoms are the hydrogen ^{1}H and carbon ^{13}C, with a spin of ½ and two possible spin states. Without external forces, the atoms and their spin can arrange freely and are in a disordered state. Under the influence of an external magnetic field, the magnetic moments align. ^{1}H and ^{13}C atoms can either be aligned against the field in a higher energy state or with the field in a lower energy state. The difference in energy between the two states increases with increasing external field strength. The nuclei can only absorb energy that equals this energy gap. The energy is varied by changing the frequency of the radiation and absorbance results in a peak in the spectrum. Nuclei of the same isotope resonate at the same frequency if they experience the same magnetic field. However, the electrons of the isotopes shield the nuclei from the external field because they possess their own small magnetic field, which opposes the external field. Therefore, a nucleus surrounded by a high electron density experiences a weaker magnetic field and resonates at lower frequencies. The electron density is influenced by bond type, structure and neighbouring atoms. Thus, the resonating frequencies provide information on these properties. Different machines for NMR spectroscopy work with different magnetic field strength, resulting in different resonance frequencies. To enable comparison, the spectra are expressed in chemical shift δ (ppm). The chemical shift is calculated, using a reference frequency ($f_{reference}$) of a material with a chemical shift of 0, often tetramethyl silane, and the resonance frequency measured for the sample (f_{sample}) as equation 1 states. The unit ppm results from dividing Hz by MHz. [77]

$$\partial = \frac{f_{reference} - f_{sample}}{f_{reference}} \tag{1}$$

2.5.3 Soxhlet extraction

The Soxhlet extraction technique is a simple way to identify if soluble components are present in a solid sample. The experimental setup is schematically illustrated in Figure 17. The sample is flooded with a chosen solvent by heating the still pot in the bottom via an oil bath and consequently evaporating the solvent. The solvent then condenses above the thimble, in which the sample is positioned due to the cooler on top of the apparatus. The chamber, containing the sample, slowly fills until it reaches the height of the siphon exit. At this point the chamber empties completely, the solvent flows back into the still pot, and the process starts again. The sample is weighed before and after the test to determine weight loss. After extraction the solvent can be analysed further to examine if or which molecules were dissolved during the test. [78]
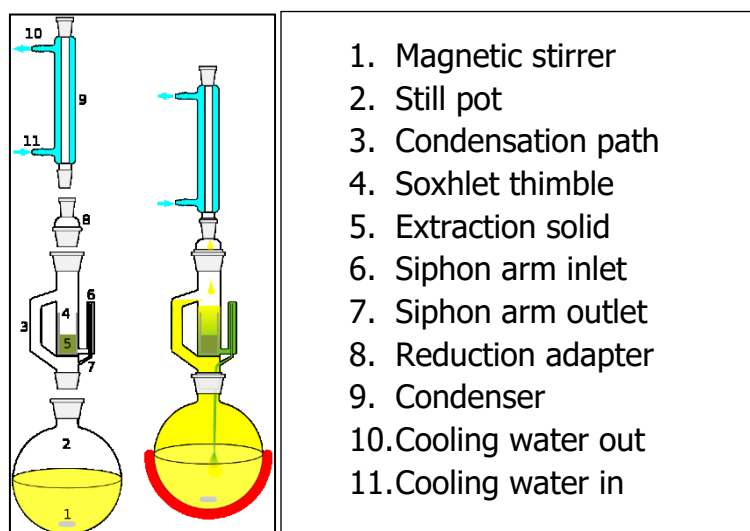

1. Magnetic stirrer
2. Still pot
3. Condensation path
4. Soxhlet thimble
5. Extraction solid
6. Siphon arm inlet
7. Siphon arm outlet
8. Reduction adapter
9. Condenser
10. Cooling water out
11. Cooling water in

Figure 17: Schematic experimental setup of a Soxhlet extraction. Reprinted from [79].

2.5.4 Differential scanning calorimetry

Differential scanning calorimetry (DSC) provides information on exo- or endothermicity of a process, by measuring the difference in the heat flow of a sample and a reference sample while they are subjected to a controlled temperature program. [80] A pan containing the sample and a pan containing the reference sample, commonly air, are placed in testing cells and their temperature is monitored. There are two types of DSC,

namely power-compensation DSC and heat-flux DSC. The power-compensation DSC varies and records the power input that is required to heat, the samples which are in separate cells, following a temperature program. The heat-flux DSC provides constant power input to heat the samples and the resulting differences in temperature are measured. The DSC is used to characterise processes that influence the required heat flow to heat a material, such as the glass transition, melting or recrystallisation of thermoplastics, and chemical reactions like curing of thermosets and elastomers. [81]

2.5.5 Dynamic creep test

Dilatometry can be implemented to evaluate the vitrification temperature by heating the sample at a constant rate and applying a small static load. However, not the thermal expansion is measured but the strain depending on the temperature. A sample strip is clamped into the measurement chamber and the chamber is set to the starting temperature. The sample should be very thin to allow a homogenous temperature distribution in the whole specimen during heating. A constant load is applied, the temperature is increased at a constant rate, and the elongation over temperature is recorded. Below the vitrification temperature, the strain rate is constant, and the elongation increases linearly. When the rate of exchange through transesterification becomes higher than the deformation rate, the elongation starts to increase non-linearly. T_v is defined as the point, at which the elongation first leaves linearity. [52]

3 EXPERIMENTAL

In order to realize dismantable adhesive bonds, two different concepts were evaluated. In the first approach, formulations with functional fillers in a commercially available adhesive were developed. The second approach comprises the development of vitrimers to facilitate a bond separation at increased temperatures as well as to allow rejoining of separated surfaces. In the following section, the two concepts are described separately. To allow a direct comparison of the different concepts, the most promising formulations were compared by lap shear testing.

3.1 Equipment

The equipment used for characterisation and material testing is listed in Table 1.

Table 1: Instruments used

Machine	Manufacturer	Type
Infrared spectrometer	PerkinElmer Inc.	Spectrum One
NMR spectrometer	Agilent Technologies.	Varian 400
Tensile testing machine	Zwick/Roell	Z010
Creep testing machine	Anton Paar GmbH	MCR 502
Dynamic mechanical analyser	PerkinElmer Inc.	DMA 8000
Differential scanning calorimeter	PerkinElmer Inc.	DSC 4000
Hot-press	Dr. Collin GmbH	COLLIN P 300 E+
Damp heat oven	Weiss Umwelttechnik	WKL 64/40

3.2 Functional filler concept

3.2.1 Materials

The investigated matrix for the functional fillers is a condensation-curing 2-component alkoxy-based silicone adhesive, consisting of Novasil S49 and the hardener Ottocure S-CA2010 in a weight ratio of 10.6 to 1. The adhesive was supplied by Hermann Otto GmbH (Germany) and is commonly used for photovoltaic applications. The adhesive system will be referenced as Novasil in the following sections.

The investigated fillers are listed in Table 2 with their respective expansion temperatures and particle sizes as stated by their suppliers.

Table 2: Fillers used

Name	Supplier	Expansion temperature, °C	Abbreviation	Particle size, µm
Thermally expandable microspheres				
909 DU 80	Nouryon	120-190	EXP	18-24
E-micro DU608S	Nanosphere	150-194	NS-DU	18-31
E-micro D280C	Nanosphere	150-200	NS-D	24-39
Expandable graphite				
BLG 300 L-LT	RMC Remacon GmbH	>140	EG300	300
BLG 40 T	RMC Remacon GmbH	>200	EG40	75
Nanoferrites				
Magnetite + SiO_2 coating	Iolitec	N/A	NF	38-44 nm

3.2.2 Expansion tests

The three types of thermally expandable microspheres (TEM) and two types of expandable graphite (EG) have been tested for their expansion behaviour. The evaluated parameters were temperature, heating time and expansion ratio. The approximate temperature range needed to trigger expansion was determined by placing the functional fillers in glass vials and heating them in a convection oven. To gather further information on their degree of expansion in dependence of time and temperature, the functional fillers were mixed with Novasil with a concentration of 10 wt.%, 30 wt.% and 50 wt.%. As a reference, the unfilled adhesive was also tested. The non-cured mixtures were spread onto an aluminium foil and a sample sheet with 1-2 mm thickness was produced. To ensure complete curing, the sheets were stored at room temperature for at least 48 h. The individual specimens were cut into squares with an area of approximately 1 cm^2. Every type of filler was tested for four different temperature levels. On each temperature level, the specimens were kept in the convection oven for 15 min and 1 h. Table 3 lists the applied temperature levels depending on the functional fillers. To calculate the expansion ratio of the functional filler embedded in the matrix, the dimensions of the test specimens were measured before and after expansion.

Table 3: Applied temperatures for the expansion test

Temperature, °C	EXP	NS-DU	NS-D	EG300	EG40
100	X				
125	X	X	X		
150	X	X	X	X	
175	X	X	X	X	X
200		X	X	X	X
225				X	X
250				X	X
275					X

3.2.3 Inductive heating

To examine the influence of the filling level of nanoferrites on their suitability for inductive heating, the respective particles were mixed with the adhesive with concentrations of 10 wt.%, 20 wt.% and 30 wt.%. Additionally, an adhesive formulation with 30 wt.% NF and 30 wt.% EXP was cured in a 1 mm layer between two microscope slides. The samples were stored for at least 48 h at room temperature to ensure complete curing. The induction heating experiments were performed at the Chair of Automation at the Montanuniversitaet Leoben, using a self-made setup. The samples were placed in the centre of an induction coil, which was connected to a power supply. Due to technical limitations of the cooling system the duration of heating was limited, and pulsed operation was done in order to avoid overheating. The temperature was measured constantly by a thermographic camera, which was placed above the specimen. The experimental parameters used for the samples with NF only are listed in the second column of Table 4, and parameters for the samples including EXP are listed in the third column.

Table 4: Induction heating parameters

Parameter	Novasil + NF	Novasil + NF + EXP
Power, kW	10	10
Coil type	Ring	Ring
Coil diameter, cm	5	5
Coil turns	3	5
Frequency, kHz	210	180
Pulse duration, ms	3000; 500	500
Number of pulses	1; 40	670
Time between pulses, ms	-; 200	200

3.3 Vitrimeric adhesive concepts

3.3.1 Materials

The materials used to establish the vitrimeric adhesive are listed in Table 5. All chemicals were obtained from commercial sources and used without further purification unless stated otherwise.

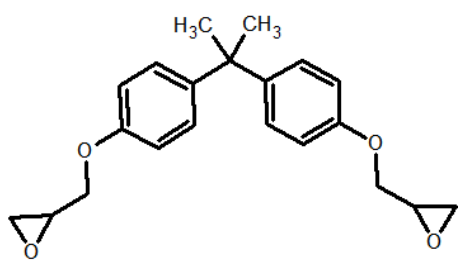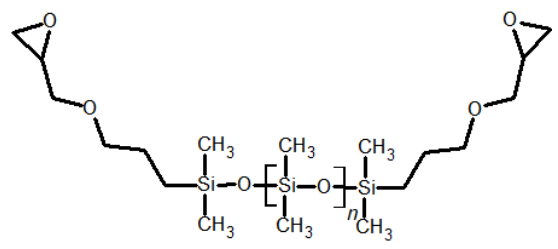**Table 5: Chemicals used for vitrimeric elastomers**

Name + abbreviation	Supplier	Chemical structure
Epoxides		
Bisphenol A diglycidyl ether DGEBA	Sigma-Aldrich	
Epoxy terminated poly(dimethylsiloxane) Ep-PDMS	Sigma-Aldrich	$M_n = 800$ g/mol

Table 5 (continued)

Curing agents

| Hexahydro-4-methylphthalic anhydride | Sigma-Aldrich | |
| MHHPA | | |

| Succinic anhydride functionalized poly(dimethylsiloxane) | ABCR-GmbH | |
| SA-PDMS | | $M_n = 700$ g/mol |

| Pripol 1040 | Croda Coatings & Polymers | |
| Pripol | | 302 g/(mol COOH) |
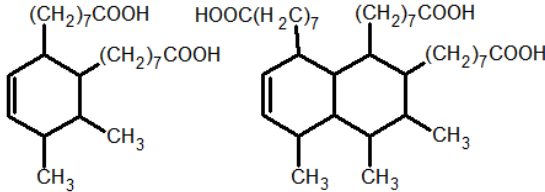
Table 5 (continued)

	Catalysts	
Zinc acetylacetonate hydrate Zn(AcAc)$_2$	Sigma-Aldrich	
1,5,7-triazabicyclo [4.4.0]dec-5-ene TBD	Sigma-Aldrich	
1,5-diaza-bicyclo [4.3.0]non-5-ene DBN	Sigma-Aldrich	
n-butylamine BA	Sigma-Aldrich	H$_3$C(CH$_2$)$_3$NH$_2$
Dibutylamine DBA	Sigma-Aldrich	(H$_3$C(CH$_2$)$_3$)$_2$NH
2,2,4-trimethyl-1,6-hexamethylenediamine TMHMDA	Sigma-Aldrich	
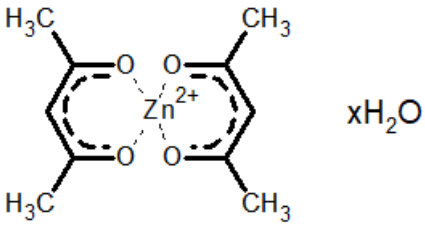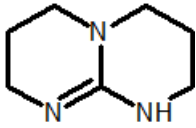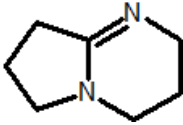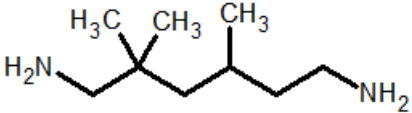
3.3.2 Synthesis of an epoxy-anhydride vitrimer

Vitrimeric samples were produced by reacting bisphenol A diglycidyl ether (DGEBA) and epoxy terminated poly(dimethylsiloxane) (Ep-PDMS) with the anhydrides hexahydro-4-methylphthalic anhydride (MHHPA) and succinic anhydride functionalized poly(dimethylsiloxane) (SA-PDMS) in a molar ratio of 2 epoxide groups to 1 anhydride group. $Zn(AcAc)_2$ in a concentration of 10 mol% to the epoxy groups was added as a catalyst.

First, $Zn(AcAc)_2$ and the anhydride were mixed in a glass vial on a magnetic stirrer set to 150°C, where it was kept until the catalyst completely dissolved and the water and low molecular weight by-products evaporated. The solution was cooled down to room temperature, mixed with the epoxy component and stirred manually until a homogenous resin was obtained. The resin was poured in a PTFE mould and cured in an oven at 120°C overnight. Complete curing was confirmed via ATR-FTIR spectroscopy by observing the shift of the characteristic signals for anhydride groups to signals for ester moieties and the disappearance of the epoxide signal. Hydroxyl groups form during crosslinking and can be detected via FTIR spectroscopy.

3.3.3 Reprocessing tests

All samples were tested on their reprocessability after curing. The samples were manually grinded, wrapped in aluminium foil and placed between two aluminium strips to allow to apply an external force on the grinded material. Afterwards, they were placed in a screw clamp and tightened manually. The experimental setup is depicted in Figure 18.
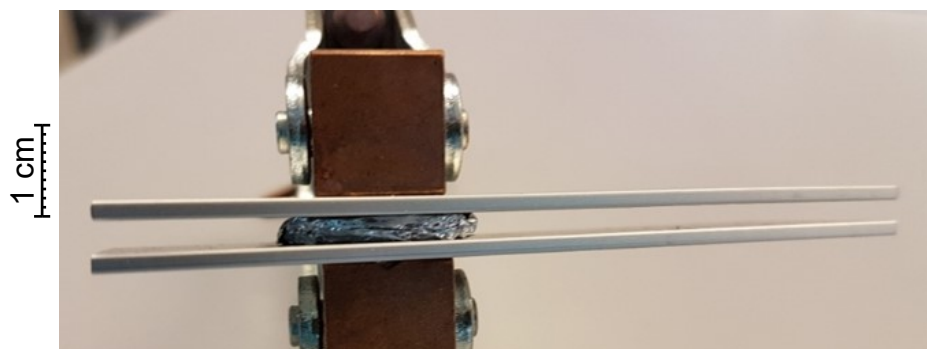

Figure 18: Setup for qualitative reprocessing tests.

To rejoin the grinded materials, the samples were placed in an oven for a selected duration at elevated temperatures. The success of reprocessing was evaluated by breaking the reproduced samples in half and optically inspecting the interface on visible grain boundaries. FTIR scans were done after the samples were reprocessed, to ensure that the reshaping was the result of transesterification and that no chemical degradation occurred.

3.3.4 Catalyst selection

Different catalysts were implemented in the vitrimer formulation to examine the influence on curing behaviour, material elasticity and reprocessability. For this, Ep-PDMS was cured with SA-PDMS in a molar ratio of 2 epoxy groups to 1 anhydride group, using different catalysts and catalyst concentrations. The alternative catalysts were the primary amine *n*-butylamine (BA); the secondary amine dibutylamine (DBA); and the tertiary amines 1,5,7-triazabicyclo[4.4.0]dec-5-ene (TBD) and 1,5-diaza-bicyclo[4.3.0]non-5-ene (DBN); with primary and secondary amines being covalently bonded to the network.

Samples containing TBD or DBN were produced by mixing the catalyst with the epoxy and anhydride components in the respective ratio and stirring them at 100°C until a homogenous mixture was achieved. Samples were prepared with either TBD or DBN at concentrations of 10 mol% and 20 mol% to the epoxy groups.

Samples containing the covalently bonded catalysts BA and DBA were produced according to the work of Altuna et al. [73] To achieve covalent bonding, the catalyst was added to Ep-PDMS in the respective ratio and placed on a magnetic stirrer for 1 h at 100°C, followed by 30 min at 130°C. SA-PDMS was added in a stoichiometric ratio and the mixture was stirred at 100°C until it was homogenous. Samples were prepared with molar ratios of 0.1 mol BA and 0.2 mol DBA per mol of epoxy groups. SA-PDMS was added in a ratio of 0.4 mol per mol epoxy groups to keep the formulation stoichiometric.

The mixtures were cast into PTFE moulds and placed in a convection oven. Curing was done overnight at 130°C. FTIR spectroscopy was utilized to confirm complete curing and the presence of characteristic signals for hydroxyl groups. Reprocessing at 180°C for 1 h, as well as qualitative examination of the elasticity before and after reprocessing were further performed for catalyst selection.

3.3.5 Synthesis of an epoxy-acid vitrimer

Ep-PDMS was cured with the fatty acid Pripol 1040, which consists of 77% trimers and 23% dimers with a carboxyl equivalent of 302 g/mol. Samples were produced, using DBA, BA and TMHMDA as catalysts. The composition of the samples is listed in Table 6. DBA and BA were reacted with Ep-PDMS as described in 3.3.4 before Pripol was added in a stoichiometric amount of epoxide to carboxyl groups. TMHMDA was reacted with Ep-PDMS at 60°C for at least 12 h.

Table 6: Composition of acid cured vitrimeric elastomers

Ep-PDMS, mol epoxide	Pripol, mol carboxyl	Catalyst, mol NH
1	0.8	BA; 0.2
1	0.8	DBA; 0.2
1	0.6	TMHMDA; 0.4

Pripol and Ep-PDMS tend to separate at room temperature. Therefore, the mixture was heated to 150°C in a convection oven and manually stirred until partial crosslinking was achieved, preventing a separation during curing. Curing was done overnight at 120°C and the conversion of the functional groups was confirmed by FTIR spectroscopy. The samples were reprocessed at 160°C for 5 h. Additionally the sample containing BA as a catalyst was tested at various reprocessing parameters: 160°C for 7 h, 160°C for 4 h, at 180°C for 3 h and 180°C for 2 h.

3.3.6 Characterisation

The polymeric network, consisting of Ep-PDMS, Pripol 1040 and BA with a ratio of epoxide groups to amine groups to carboxyl groups of 1:0.2:0.8 was characterised by mechanical testing and spectroscopic techniques.

The curing reaction was monitored by DSC and FTIR measurements using transmissive FTIR spectroscopy with the uncured resin being spin-coated onto a silicon wafer. The curing was carried out at 120°C. The shift of the carbonyl peak in the FTIR spectra was considered to determine the conversion. DSC measurements were carried out with a heating rate of 20 K/min from -70°C to 300°C.

Verification of catalyst bonding

To demonstrate that the catalyst BA is covalently bonded to the PDMS backbone and cannot leach out of the material, a Soxhlet extraction with hexane as solvent was carried out. The test was done for 23 h at a temperature of 90°C. Additionally the material was kept in the solvent for 26 h at room temperature. The sample was weighed before and after the extraction, and FTIR spectra were recorded to monitor any changes in chemical structure. Reprocessing tests were conducted at 160°C for 5 h, comparing the sample after the extraction with a sample that did not undergo the test.

To verify the existence of bonded amine groups ^{13}C-NMR spectra of Ep-PDMS and Ep-PDMS reacted with BA were recorded at 399,84 MHz with tetramethylsilane as reference.

Tensile test and reprocessability

Tensile tests were carried out to quantify the mechanical properties of the material as well as the reprocessability. The tensile tests were carried out with a testing speed of 1 mm/min for tensile modulus determination and continued with 50 mm/min on virgin and reprocessed material. No pre-load was applied, and the tensile modulus was calculated with the regression model.

The virgin samples were prepared by casting a sheet between two steel plates with distance holders of 1 mm thickness from which the specimens were punched out. The reprocessed samples were produced by grinding the virgin material after the tensile test and placing it in a hot-press at 160°C for 5 h. Distance holders of 1mm thickness were used and the press applied a pressure of 6 bar. The reprocessed sheets were then punched out again to obtain tensile specimens. The sample geometry of the test specimen is illustrated in Figure 19.
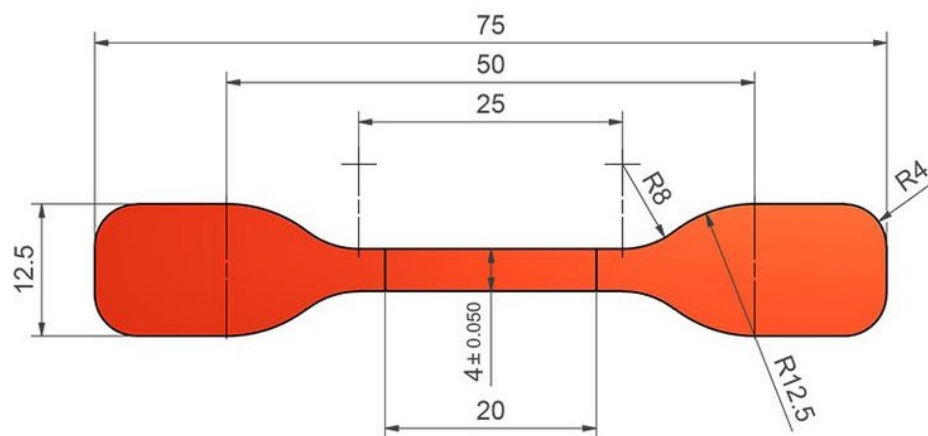
Figure 19: Specimen geometry for tensile tests. Figure modified from [82]

<u>*Dynamic creep tests*</u>

The vitrification temperature was determined by creep tests with loads of 20 kPa and 40 kPa and ramping the temperature. The heating rate was 3 K/min, starting at 25°C and heating up to 250°C. The samples were produced by casting a sheet between two metal plates with distance holders of 1 mm thickness and rectangular specimens of 10 mm x 30 mm were cut out. The test was repeated for samples with DBA as catalyst with a load of 20 kPa.

3.4 Lap shear tests

To evaluate the practical use of the most promising systems and to allow a comparison to the reference adhesive Novasil, lap shear tests under different conditions were carried out. The lap shear tests were done with a pre-load of 0.5 MPa and a test speed of 50 mm/min. All samples were tested without pre-conditioning as well as after

temperature cycle tests and damp heat tests. The temperature cycle tests were carried out by Lukas Neumaier at Silicon Austria Labs in Villach (Austria) for 50 cycles from -40°C to 85°C. The damp heat tests were done for 2000 h at 85°C and 85 % relative humidity. The vitrimeric samples were also tested on heat resistance for 930 h at 120°C in a convection oven.

The vitrimeric samples were tested at 160°C, at room temperature and after rejoining. Rejoining was done for 5 h at 160°C. The functional filler systems were tested at room temperature and after triggering the expansion. The thermal triggering of the expansion was done in a convection oven, 30 min at 150°C for the thermally expandable microspheres and 1 h at 225°C for the expandable graphite.

Five lap shear specimens for each parameter were prepared by bonding aluminium bars with an overlap of 13 mm (see Figure 20). The bond line had a thickness of 1 mm. As reference, samples with unfilled Novasil adhesive were prepared as well and tested under all conditions. Table 7 contains an overview over the produced samples and the different conditions the samples were tested with. The listed samples and condition were repeated three times: without weathering, after temperature cycle tests and after damp heat tests. The vitrimeric samples after heat resistance tests were only tested at room temperature (RT) and were not rejoined.

Table 7: Lap shear tests overview

Samples	RT	RT after trigger	160°C	RT after rejoining	Total
Novasil pure	5	5	5		**15**
Novasil + 30 wt.% EXP	5	5			**10**
Novasil + 50 wt.% EXP	5	5			**10**
Novasil + 30 wt.% EG300	5	5			**10**
Novasil + 50 wt.% EG300	5	5			**10**
Vitrimeric adhesive	5		5	5	**15**
Total	**30**	**25**	**10**	**5**	**70**

The samples were prepared by applying the adhesive materials onto an aluminium bar, a microscope slide served as distance holder for an even bond thickness and as barrier for the defined overlap. The second bar was placed on top of the adhesive and microscopic slide and pressed down by a weight of 500 g. A spacer below the second bar provides parallelism between the bars (see Figure 20). The vitrimeric material was partially crosslinked at 150°C for approximately 2 h in a convection oven before applying it onto the aluminium bar, to achieve a viscosity high enough to prevent the material from flowing off the bar during curing.
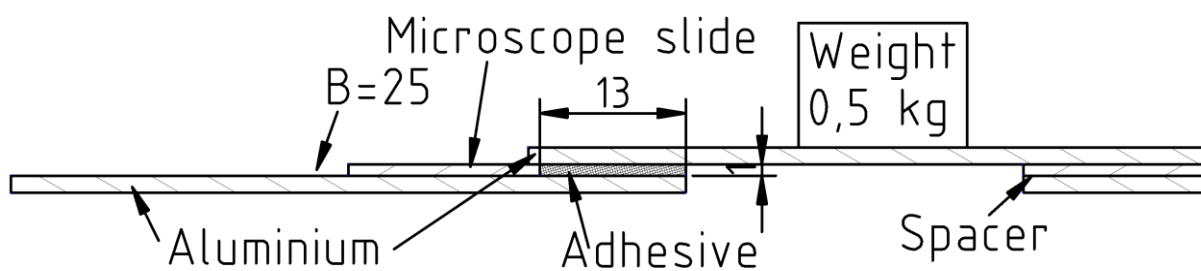
Figure 20: Lap shear specimen dimensions and production setup.

4 RESULTS AND DISCUSSION

4.1 Functional fillers

4.1.1 Expansion tests

In order to characterise the potential of the investigated functional fillers to expand and subsequently, to cause a separation of bonded surfaces, suitable filling degrees in the Novasil adhesive, expansion temperatures and heating times have been evaluated. Figure 21 shows the resulting expansion of the prepared specimens with 10 wt.%, 30 wt.% and 50 wt.% EXP, as well as unfilled reference samples after being in the oven at 125°C, 150°C, 175°C and 200°C for 15 minutes and 1 hour. When comparing the specimens after 15 minutes and 1 hours, it is obvious that the expansion has reached its maximum before 15 minutes and longer heating does not increase the expansion ratio any further. On the contrary, longer durations even reduce the resulting expansion at temperatures of 175°C and higher, due to a degradation of the material after prolonged exposure to heat. This can be explained either by thermal degradation of the thermoplastic shell of the thermally expandable microspheres or by rupturing of the thermoplastic shell from the expansion being too high. Degradation of the thermoplastic shell of TEMs is considered to be more likely because, as previously stated, no significant further expansion can be observed after 15 minutes in the oven. EXP already expands at 125°C, while samples containing NS-D (see appendix, Fig. i) and NS-DU (see appendix, Fig. ii) start at 150°C. Despite the higher starting temperature, NS-D and NS-DU still degraded after 1 h at 175°C, resulting in a narrower process window. Furthermore, EXP reaches a higher expansion ratio, with approximately 21x increase of its volume after 15 minutes at 150°C compared to approximately 7x increase for NS-DU and 12x for NS-D after 15 minutes at 175°C, all values being for samples with 50 wt.% functional filler. Therefore, further tests were conducted with EXP due to their preferable expansion behaviour at the relevant temperatures.
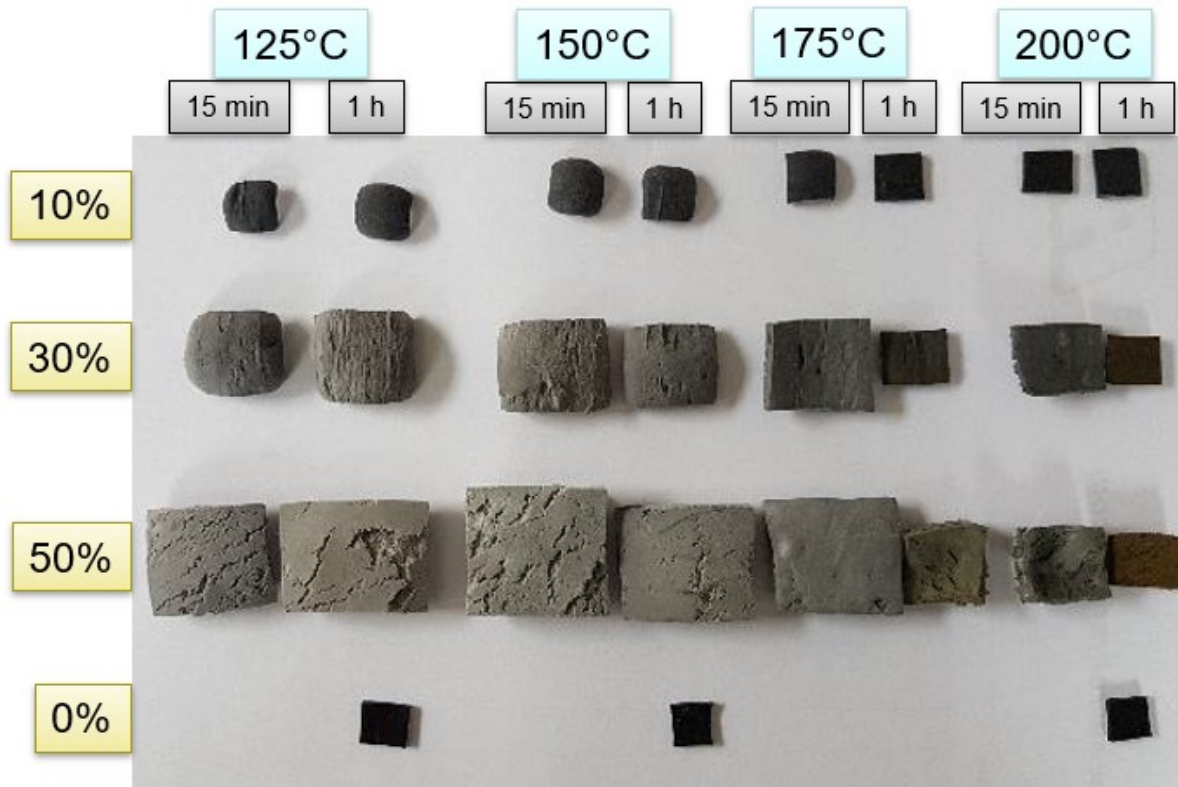
Figure 21: Expansion of Novasil samples filled with EXP in dependence of time, temperature and filler content.

Figure 22 shows the results of the expansion test for EG300, which has been performed in a similar manner to samples filled with TEM at temperatures of 175°C, 200°C, 225°C and 250°C. The expandable graphite generally showed less expansion compared to TEM. Furthermore, the rate of expansion is slower than for microspheres, increasing the expansion ratio with longer durations in the oven and no visible signs of degradation. The expansion also takes place at higher temperatures due to their usual field of application, which is fire protection. The maximum expansion ratio stated in the material datasheet provided by the supplier, was not reached, since the applied temperature was below the suggested temperature for maximum expansion of 1000°C. EG40 (see appendix, Fig. iii) could not be expanded in a temperature range (150°C ~275°C) that is reasonable for the intended application for dismantable adhesives.
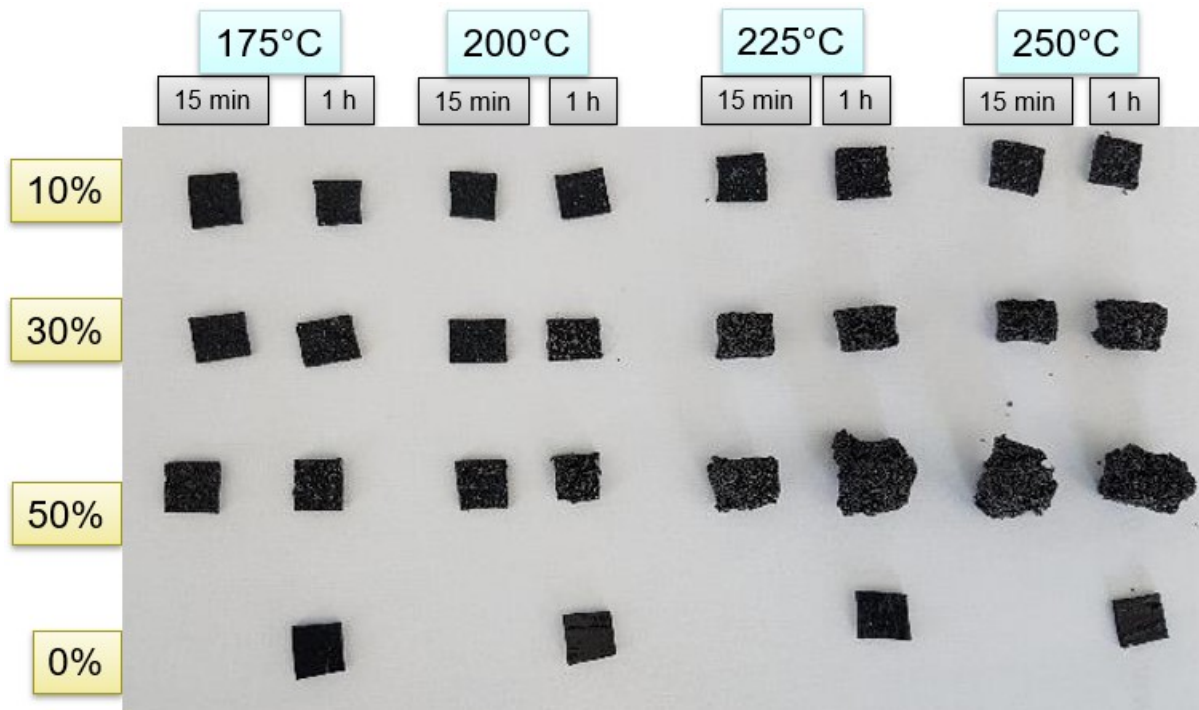
Figure 22: Expansion of Novasil samples filled with EG300 in dependence of time, temperature and filler content.

Table 8 includes the calculated maximum volumetric expansion for each sample, in Tab. i in the appendix all expansion ratios are listed. The volumetric expansion was calculated according to equation 2 with β being the expansion ratio, V_0 the calculated sample volume before expansion and V_E the volume after expansion. The volumes were calculated from the measured dimensions of the samples. Inaccuracies are estimated to be +/- 50 % volumetric expansion due to warpage caused by hindrance of expansion of TEM-filled samples by the aluminium and unevenness of the surface. Due to the air circulation in the convection oven, the calculated expansion ratio for EG might be prone to errors, due to inaccuracies in determining the sample dimensions, since expanded graphite flakes were partially blown away from the sample surface in the convection oven.

$$\beta = \frac{V_E}{V_0} \tag{2}$$

EXP achieved a more than two times higher expansion than EG300. Furthermore, TEM required less time to react to the temperature trigger. However, the TEM-filled samples

still exhibited a rather homogeneous surface after expansion, while the surface of the EG-filled samples was very rough after expansion, with loosely connected graphite flakes on top. It is expected that larger particle size and orientation of graphite flakes at the bonding interface facilitate a thermally triggered disbonding.

Table 8: Maximum expansion ratio of samples with functional fillers

Filler content, wt.%	Highest calculated volumetric expansion ratio				
	EXP	**NS-DU**	**NS-D**	**EG300**	**EG40**
10	3	2	2	2	1
30	11	6	7	6	1
50	21	7	12	9	1

4.1.2 Inductive heating

As an additional concept to trigger the expansion of EG by external stimuli, inductive heating of nanoferrites has been explored. This approach allows to trigger the expansion of the functional fillers throughout the volume of the sample, which reduces the distance for thermal conduction, compared to heating from the surface via a convection oven. This results in higher heating rates as polymers usually have low thermal conductivities and the adhesive can be heated selectively, reducing energy losses from heating unnecessary parts. Furthermore, triggering the expansion via inductive heating allows for a continuous separation process of the photovoltaic modules, since an induction coil does not require a closed space, while an open convection oven would result in high energy losses due to hot air leaving the oven. Studies report on the potential application of induction heating for e.g. selectively heating thermoplastic matrices of composites, [29] thermally triggering self-healing polymers, [34] welding of thermoplastic materials, and curing of thermosets [83] with promising results.

To realize adhesive connections, which can be disbonded by applying an alternating electromagnetic field, 10, 20 and 30 wt.% nanoferrites as susceptor particles alone and together with 30 wt.% expandable fillers (EXP) are implemented as fillers in Novasil. The sample temperatures were continuously measured by the means of thermography. Figure 23 shows a thermographic image of a Novasil sample (26 mm x 25 mm x 1 mm, between two microscope slides) containing 30 wt.% NF and 30 wt.% EXP inside the induction coil. The temperature was measured as area average within the square on the sample. The sample exhibits a homogenous heat distribution throughout the whole heating process. The measured absolute temperature values of the samples might differ slightly from the actual temperature, since the samples are no perfect emitters. However, the heating rate and the increase in temperature are accurate.
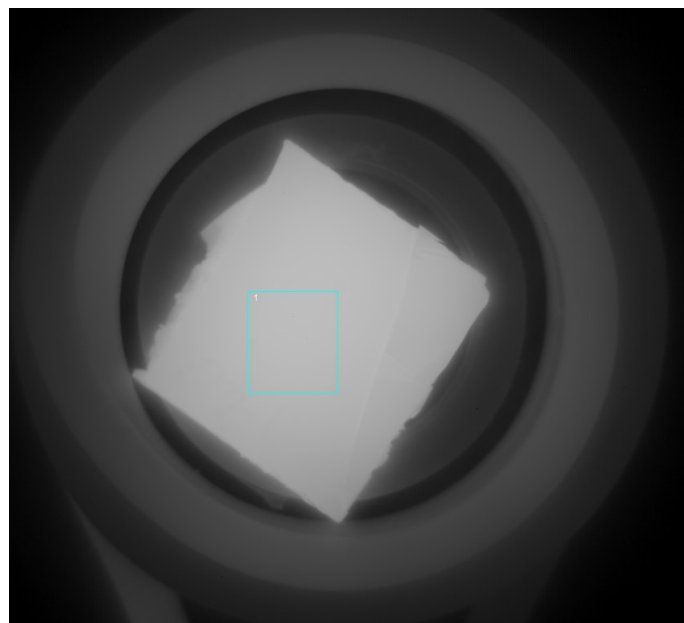
Figure 23: Thermographic image of a Novasil sample containing 30 wt.% NF and 30 wt.% EXP, placed inside the induction coil.

Figure 24 illustrates the influence of NF content on inductive heating as a function of temperature over time for Novasil samples filled with 10 wt.%, 20 wt.% and 30 wt.% NF. Within three seconds the material temperature increased by nearly 15°C with 30 wt.% NF. With filler contents of 10 wt.% and 20 wt.% the temperature rises roughly 5°C and 10°C, respectively. This implies an increase of 5°C per 10 wt.% of NF added to the adhesive.
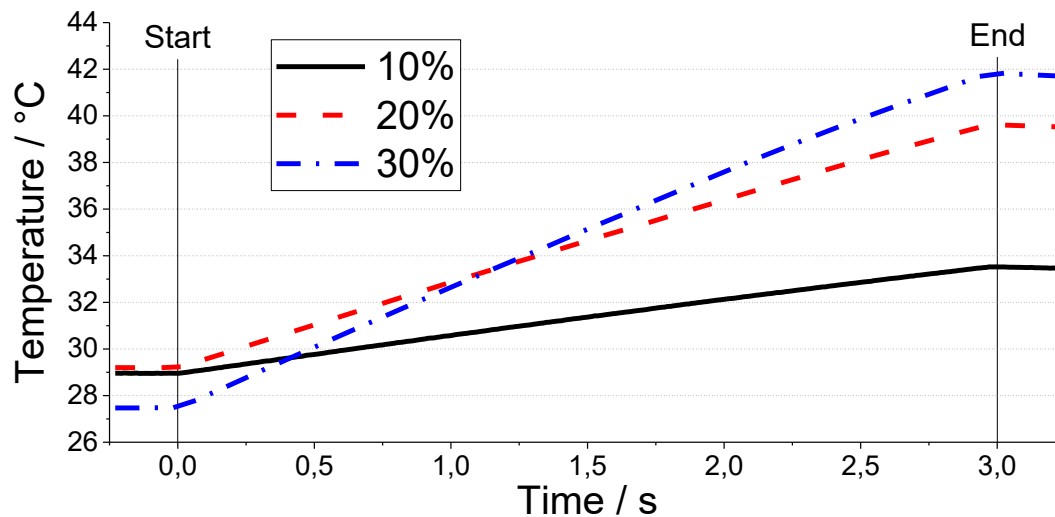
Figure 24: Influence of filler content on inductive heating effectiveness for Novasil samples filled with 10 wt.% (black solid line), 20 wt.% (red dashed line) and 30 wt.% (blue dot dashed line) of NF-filler.

Figure 25 shows the temperature evolvement over time for a sample filled with 30 wt.% NF and 30 wt.% EXP. The temperature shows a nearly linear increase up to 80°C, reaching it within 50 seconds. The gradient then starts to decrease, and the temperature approximates a plateau of about 136°C. This plateau indicates a magnetic saturation of the iron oxide particles. [84] Noticeably, in these experiments a temperature increase of 100°C was obtained within less than 10 min and more than 60°C in 100 s. The temperature of expansion for EXP was reached after 135 s, and the expansion took place for another 135 s. Figure 26 shows the sample before and after expansion. The bond-line thickness was more than doubled by expansion of EXP triggered via inductive heating, and therefore proves that inductive heating is applicable as triggering mechanism for expandable fillers.
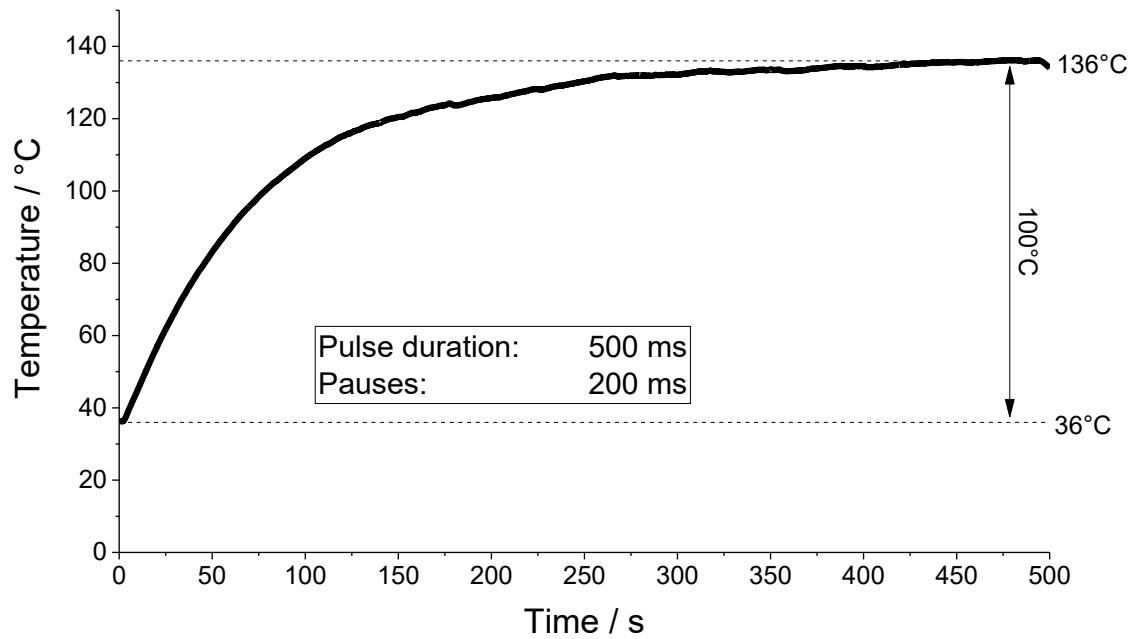
Figure 25: Temperature over time for a Novasil sample containing 30 wt.% NF and 30 wt.% EXP during inductive heating with 180 kHz.

Figure 26: Specimens filled with 30 wt.% NF and 30 wt.% EXP before (left) and after (right) expansion via inductive heating.

When comparing the heating curves of Novasil filled with 30 wt.% NF only and Novasil filled with 30 wt.% NF and 30 wt.% EXP, a large difference in heating rate is noticeable (see Figure 27). Different coils were available for their respective heating, resulting in a frequency of 210 kHz for samples containing only NF and 180 kHz for samples with NF and EXP. At 210 kHz, a temperature difference of 65°C is reached after 27 s, more than twice as fast as for 180 kHz. The results correspond with reports of Bayerl et al., [29] where the maximum heating rates were achieved at 430-450 kHz and temperatures of more than 200°C were reached. This temperature range would suffice to expand EG as well. If and how much EXP influences the inductive heating requires further research.
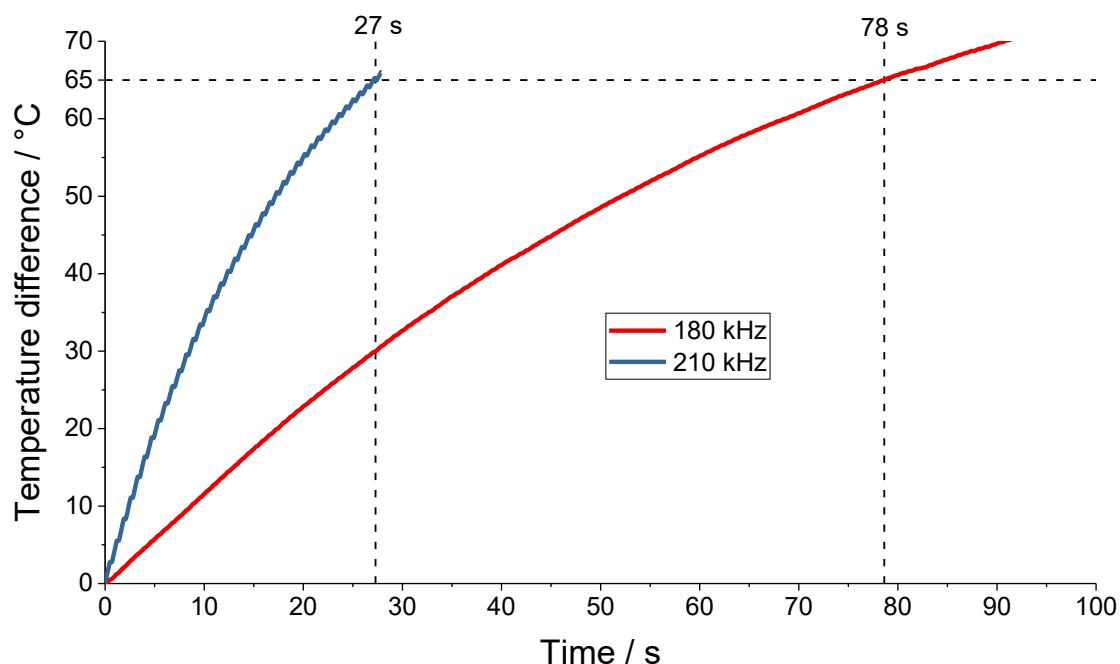
Figure 27: Inductive heating of Novasil samples containing 30 wt.% NF at 210 kHz (blue) and 30 wt.% NF + 30 wt.% EXP (red) at 180 kHz.

The results prove that using inductive heating to trigger thermally expandable fillers is possible within reasonable time and suggests that high heating rates are achievable by optimizing the parameters. In case of a metallic substrate, induction heating can also be used to heat the substrate to a temperature of adhesive failure, in this case more than 300°C. This method was not tested and requires higher temperatures but would allow for disbonding of adhesives without functional fillers.

4.2 Epoxy-anhydride vitrimer

The starting products to achieve a dynamic epoxy-anhydride network were characterised by means of FTIR spectroscopy. Figure 28 shows the FTIR spectrum of DGEBA and its characteristic signals in the mid IR region. The signal at 3056 cm^{-1} can be assigned to the stretching vibration of C-H of the oxirane ring, signals in the region of 2966 cm^{-1} to 2872 cm^{-1} can be accounted to the stretching vibration of aromatic and aliphatic C-H and C-H_2. The stretching vibration of carbon bonds in aromatic rings results in a signal at 1607 cm^{-1} for C=C double bonds and 1507 cm^{-1} for C-C single

bonds. The signals at 1229 cm^{-1} and 1182 cm^{-1} belong to the stretching vibration of C-C-O-C. The signal of the stretching vibration of C-O-C bonds for ethers locates at 1032 cm^{-1}. The signal at 914 cm^{-1} belongs to the stretching vibration of the C-O bonds in the oxirane ring, with another signal at 826 cm^{-1} for the C-O-C stretching vibration. At 770 cm^{-1} is the characteristic peak for the rocking vibration of C-H$_2$. [85,86]
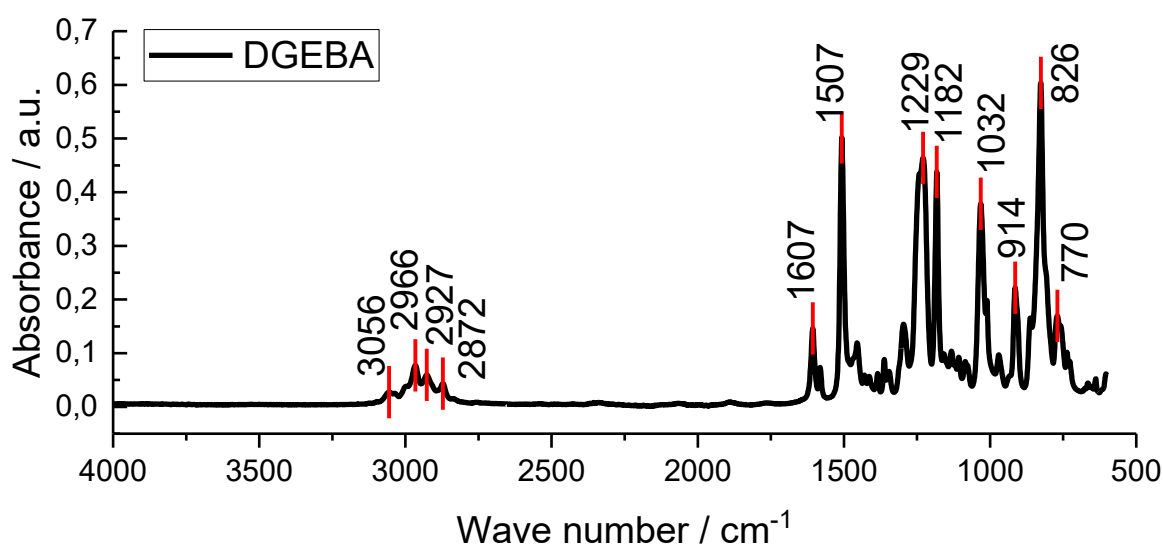
Figure 28: FTIR spectrum of DGEBA.

Figure 29 contains the FTIR spectrum of MHHPA and its characteristic signals in the mid IR region. Signals in the region 2953 cm^{-1} to 2871 cm^{-1} can be assigned to the stretching vibration of C-H, C-H$_2$ and C-H$_3$. The signal at 1776 cm^{-1} can be accounted to the stretching vibration of the C=O bonds. The stretching vibration of the C-C bonds results in a signal at 1109 cm^{-1}. The signal at 892 cm^{-1} belongs to the deformation vibration of the C=O bonds. [87,88]
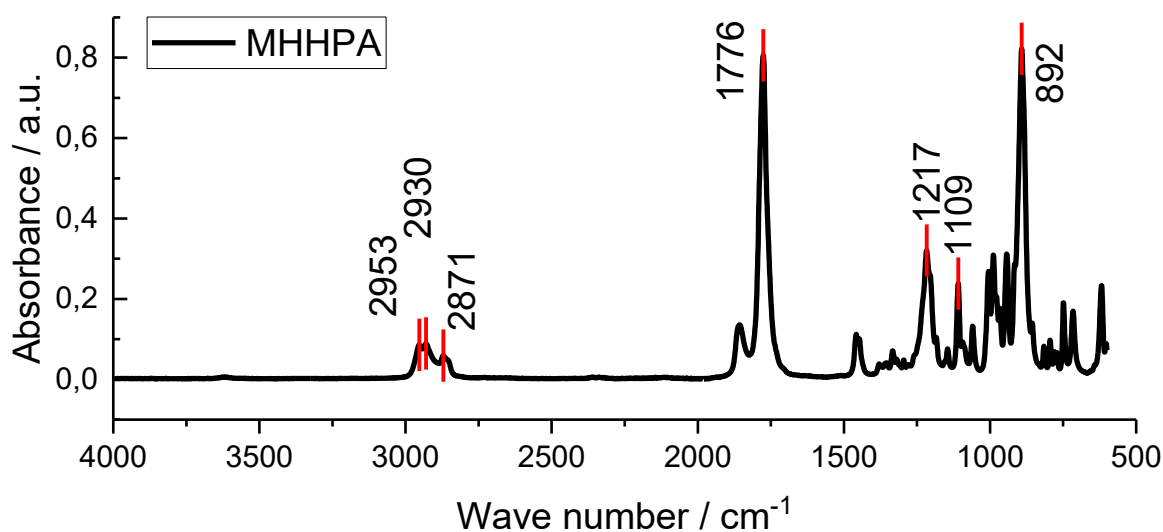
Figure 29: FTIR spectrum of MHHPA.

Figure 30 contains the FTIR spectrum of epoxidized PDMS and its characteristic signals. The signal at 2960 cm^{-1} belongs to the stretching vibration of C-H$_3$. The signal at 2871 cm^{-1} can be assigned to the stretching vibration of C-H and C-H$_2$. At 1257 cm^{-1} locates the signal for the deformation vibration of C-H$_3$. The signals at 1077 cm^{-1} and 1013 cm^{-1} can be accounted to the stretching vibration of Si-O-Si. The stretching vibration of C-O in the oxirane ring results in a signal at 911 cm^{-1}. The signal at 789 cm^{-1} belongs to the rocking vibration of C-H$_3$ and the stretching vibration of Si-C. [89,90]
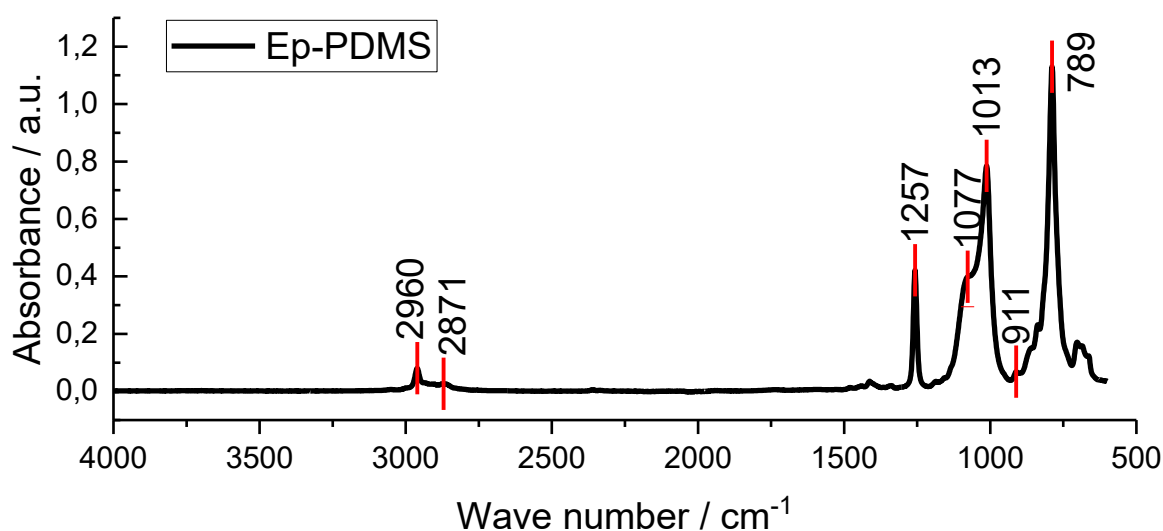
Figure 30: FTIR spectrum of epoxidized PDMS.

Figure 31 contains the FTIR spectrum of SA-PDMS and its characteristic signals. The signal at 2961 cm^{-1} belongs to the stretching vibration of C-H$_3$. The signals at 2905 cm^{-1} and 2866 cm^{-1} can be assigned to the stretching vibration of C-H and C-H$_2$. The stretching vibration of C=O results in a signal at 1783 cm^{-1}. The stretching vibration of C-O in the anhydride ring locates at 912 cm^{-1}. The signal at 790 cm^{-1} can be accounted to the rocking vibration of C-H$_3$ and the stretching vibration of Si-C. [76,89]
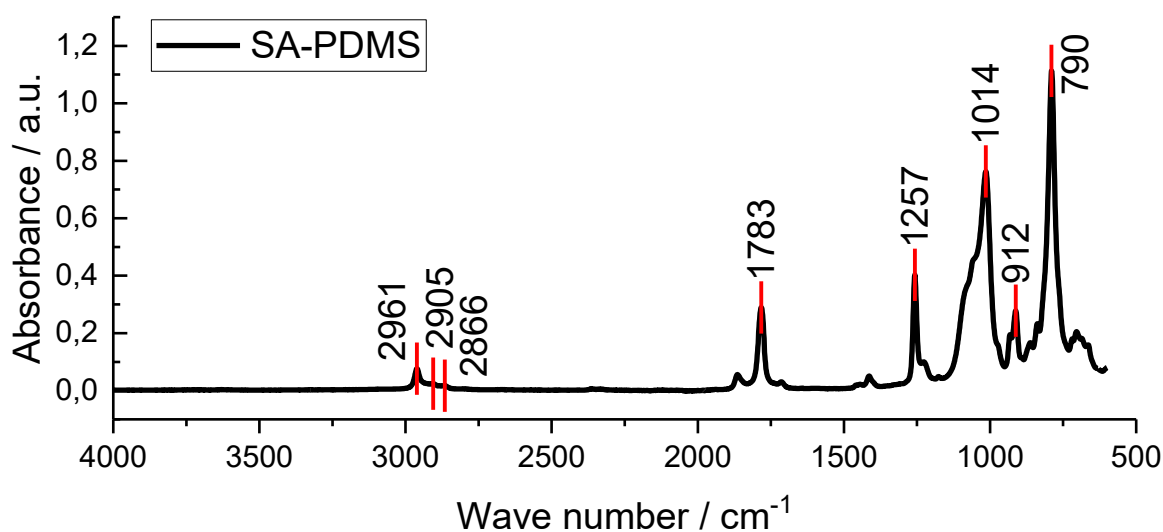
Figure 31: FTIR spectrum of SA-PDMS.

4.2.1 Curing of epoxy-anhydride networks

Figure 33, Figure 35 and Figure 37 show the infrared spectra of the cured and uncured samples (A), consisting of DGEBA/SA-PDMS (see Figure 33), Ep-PDMS/MHHPA (see Figure 35) and Ep-PDMS/SA-PDMS (see Figure 37), as well as a detailed image of the appearance of a broad signal in the range of 3000 cm^{-1} to 3650 cm^{-1}, which can be assigned to hydroxyl groups (B), the shift of anhydride C=O stretching signals to lower wave numbers accounting for ester linkages (C) and the consumption of the epoxide groups based on the decrease of the signal for C-O stretching of the oxirane ring (D). The individual spectra are normalized for better comparison. Figure 32 schematically illustrates the curing reaction of DGEBA with SA-PDMS in a molar ratio of 2:1, resulting in a crosslinked network with beta hydroxyl ester linkages. The curing of Ep-PDMS with

SA-PDMS runs analogously. MHHPA only contains one anhydride functional group that can react with Ep-PDMS, and therefore a molar ratio of Ep-PDMS to MHHPA of 1:1 is required.
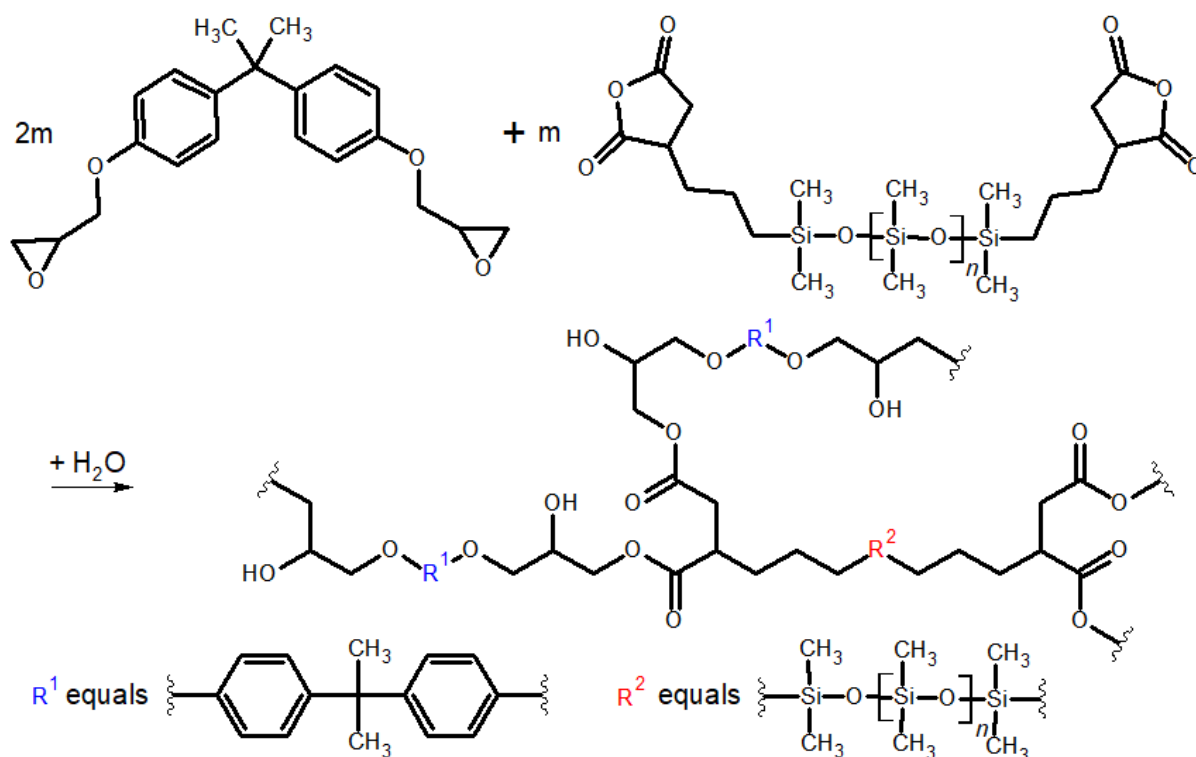

Figure 32: Schematic illustration of the curing reaction of DGEBA with SA-PDMS in a molar ratio of 2:1.

DGEBA cured with SA-PDMS in the presence of 10 mol% $Zn(AcAc)_2$ results in a hard and brittle thermoset, which cannot be stretched by hand. The FTIR spectrum (see Figure 32) confirms complete curing at 120°C overnight and the existence of ester and hydroxyl groups in the network. After reprocessing the material for 1 h at 180°C, the material fragments adhered to each other, but grain boundaries were still visible (see Figure 34) and mechanical separation along the interfaces was possible. However, this might be due to insufficient contact of the hard particles and does not necessarily mean that the transesterification rate is low. This was not investigated any further, since a thermoset material is not suitable for the application in the PV module.
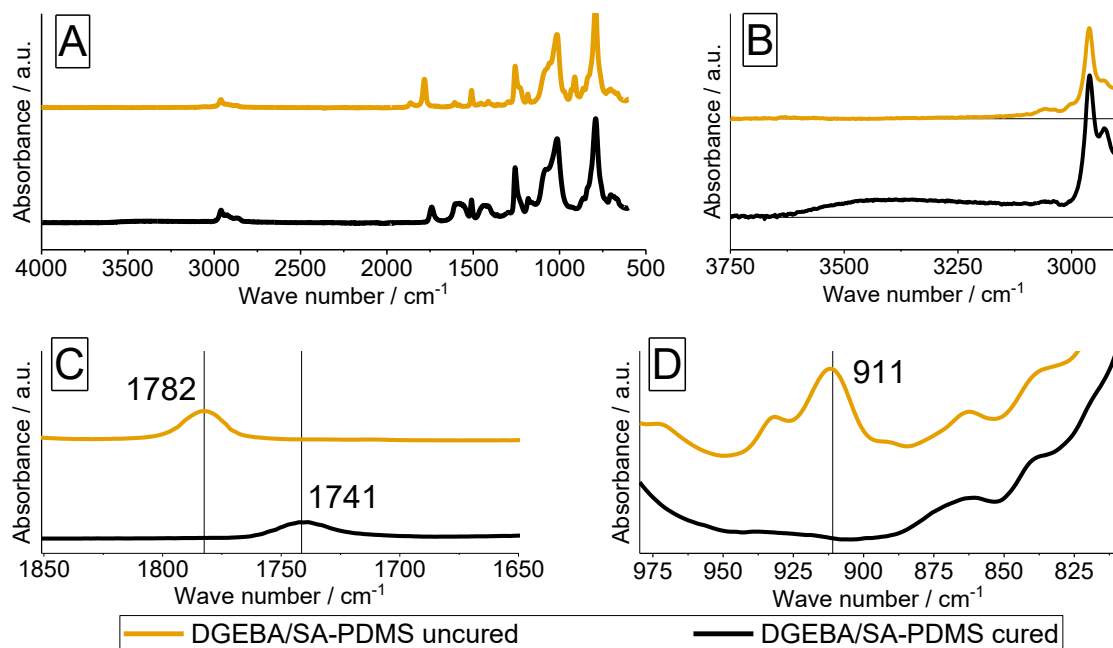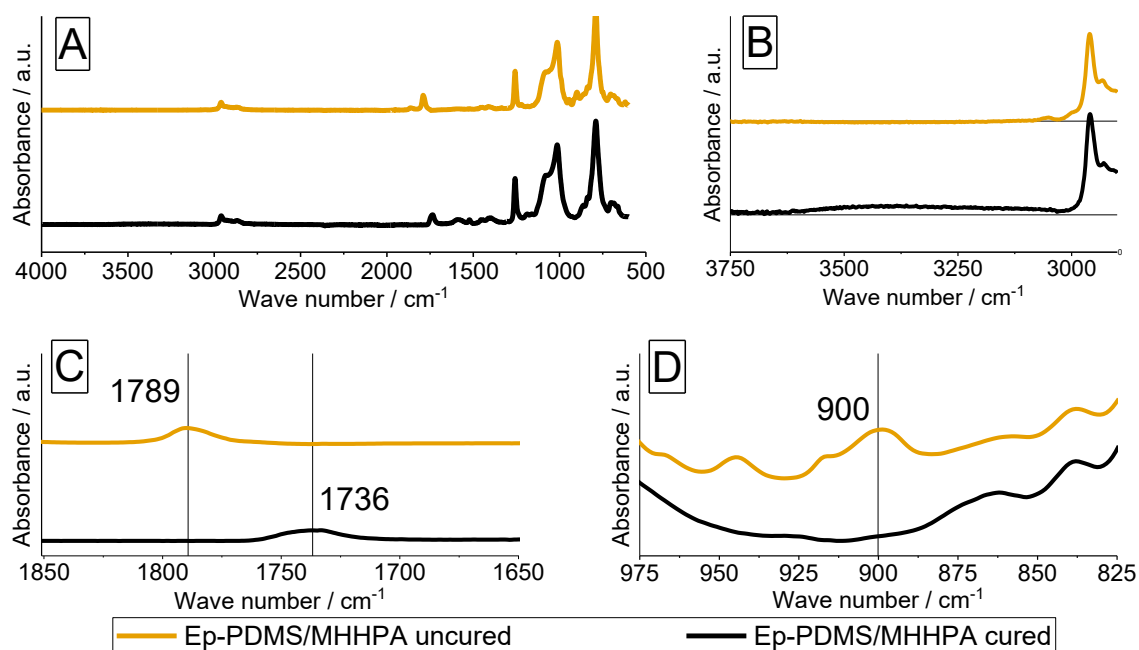
Figure 33: FTIR spectrum of uncured and cured DGEBA with SA-PDMS and 10 mol% Zn(AcAc)$_2$ (A), generation of hydroxyl groups (B), shift of C=O peak (formation of ester groups) (C) and consumption of epoxide groups (D) after curing at 120°C overnight.

Figure 34: DGEBA cured with SA-PDMS, catalysed by 10 mol% Zn(AcAc)$_2$ after reprocessing for 5 h at 160°C.

Curing Ep-PDMS with MHHPA catalysed by 10 mol% Zn(AcAc)$_2$ at 120°C overnight produces a soft, elastomer-like network. The establishment of the vitrimeric network is confirmed by the means of FTIR spectroscopy (see Figure 35). Despite the

elastomeric appearance, the material tolerates only small deformations until failure with very low fracture toughness. Reprocessing was possible at 180°C for 1 h (see Figure 36, left) with no visible grain boundaries, but slightly rough interfaces after breaking the reprocessed sample. Whether or not the roughness comes from breaking the samples or insufficient reprocessability was not examined, because the Ep-PDMS cured with SA-PDMS resulted in a similar material and MHHPA is not a preferable curing agent since it is included in the candidate list of substances of very high concern. [91]

Figure 35: FTIR spectrum of uncured and cured Ep-PDMS with MHHPA and 10 mol% Zn(AcAc)$_2$ (A), generation of hydroxyl groups (B), shift of C=O peak (formation of ester groups) (C) and consumption of epoxide groups (D) after curing at 120°C overnight.

Figure 36: Ep-PDMS cured with MHHPA (left) and SA-PDMS (right) with 10 mol% Zn(AcAc)$_2$ and reprocessed at 180°C for 1 h.

The fully PDMS-based sample, achieved through curing Ep-PDMS with SA-PDMS in the presence of 10 mol% Zn(AcAc)$_2$ at 120°C overnight, exhibits similar properties compared to Ep-PDMS with MHHPA: Elastomeric, but only small deformations are possible before failure. The FTIR spectrum in Figure 37 confirms complete curing and the formation of the vitrimeric network. The system is fully reprocessable at 180°C for 1 h, without any visible grain boundaries or defects in the interfaces after breaking the sample (see Figure 36, right).
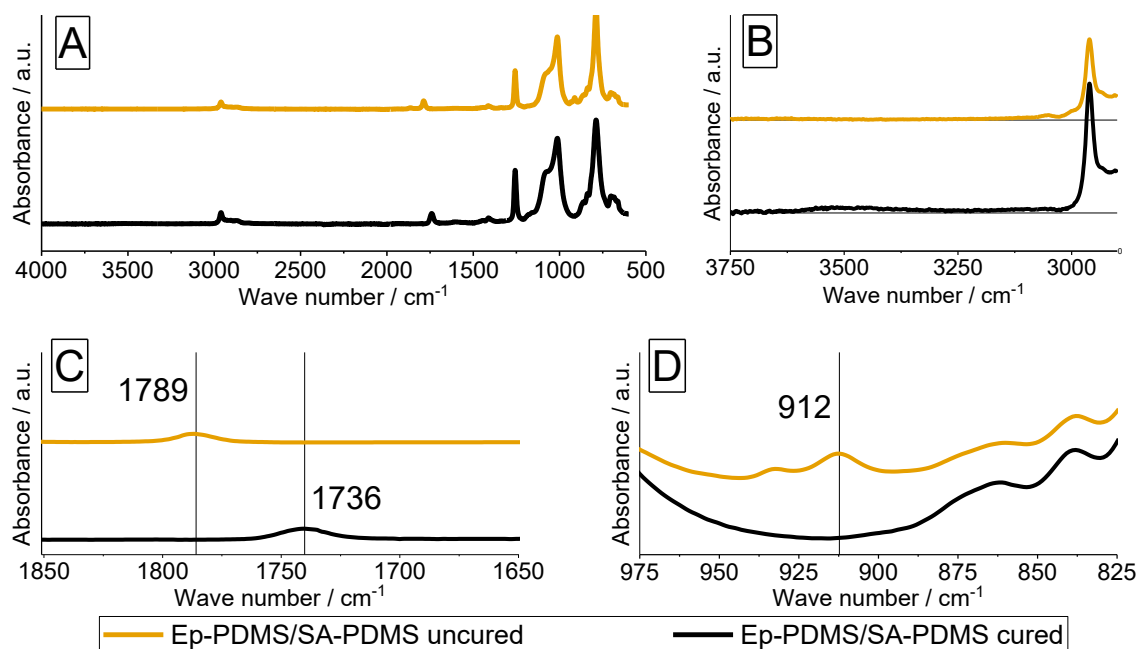
Figure 37: FTIR spectrum of uncured and cured Ep-PDMS with SA-PDMS (A), generation of hydroxyl groups (B), shift of C=O peak (formation of ester groups) (C) and consumption of epoxide groups (D) after curing at 120°C overnight.

4.2.2 Evaluation of catalysts for epoxy-anhydride systems

With the goal to increase elongation and flexibility while maintaining the reprocessability of the vitrimeric network Ep-PDMS was crosslinked with SA-PDMS and various catalysts were tested with the formulation. Complete conversion of epoxide groups and carboxyl groups as well as the formation of hydroxyl groups were confirmed via FTIR spectroscopy after curing at 120°C overnight (see Figure 37). A qualitative comparison of the samples indicates that the catalysts influence the elongation and fracture toughness of the material. BA in a ratio of 0.2 mol to Ep-PDMS as well as TBD in a concentration of 20 mol% to the epoxy groups allowed full reprocessability, resulting in an interface as seen in Figure 36 (right), and a slightly increased elongation of the material was observed. A ratio of 0.4 mol DBA to Ep-PDMS and a concentration of 20 mol% DBN to the epoxy groups resulted in full reprocessability as well but did not increase the elongation of the material at all. 10 mol% TBD and DBN to the epoxy groups showed insufficient reprocessability (see Figure 38). In general, the material still exhibits rather low toughness and only tolerates small deformations. An increase in elongation and toughness could most likely be achieved by increasing the molecular weight, and therefore the chain length of the PDMS precursors.

Figure 38: Ep-PDMS cured with SA-PDMS and reprocessed at 180°C for 1 h.

4.3 Epoxy-acid vitrimer

To achieve a material with higher flexibility, Pripol was used as curing agent for Ep-PDMS. Pripol was characterised by the means of FTIR spectroscopy, illustrated in Figure 39. The broad absorption band between 3500 cm^{-1} and 2500 cm^{-1} can be assigned to the stretching vibration of O-H. The signals at 2922 cm^{-1} and 2852 cm^{-1}

can be accounted to the stretching vibration of $C-H_2$ and $C-H_3$. The signal at 1706 cm^{-1} can be attributed to the stretching band of the C=O groups. At 1457 cm^{-1} locates the signal of the deformation vibration of $C-H_2$. The signal at 1412 cm^{-1} belongs to the stretching of C-O and deformation of O-H. The signals at 1283 cm^{-1} and 1236 cm^{-1} can be assigned to the stretching vibration of C-O. The deformation vibration O-H absorbs at 935 cm^{-1} and the deformation of $(C-H_2)_n$ at 723 cm^{-1}. [67]
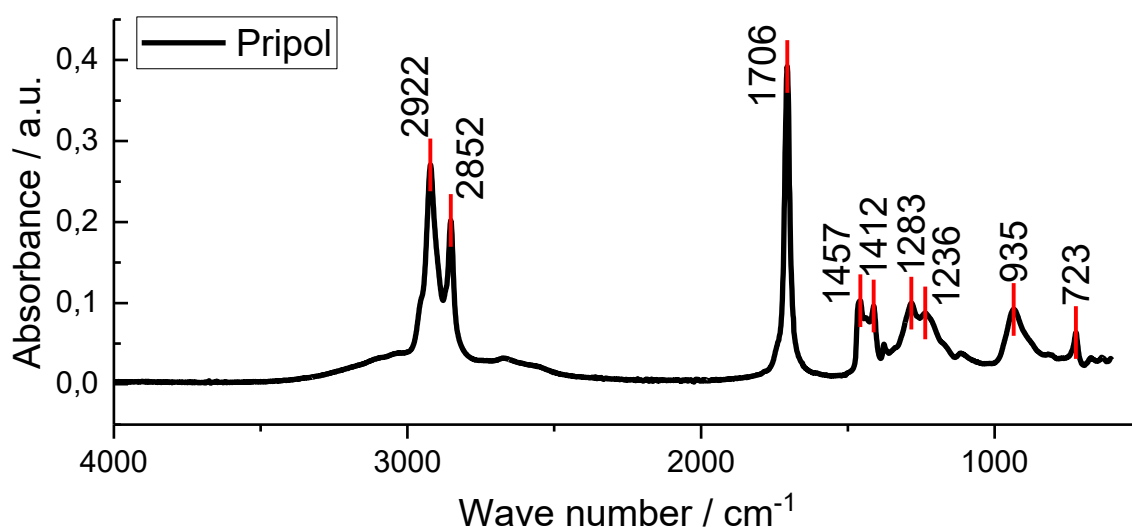
Figure 39: FTIR spectrum of Pripol 1040.

4.3.1 Curing of epoxy-acid networks

Figure 40 shows the infrared spectrum of the partially cured and fully cured Ep-PDMS with Pripol and covalently bonded BA in a molar ratio of 0.2 to Ep-PDMS as a catalyst (A) as well as a detailed image of the appearance of a broad hydroxyl signal in the range of 3000 cm^{-1} to 3650 cm^{-1} (B), the shift of carbonyl signal (carboxyl acid groups are converted to ester moieties) to higher wave numbers (C) and the consumption of the epoxide groups (D) after curing at 120°C overnight. The infrared spectra of the samples with DBA in molar ratio of 0.4 to Ep-PDMS as catalyst are congruent with the measured spectra with BA as a catalyst and are therefore not illustrated separately.

Since the polymeric network has been partially cured for approximately 2 h at 150°C to improve the handling, an ester signal is present in both spectra and the epoxide signal has a lower intensity compared to pristine Ep-PDMS. For the same reason signals

for hydroxyl groups are present in both spectra as well. In addition, Pripol contains hydroxyl groups inherently. The broad signal for O-H stretching increases in intensity and shifts towards higher wave numbers. The signal for C=O stretching of carboxyl groups at 1710 cm^{-1} and the small epoxide signal at 911 cm^{-1} deplete, while the signal for C=O stretching of ester groups at 1740 cm^{-1} increases in intensity.

After curing at 120°C overnight, the samples show rubber like properties and exhibit a comparably high elasticity, determined by qualitative comparison of the produced samples with the anhydride cured systems, considering that no fillers or other reinforcements were used. The fracture toughness is still rather low, compared to the reference silicone rubber but it is significantly higher than for the anhydride cured networks. Qualitatively, no difference between the samples using DBA and BA was observed. Both achieved complete reprocessability (see Figure 41). The interface exhibits a certain roughness, but no visible signs of degradation could be observed, and the reprocessed samples seem to have very similar properties to the virgin material. Altuna et al. postulated that DBA allows for faster reshaping due to less steric hindrance, while BA provides a slightly higher strength due to the extra crosslinking sites. [73] Therefore, the use of BA might have a favourable effect on creep behaviour in long-term use and it was chosen for further tests. While it achieved complete reprocessability with no degradation for all tested parameters, 5 h at 160°C was chosen to be the safest option in terms of full reprocessability and avoidance of degradation.
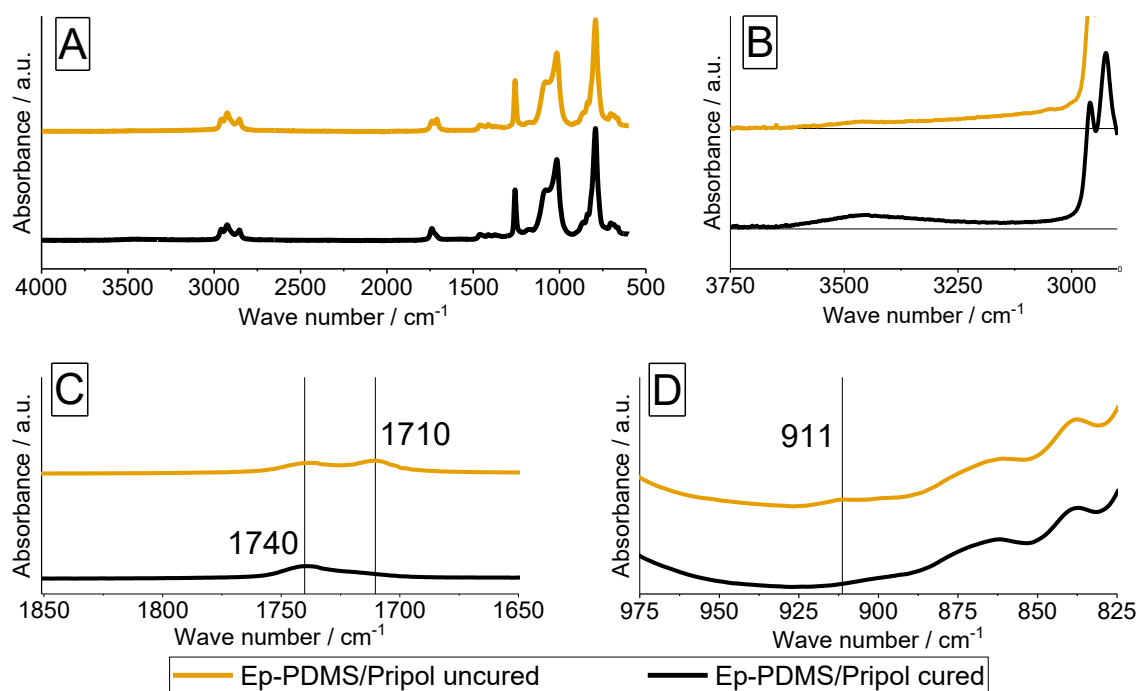
Figure 40: FTIR spectrum of uncured and cured Ep-PDMS with Pripol and 0.2 mol BA (A), generation of hydroxyl groups (B), shift of C=O peak (formation of ester groups) (C) and consumption of epoxide groups (D) after curing at 120°C overnight.

Figure 41: Ep-PDMS cured with Pripol and reprocessed at 160°C for 5 h.

Figure 42 shows the cure kinetics of Ep-PDMS with Pripol and BA by FTIR spectroscopy, determined by the shift of the carbonyl signal from conversion of the carboxyl acid groups to ester moieties. There is no initiation period visible due to the necessary pre-crosslinking of the system. Therefore, the typical S-shape of a conversion curve does

not appear as the material is already at the state of maximum conversion rate. The data point after a duration of 700 min is assumed as 100 % conversion, but the percentage for the intermediate measurement points could not be determined.
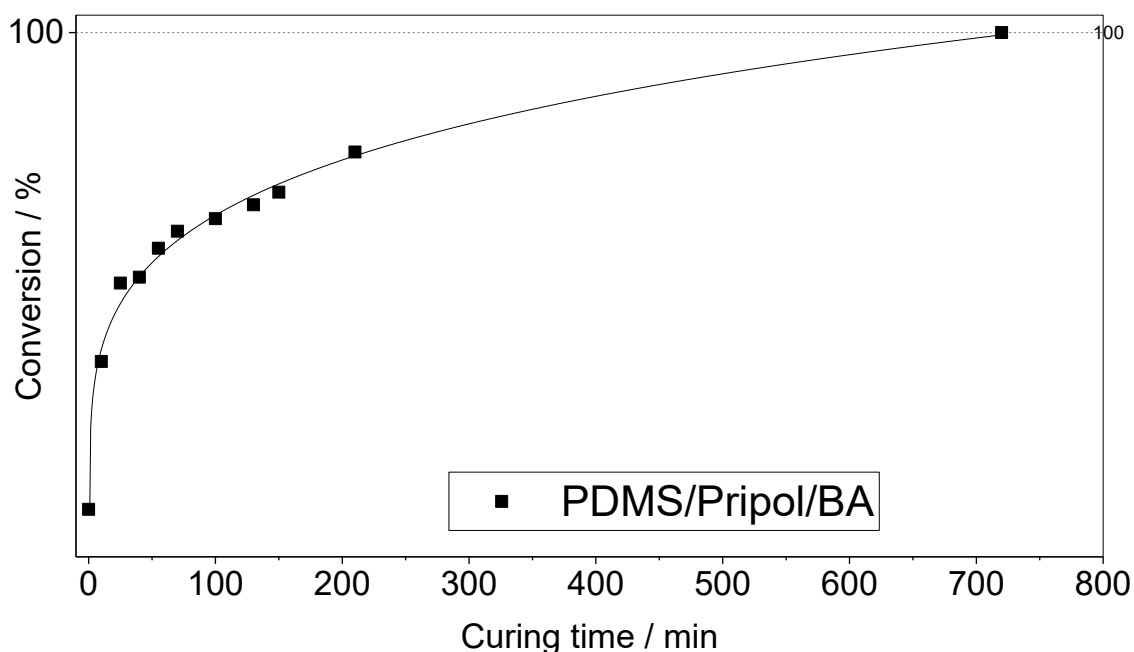
Figure 42: Conversion of carboxyl groups to ester moieties of Ep-PDMS/Pripol/BA determined by the shift of the carbonyl signal over curing time at 120°C.

Figure 43 contains the DSC graph of samples with BA as catalyst. The curve of the second heating was shifted by -4 W/g to improve visibility. The exothermic peak of the crosslinking reaction is rather small due to the necessary pre-crosslinking during sample preparation. No remaining endothermal or exothermal peaks appear during cooling and the second heating, confirming that the material is indeed fully crosslinked. There is a slight indication that the glass transition ranges around -50°C but an evaluation at low temperatures is not possible due to limited cooling range for the used calorimeter. The first and second heating curves further suggest that the materials are thermally stable in the tested temperature range for short-term exposure.
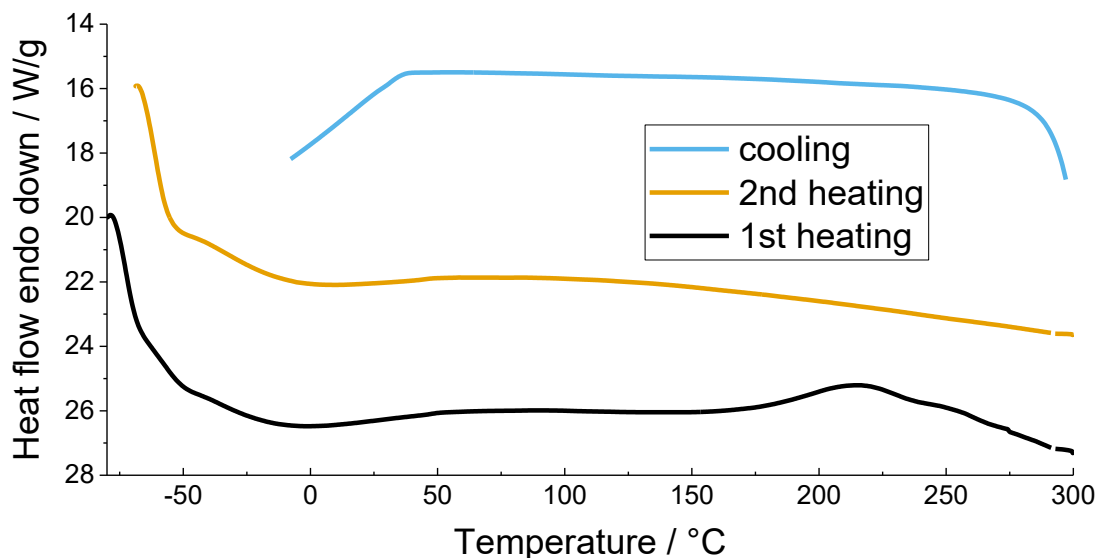
Figure 43: DSC graph of Ep-PDMS cured with Pripol and BA as catalyst.

Figure 44 shows a comparison of the FTIR spectra for pristine Ep-PDMS, Ep-PDMS reacted with TMHMDA, cured and uncured Ep-PDMS with Pripol and TMHMDA as catalyst. The pre-crosslinking of Ep-PDMS with TMHMDA is clearly visible by the generation of hydroxyl peaks (B) and could also be qualitatively observed by an increase in viscosity. The epoxy peak at 911 cm^{-1} decreases slightly during the reaction (D). The addition of Pripol gives rise to a C=O peak (carboxylic acid groups) that shifts due to the formation of ester moieties during curing (C).

TMHMDA seems to be a very effective catalyst for the curing reaction as the pre-reacted Ep-PDMS was easily mixed with Pripol at room temperature, creating a homogenous mixture without phase separation. While this was not possible with DBA or BA even at higher concentration, it could also be due to the increased viscosity of Ep-PDMS with TMHMDA. The cured material exhibits increased hardness and more brittle behaviour compared to the samples with BA and DBA as catalyst in a qualitative comparison, which probably derives from the higher number of crosslinks. A certain amount of crosslinks are permanent amine crosslinks due to the reaction of Ep-PDMS with TMHMDA. One TMHMDA molecule can react with up to 4 epoxide groups, which decreases the average distance between crosslinks and consequently, the elastic behaviour of the material. Reshaping is possible, but a few grain boundaries were still

visible afterwards. A decrease in TMHMDA content could possibly increase the elongation and reprocessability of the system by decreasing the permanent crosslinks and increasing dynamic bonds. Li et al. report on a full reprocessability of dynamic networks with 40 mol% permanent crosslinks. [53] An additional investigation on the influence of permanent crosslinks on dynamic networks has not been performed in this study and is a matter of future research activities. Nonetheless, the results indicate that conventional amine hardeners can be implemented as transesterification catalysts. The use of covalently bonded catalysts enables the application of vitrimeric materials in long-term instalments by decreasing the risk of catalyst migration or leaching.
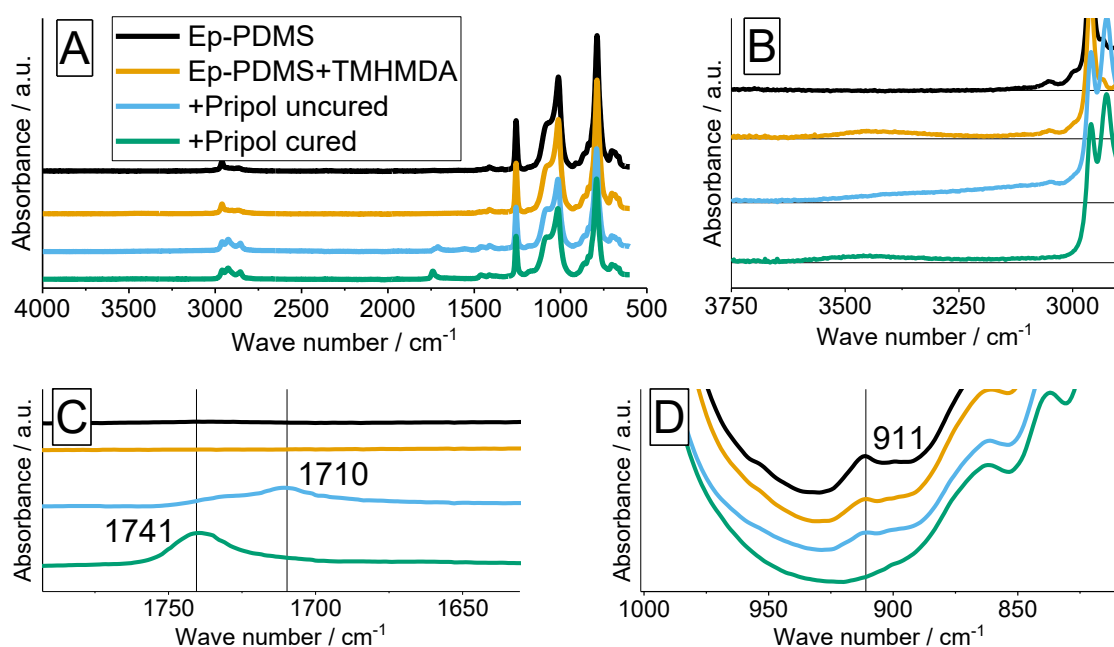
Figure 44: FTIR spectrum of Ep-PDMS, Ep-PDMS reacted with TMHMDA at 60°C overnight, and uncured and cured (120°C overnight) mixture thereof with Pripol (A), generation of hydroxyl groups (B), shift of C=O peak (formation of ester groups) (C) and consumption of epoxide groups (D).

Figure 45: Ep-PDMS cured with Pripol with TMHMDA as catalyst and reprocessed at 160°C for 5 h.

4.3.2 Evaluation of the covalent attachment of *n*-butylamine to Ep-PDMS

A comparison of FTIR spectra of Ep-PDMS before and after the reaction with *n*-butylamine did not reveal significant changes in the characteristic regions for amine and hydroxyl moieties or a strong decrease of the signal for epoxide groups, which could confirm the covalent bonding of the catalyst to Ep-PDMS. This observation can be explained by the fact that the epoxide groups were only partially reacted with a molar ratio of 0,1 mol BA per mol of epoxy groups with a further reduction of the conversion due to non-optimized reaction conditions, leading to partial evaporation of unreacted *n*-butylamine. It is expected that these reaction conditions lead to a comparably low conversion for the respective sample, lying below the detection limit for FTIR spectroscopy.

However, it has been noted that without implementing catalyst, the mixture of Ep-PDMS and Pripol could not be brought to a homogenous solution, even after 7.5 h at 150°C on a magnetic stirrer.

Therefore, in order to determine whether the catalyst is covalently bonded to Ep-PDMS, Soxhlet extraction was performed in addition to an investigation of the material after reaction by means of ^{13}C-NMR spectroscopy.

The target of the Soxhlet extraction was to confirm that the catalyst cannot be leached out of the polymer matrix, and therefore a transesterification is still possible after extraction. The Soxhlet experiment resulted in a weight loss of 5 wt.% after the extraction. The comparably high weight loss is accounted to a high amount of low molecular weight components such as cyclic siloxanes in the crosslinked polysiloxane.

Nonetheless, the sample did not show strong signs of degradation and only exhibited slight embrittlement by a qualitative test, which may be accounted to the removal of the low molecular weight components. Furthermore, reprocessing tests were successful after the Soxhlet extraction, suggesting that the catalyst cannot be leached.

Figure 46 shows the 13C-NMR spectrum of Ep-PDMS, with characteristic signals of the respective carbon atoms (a-g) assigned to the chemical structure as depicted in the graph. The signals for the epoxide rings appear at 44,35 ppm (a) and 50,85 ppm (b), respectively. The solvent peak for CDCl3 is observed at 76,98 ppm.

After the reaction of Ep-PDMS with BA, a number of additional signals appear in the spectra as shown in Figure 47. Most notably, new signals are detected at 68,82 ppm (i) and 65,40 ppm (h) which are likely due to the carbon atoms in alpha position of the tertiary amine and suggest that BA is indeed covalently bonded. Due to the fact that Ep-PDMS was only partially reacted with BA, the peaks from the epoxide rings of Ep-PDMS are still present at 44,35 ppm (a) and 50,86 ppm (b). The signals in the range of 20 ppm to 35 ppm were not assigned in detail due to the fact that the formation of side products could not be excluded. Nonetheless, the peaks in this range also indicate the presence of aliphatic CH2 groups of the bonded catalyst. The absence of characteristic signals of the alpha carbon of *n*-butylamine at 41,66 ppm further suggests that no residual BA is present. The 13C-NMR spectrum of BA is shown in Figure 48 as a reference.

At the current point in time, it cannot be excluded that the formation of side products occurred and that further etherification reactions between the hydroxyl groups and remaining epoxy groups took place at the chosen reaction conditions. At the time of writing, the detailed evaluation and assignment of the reaction products is still ongoing and a matter of further research.

Nevertheless, the combination of the performed Soxhlet extraction with successful reprocessing tests and the results from 13C-NMR spectroscopy indicate that the reaction of Ep-PDMS with BA was successful, and the catalyst is indeed covalently bonded.
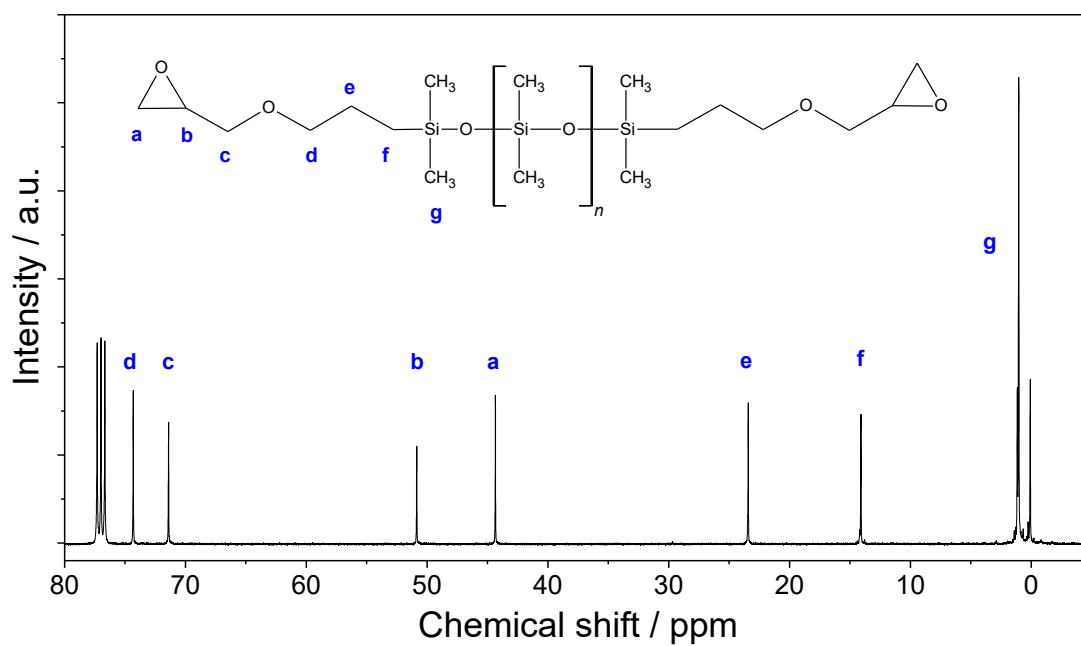
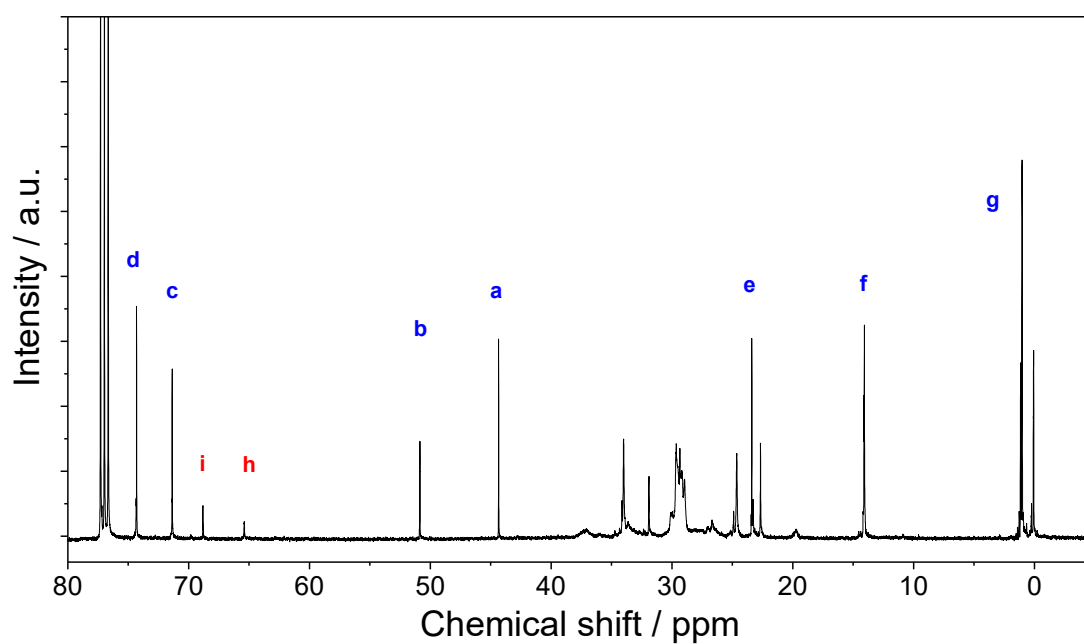**Figure 46: ^{13}C-NMR spectrum of Ep-PDMS.**

Figure 47: ^{13}C-NMR spectrum of Ep-PDMS after reaction with BA in a molar ratio of 5:1.
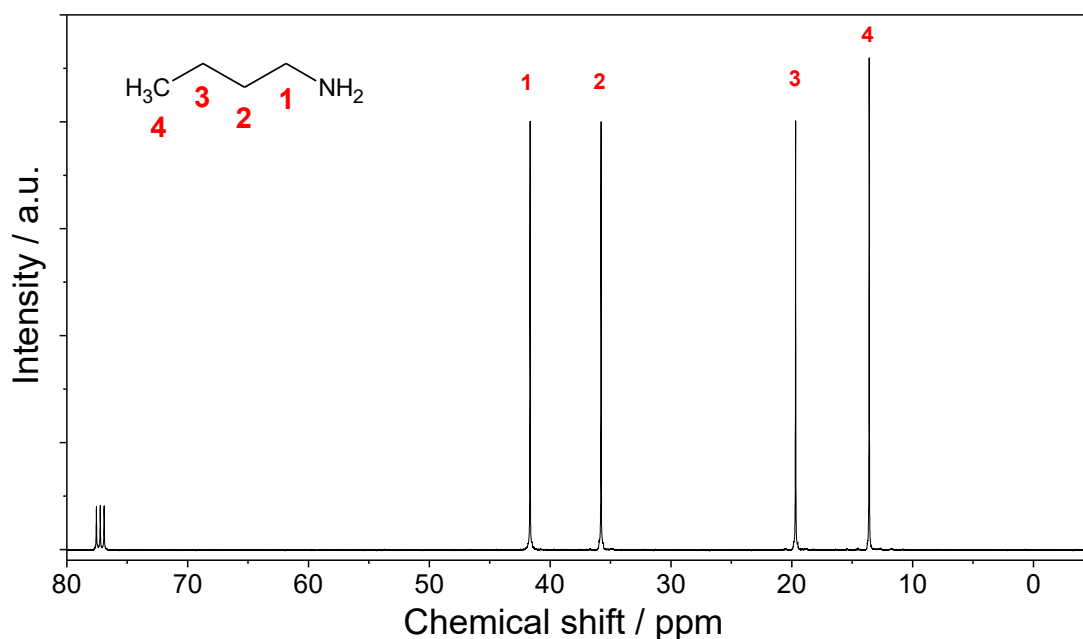
Figure 48: ^{13}C-NMR spectrum of *n*-butylamine.

4.3.3 Tensile tests

Tensile tests on samples of Ep-PDMS cured with Pripol and BA as covalently bonded catalyst were performed to determine the mechanical properties of cured samples before and after reprocessing.

Figure 49 shows the results of the tensile tests done on the virgin and reprocessed vitrimer. The virgin material achieved an average of 40 % elongation at break, 0.40 MPa stress at break with a tensile modulus of 0.84 MPa. After reprocessing the samples in the hot-press at 160°C for 5 h, the test results show an average of 19 % elongation at break, 0.35 MPa stress at break and a tensile modulus of 1.56 MPa. While the maximum elongation decreases by half, the maximum stress only decreases slightly. A comparison of FTIR spectra before and after reprocessing showed no signs of thermo-oxidative degradation. The reference adhesive Novasil exhibits a stress at break of 2-3 MPa and 200-500 % elongation at break according to its technical datasheet. Without any reinforcing fillers the produced vitrimeric elastomer reaches approximately one fifth of the properties of Novasil, when compared to the lower

values. It is expected that with an implementation of filler components and tailoring of the formulation, the achieved mechanical properties can still be improved, since silicone rubbers are known to have low tensile strengths when unreinforced. [92]
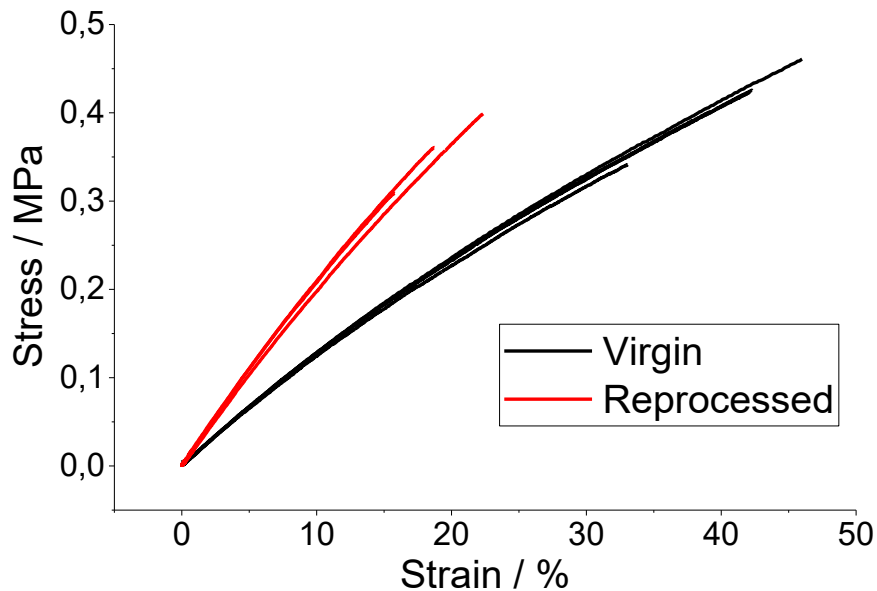
Figure 49: Stress-strain curves of virgin and reprocessed vitrimeric elastomers.

The material exhibits stiffer behaviour after reprocessing, represented by an increase of tensile modulus by approximately 85 %, which might be due to residual stresses as the reprocessing was done under pressure, while the original casting process did not involve any external pressure. It is expected that tempering the samples after reprocessing can potentially increase the maximum elongation by allowing a relaxation of the residual stresses.

Another possible improvement of the material properties after reshaping could be done by the process itself. The reprocessing was done using a hot-press with distance holders where the grinded material was poured in the middle, piling up to a cone. The amount of material was too low to completely fill the volume between the distance holders. Therefore, the pressure was only applied vertically and not in-plane, which might also decrease the material properties after reprocessing. The use of dipping edges in the hot-press would allow pressure from all sides to ensure better contact in-plane.

4.3.4 Creep tests

Figure 50 illustrates the results of the creep or dilatometry tests for samples with BA and DBA. The sample using DBA exhibits a vitrification temperature of 93°C, tested at a load of 20 kPa. BA was determined with a load of 20 kPa and 40 kPa as well, to increase the visibility of the transition from elastic solid to viscoelastic liquid. The evaluated vitrification temperatures are at 141°C for 20 kPa and 125°C for 40 kPa. Due to the increased rise of the slope at 40 kPa, the evaluation is more accurate and 125°C is further considered to reflect the vitrification temperature of the sample containing BA more precisely. The results confirm that DBA has a higher effectiveness as a transesterification catalyst. However, for a potential application in photovoltaic modules, the vitrification temperature should not be below 100°C to avoid creep as much as possible. Below the vitrification temperature, the slopes of the elongation curves are almost parallel for both samples, indicating similar behaviour.
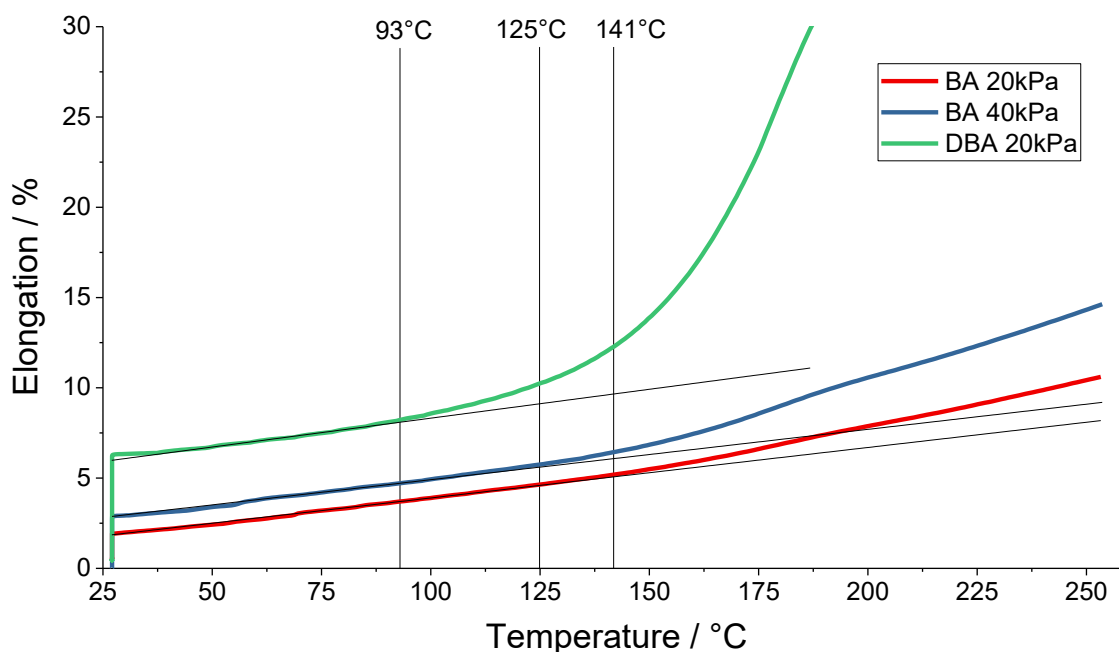
Figure 50: Elongation of Ep-PDMS/Pripol with BA and DBA versus temperature.

4.4 Lap Shear tests

4.4.1 Evaluation of aging and weathering resistance

Accelerated aging tests were performed in order to evaluate the stability of the developed material systems and to assess their applicability for photovoltaic modules. The climate cycle test did not influence the FTIR spectra or the functionality of the tested samples after 50 cycles from -40°C to 85°C. The pure Novasil samples as well as the ones filled with expandable graphite did not show changes after 2000 h in the damp heat chamber at 85°C and 85 % relative humidity. However, the thermally expandable microspheres and the vitrimeric samples showed strong signs of degradation. The EXP-filled samples could not be expanded anymore after the exposure to damp heat. It could not be determined if the blowing agent inside the microspheres migrated or if the thermoplastic shell collapsed.

The vitrimeric samples showed a strong hydrolytic degradation and completely de-crosslinked, visible in the FTIR spectra as well as due to significant changes in the physical appearance, which changes from a brown, elastomeric solid to a viscous dark brown liquid. Figure 51 shows the FTIR spectrum of the vitrimeric samples before and after the damp heat test. The appearance of a new signal at 1710 cm^{-1}, which can be assigned to C=O of carboxyl groups as well as the increase of the signal for hydroxyl groups between 3000 cm^{-1} and 3600 cm^{-1} are accounted to hydrolytic degradation. Therefore, the vitrimeric samples could not be tested mechanically after damp heat tests. Quenching the functional groups of the transesterification or the addition of stabilizing additives might be possible to improve the weathering resistance of the vitrimeric elastomer
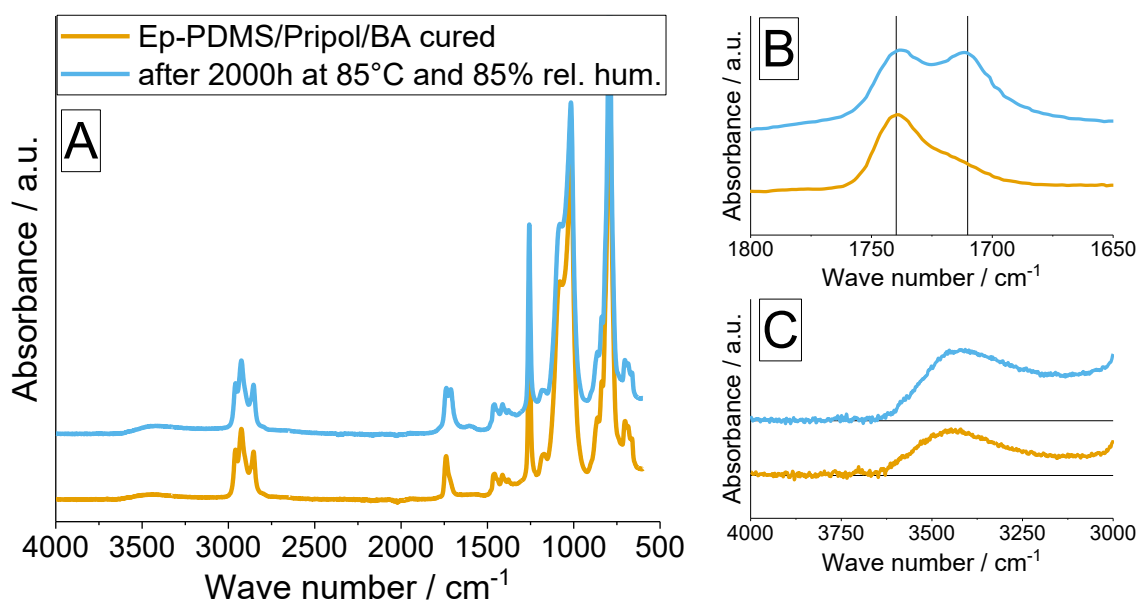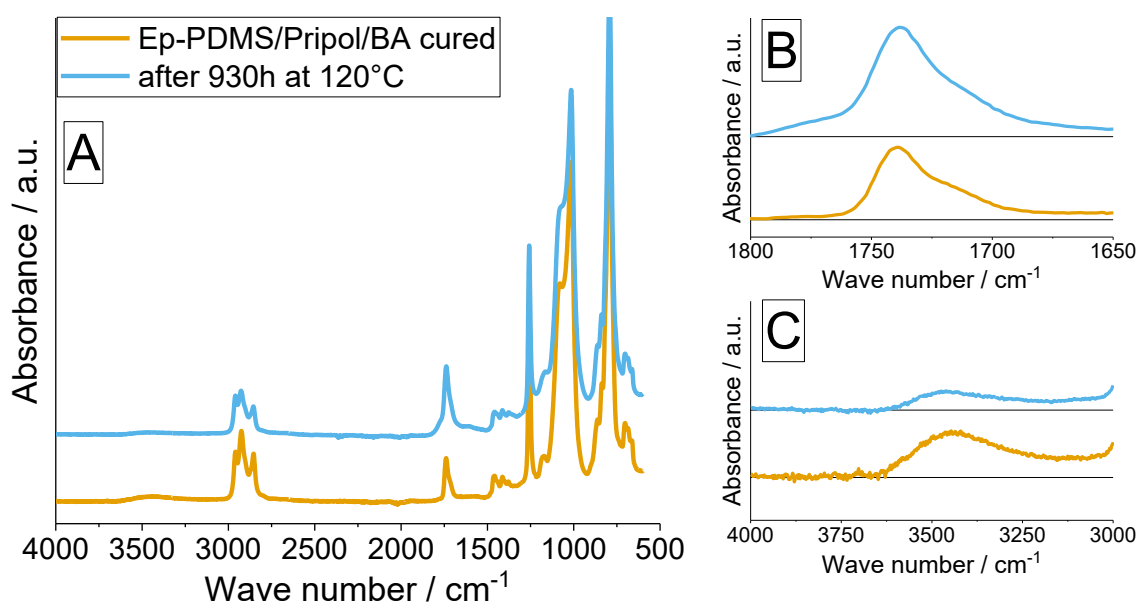
Figure 51: FTIR spectrum of Ep-PDMS cured with Pripol and BA as catalyst before (orange line) and after (blue line) damp heat tests (A), partial formation of carboxyl groups (B), and increase of signals for hydroxyl groups (C).

The vitrimeric samples stored at 120°C for 930 h showed a change of chemical structure in the infrared spectrum as well (see Figure 52). The long exposure to high temperature resulted in a partial conversion of the hydroxyl groups to carbonyl group, visible in a decrease of the signal for hydroxyl groups between 3000 cm^{-1} and 3600 cm^{-1} and an increase of the C=O stretching signal around 1740 cm^{-1}. While the material itself stayed crosslinked, the reduction in hydroxyl groups decreases its vitrimeric properties and hence could not be rejoined after the tests.

Figure 52: FTIR spectrum of Ep-PDMS cured with Pripol and BA as catalyst before (orange line) and after (blue line) storage for 930h at 120°C (A), increase of carbonyl groups (B), and decrease of hydroxyl groups (C).

4.4.2 Result overview

Figure 53 gives an overview of the results for the lap shear test for all samples that withstood the weathering tests. Tab. ii in the appendix includes all results quantitatively. Overall, a significant decrease of mechanical properties after damp heat tests is visible, whereas temperature cycling tests do not lead to a significant change. For the filled samples, EG exhibits a stronger influence than EXP, while little to no difference was found when comparing the filling levels of 30 wt.% to 50 wt.%. The vitrimeric samples achieve approximately 20 % of the mechanical properties of pristine Novasil, correlating with the results of the tensile tests. EG after expansion is not listed because both 50 wt.% as well as 30 wt.% filling level resulted in complete disbonding of the connection for aged and unaged samples.

The sample names denote their material, with Vit standing for the vitrimeric sample and NS for pure Novasil; the amount of filler, with low being 30 wt.% and high 50 wt.%; the pre-conditioning done, with Ref being unaged samples, TC samples after temperature cycle tests, DH samples after damp heat tests, TS samples after storage

at 120°C for 930 h and Rej samples after rejoining. Lastly, the names state the conditions under which they were tested, with RT being tested at room temperature, trig being tested at room temperature after triggering the expansion mechanism and 160°C being tested at 160°C.
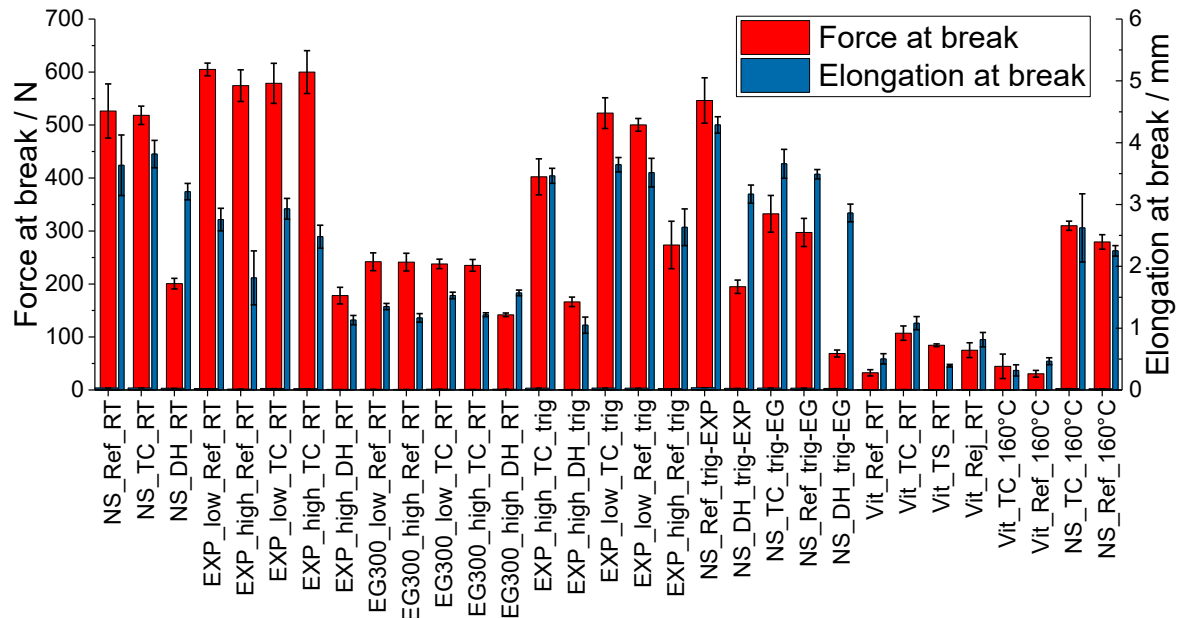
Figure 53: Overview of lap shear test results.

Upon temperature increase, EXP did not disbond for neither 30 wt.% nor 50 wt.% filling levels. In pre-tests, the adhesive matrix was destroyed completely with a microsphere content of 50 wt.% (see Figure 54). For the lap shear specimens, the adhesive just squeezed out to the sides, while the connection stayed intact. However, the pre-tests were done with a higher bonding area, which might be the reason the disbonding worked as it prevents the adhesive from expanding in axial direction.

Figure 54: Novasil filled with 50% EXP before (A) and after (B) expansion in pre-test.

The vitrimeric samples show better results after the climate cycling test than before because the unaged samples showed an adhesive failure, while the samples after the weathering test failed cohesively. This indicates that the climate cycling test served as tempering time and either improved the connection to the metallic surface by reducing residual stresses, or by a promoted rearrangement of their topology, resulting in a better penetration of the surface roughness. In these experiments the samples that showed adhesive failure had to be recombined with other sample-halves for reprocessing, so per two specimens with adhesive failures only one rejoined sample could be produced. After rejoining all samples showed cohesive failure.

4.4.3 Influence of filler content

Table 9 shows the relative influence of filler content on force and elongation at break without expansion, normalized to the values for pure Novasil, being 526.5 N and 3.6%, respectively. The addition of EXP slightly increases the strength at break and decreases the elongation at break. While the material strength barely changes from 30% to 50% filler content, the elongation at break decreases yet again to 50% of pure Novasil. EG300 has a strong influence on both force and elongation at break since both values decrease by more than 50% for both fill levels. The strong effect of the filler is attributed to its comparably large particle size of 300 µm and because its layered structure with weak connections inbetween the layers. While the addition of EG300

drastically decreases mechanical properties, the requirements for the application in the photovoltaic module are rather low and therefore the material might still be suitable. Smaller EG particles however should be preferred.

Table 9: Influence of filler content on mechanical properties of Novasil

Filler content, wt.%	Relative force at break, %		Relative elongation at break, %	
	EXP	EG300	EXP	EG300
0	100	100	100	100
30	115	46	76	37
50	109	46	50	32

4.4.4 Influence of weathering tests

Table 10 lists the relative influence of weathering tests on the mechanical properties of NS, NS filled with EXP and EG300 and the vitrimeric samples. The temperature cycling test did not have any negative influence on any of the samples, while the damp heat test heavily damaged the material. While the EG300 samples exhibit the least reduction of mechanical properties from damp heat and even an increase in elongation at break, the mechanical properties of EG300 samples were already low, which is why the decrease from damp heat tests was not as strong as for pristine and EXP-filled Novasil samples. In Figure 53, it can be seen that all NS samples, filled and unfilled, have a similar low level of mechanical properties and it can be concluded that the functional fillers do not have a significant influence on the weathering resistance of NS. As previously stated, the vitrimeric samples completely degraded during the damp heat test.

Table 10: Influence of weathering tests on mechanical properties of Novasil and vitrimeric elastomer

Parameter	Sample	None	Temperature cycle test	Damp heat test
			Conditioning	
Force at break, %	NS force	100	100	38
	EXP force	100	104	31
	EG300 force	100	98	59
	Vit force	100	331	0
Elongation at break, %	NS elongation	100	115	88
	EXP elongation	100	137	62
	EG300 elongation	100	104	135
	Vit elongation	100	215	0

4.4.5 Disbonding effectivity

Figure 55 illustrates the influence of triggering the expansion on the force at break of the lap shear samples. The results are normalized to the force at break before the triggering, with the measured value being defined as 100 %. EG300 is not included, since all samples disbonded completely. However, also the maximum force of NS samples strongly decreases when being exposed to the temperature trigger of EG300, by more than 60 % for the samples that were exposed to the damp heat test. The degradation of EXP during the damp heat test expresses itself by the damp heat samples still being at nearly 100 % after the expansion trigger. Also, the temperature cycling test seems to have had an effect on EXP, as the force at break is still very high compared to the unaged samples. Without any weathering tests, expanding EXP reduces the force at break by 20 % with 30 wt.% EXP and 55 % with 50 wt.%.
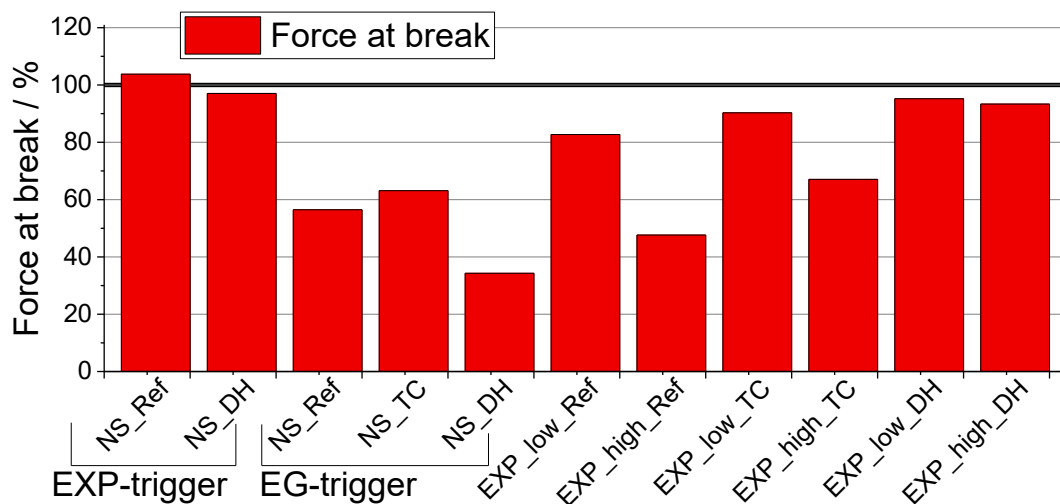
Figure 55: Relative comparison of force at break of lap shear samples after triggering the expansion mechanisms.

4.4.6 Vitrimeric samples

Vitrimeric samples demonstrate a force at break of 107.2 N and an elongation at break of 1.1 %. Compared to NS with 518.3 N and 3.8 % it achieves approximately one fifth of its strength and nearly one third of elongation. While the results match with tensile tests for material strength, the elongation at break of the vitrimeric sample is closer to NS when in a lap shear setup than in tensile tests. Considering the low fracture toughness of the vitrimeric samples this might be because during lap shear tests a crack in the bond normal to the load does not have to lead to complete failure, in contrast to tensile tests.

Figure 56 compares the test result of vitrimeric elastomer to NS, normalized to their respective unaged strength at room temperature. At 160°C NS lost 40% of strength and the vitrimeric sample loses roughly 60% of its properties. The temperature storage reduces the force at break by 20 % and the elongation decreases by more than 60 %. The results of the rejoined samples are very good, reaching more than 70 % of their original properties. However, the observed effect of a decreased force at break and elongation cannot be accounted exclusively to the vitrimeric properties of the samples

based on these results, since the relaxation time of the vitrimeric samples might be too high to have a significant impact on a monotone test like lap shear tests, even at elevated temperatures. Therefore, the use of a vitrimeric elastomer for adhesive disbonding requires further research and focus on an optimization of the material formulations and additives such as adhesion promoters and fillers. However, these results clearly demonstrate the potential of the developed elastomeric vitrimers for advanced applications such as reversible adhesive connections, where reusability, recyclability or repair and self-healing is of interest.
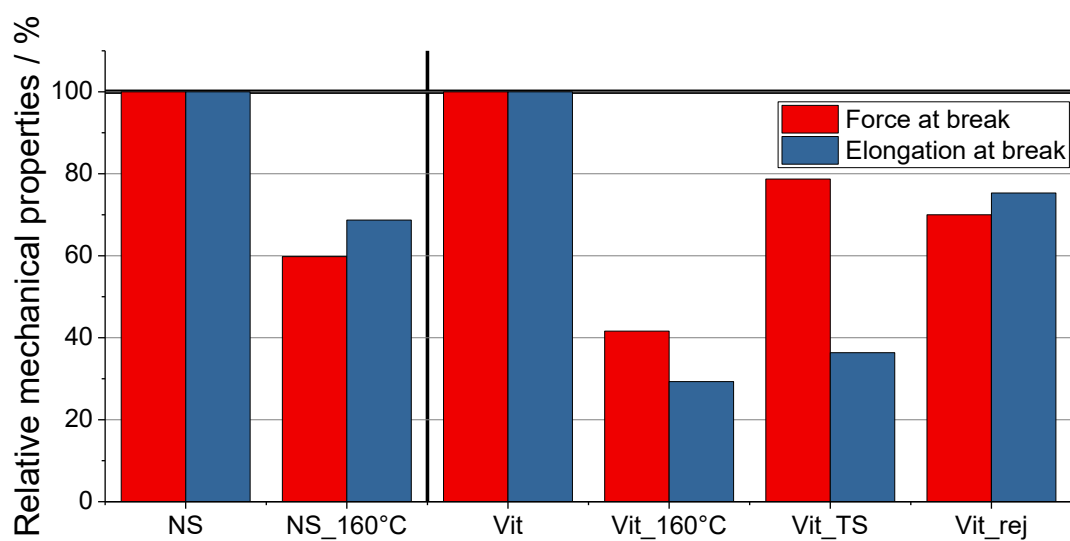
Figure 56: Lap shear result: Comparison of silicone adhesive (NS) reference to vitrimeric (Vit) samples.

5 SUMMARY

In the present thesis different concepts for dismantable and reversible adhesive connections were developed and characterised on their suitability.

In a first approach, functional fillers, which expand upon reaching certain temperatures, were implemented into a condensation-curing alkoxy-based silicone adhesive, commonly used in PV applications. 10-50 wt.% of thermally expandable microspheres (TEM) as well as expandable graphite (EG) were incorporated into the adhesive matrix to characterise the expansion behaviour in dependence on time, temperature and filler content. A strong dependence on filling levels, as well as temperature is visible for both TEM and EG samples. EG samples show a high influence of heating time, whereas TEM samples exhibit a fast expansion without any further increase in volume at longer heating times. Volumetric expansion ratios of up to 21x for 50 wt.% TEM after expansion at 150°C for 15 min, and 9x for 50 wt.% EG after expansion at 250°C for 1 h were reached with the experiments.

Moreover, inductive triggering of the thermal expansion of TEMs was carried out by adding 30 wt.% TEM and 30 wt.% NF to the silicone adhesive. By applying an alternating magnetic field at 180 kHz via a ring coil, thermally induced expansion was successfully accomplished within less than 5 min.

Further evaluation of aging stability, influence of filler content and expansion was done by lap shear tests. Lap shear specimens were prepared with filling levels of 30 wt.% and 50 wt.% of TEM and EG, as well as unfilled reference samples. The addition of EG as functional filler exhibited a stronger influence on bond strength due to its particle size and layered structure, with a decrease of approximately 50 % for both filling levels. The addition of TEM slightly increased the bond strength by 15 % and 10 % for 30 wt.% and 50 wt.% filling levels, respectively. The expansion of the functional fillers was triggered at 150°C for 30 min for TEM-filled samples and at 225°C for 1 h for EG-filled samples. The thermal expansion of EG resulted in a disbonding of the adhesive connection for both 30 wt.% and 50 wt.% filler content, whereas the thermal expansion of TEM decreased the bond strength by up to 20 % and 50 % for 30 wt.% and 50 wt.% filling levels, respectively. To evaluate the weathering stability of the

functional fillers, the samples were exposed to accelerated aging tests and the strength and elongation was compared to the unaged samples. Temperature cycling tests with 50 cycles from -40°C to 85°C did not lead to significant changes in mechanical properties. In contrast, damp heat tests for 2000 h at 85°C and 85 % relative humidity decreased the strength of all specimens alike with a remaining strength of less than 40 %, compared to the unaged and unfilled reference samples. Therefore, no influence of filler content on aging stability was observed. However, the thermally expandable microspheres suffered from degradation during the damp heat test and could not be expanded anymore. In conclusion of the results, expandable graphite has proven to be a suitable candidate to achieve a dismantable adhesive connection by implementing it into an elastomeric adhesive system. Lower expansion temperatures would be favourable and are possible to produce but appropriate types of EG are not commercially available at the moment.

In a further approach to achieve reversible and reworkable adhesive connections, vitrimeric elastomers based on PDMS were realized. By exploiting reactions of epoxide functional groups with anhydrides and carboxylic acids, covalent adaptable networks (CAN) are formed in the presence of suitable catalysts. CANs are crosslinked materials, which are capable of rearranging their topology at elevated temperatures by dynamic bond exchange. In the case of epoxy-anhydride and epoxy-acid networks, beta hydroxyl esters are formed for systems with equimolar ratios of epoxy groups to COOH/anhydride groups. These beta hydroxyl ester linkages can dynamically exchange their bonds via transesterification reaction. The rate of the exchange reaction increases with temperature, and after reaching a certain temperature, the material transitions from an elastic solid to a viscoelastic liquid and becomes able to flow and can therefore be reprocessed.

A fully PDMS-based CAN was realized by reacting epoxidized PDMS with succinic anhydride functionalized PDMS using covalently bonded *n*-butylamine (BA) as catalyst. The material exhibited very good reprocessability but only allowed low deformations before failure. To achieve higher elasticity, a vitrimeric elastomer was produced by curing epoxidized PDMS with a multifunctional fatty acid and the covalently bonded catalyst BA. The covalent bonding of BA to the epoxy component was confirmed by

means of ^{13}C-NMR spectroscopy, and additionally a Soxhlet extraction in hexane was performed to confirm that the catalyst does not leach out of the material. In tensile tests the material achieved an average strain at break of 40 % and an average strength at break of 0.40 MPa, which is approximately one fifth of the reference adhesive's strength and elongation. After reprocessing, the materials exhibited a remaining strength of 0.35 MPa and an elongation of 19%, which amounts to roughly 85 % and 50 % of the virgin material properties.

Lap shear tests to evaluate bond strength, rejoining of separated bonds, aging stability and the ability to weaken the adhesive connection were done in a similar manner to the functional fillers. In the lap shear tests, the vitrimeric elastomer achieved approximately one fifth of the reference adhesive's strength and one third in terms of elongation. Tests performed at 160°C resulted in a bond strength decrease of 60 %, compared to a reduction of 40 % for the silicone adhesive. After rejoining the tested sample interfaces, more than 70 % of the strength of the virgin samples was achieved. Aging stability was evaluated by storage at 120°C for 930 h, additionally to the damp heat and temperature cycling tests. The storage at elevated temperatures reduced the bond strength of the vitrimeric sample by approximately 20 %. Temperature cycling tests did not affect the material, however, damp heat tests resulted in hydrolytic bond cleavage, and therefore material failure. The results confirm that a vitrimeric elastomer can be used to establish reworkable and recyclable adhesive bonds. For an application in photovoltaic modules, aging stability would have to be improved by e.g. stabilizing additives or temporarily quenching the functional groups of the network during service-life, which is a matter of further research activities. Another object of further research will be to decrease the relaxation times of the vitrimeric system at elevated temperatures to further improve the bond weakening, and therefore adhesive dismantling.

6 LIST OF ILLUSTRATIONS

7 LIST OF TABLES

8 INDEX OF ABBREVIATIONS

η   viscosity

AC   alternating current

ATR   attenuated total reflection

BA   *n*-butylamine

CAN   covalent adaptable networks

DBA   dibutylamine

DBN   1,5-Diazabicyclo[4.3.0]non-5-ene

DGEBA   bisphenol A diglycidyl-ether

DSC   differential scanning calorimetry

EG   expandable graphite

EG300   expandable graphite by RMT Remacon GmbH, type BLG 300 L-LT

EG40   expandable graphite by RMT Remacon GmbH, type BLG 40 T

Ep-PDMS   epoxy terminated poly(dimethyl siloxane)

EXP   thermally expandable microspheres by Nouryon, type 909 DU 80

FTIR   fourier-transform infrared

IR   infrared

MHHPA   hexahydro-4-methylphthalic anhydride

NF   nanoferrites

NMR   nuclear magnetic resonance

Novasil   Novasil S49 with Ottocure S-CA2010

NS   Novasil S49 with Ottocure S-CA2010

NS-D   thermally expandable microspheres by Nanosphere, type E-Micro D280C

NS-DU   thermally expandable microspheres by Nanosphere, type E-micro DU608S

PDMS   poly(dimethylsiloxane)

PMMA   poly(methyl methacrylate)

Pripol   Pripol 1040

PS   poly(styrene)

PV   photovoltaic

PVC   poly(vinylchloride)

RT   room temperature

SA-PDMS   succinic anhydride functionalized poly(dimethylsiloxane)

TBD   1,5,7-triazabicyclo[4.4.0]dec-5-ene

TEM   thermally expandable microspheres

T_g glass transition temperature

TMHMDA   2,2,4-trimethyl-1,6-hexamethylenediamine

T_v vitrification temperature

wt.%   weight percent

$Zn(AcAc)_2$ zinc acetylacetonate

9 REFERENCES

[1] Official Journal of the European Union 2018(L328):82–209.

[2] Renewable energy statistics. [February 06, 2020]; Available from: https://ec.europa.eu/eurostat/statistics-explained/index.php?title=Renewable_energy_statistics.

[3] Prince MB. Semiconductor Photovoltaic Effect and Devices. In: Low W, Schieber M, editors. Applied Solid State Physics, vol. 26. Boston, MA: Springer US, 1970. pp. 223–234.

[4] Kempe M. Encapsulant Materials for PV Modules. In: Reinders A, Freundlich A, Verlinden P, van Sark W, editors. Photovoltaic solar energy: From fundamentals to applications, vol. 27. Chichester: Wiley, 2017. pp. 478–490.

[5] The structure of a photovoltaic module. [February 06, 2020]; Available from: https://ecoprogetti.com/the-structure-of-photovoltaic-module/.

[6] Knausz M. Influence of polymeric encapsulation materials on quality and reliability of PV modules. Dissertation. Leoben, 2015.

[7] Jäger-Waldau A. PV Status Report 2019, 2019.

[8] IRENA and IEA-PVPS. End of life management solar photovoltaic panels: International Renewable Energy Agency and International Energy Agency Photovoltaic Power Systems, 2016.

[9] Hutchinson A, Liu Y, Lu Y. The Journal of Adhesion 2017;93(10):737–55.

[10] Chakma P, Konkolewicz D. Angewandte Chemie (International ed. in English) 2019;58(29):9682–95.

[11] Kloxin CJ, Scott TF, Adzima BJ, Bowman CN. Macromolecules 2010;43(6):2643–53.

[12] Pröbster M. Elastisch Kleben: Aus der Praxis für die Praxis. Dordrecht: Springer, 2013.

[13]   Pizzi A, Mittal KL. Handbook of Adhesive Technology, Revised and Expanded: Taylor & Francis, 2003.

[14]   Kinloch AJ. Adhesion and Adhesives: Science and Technology: Springer Netherlands, 2012.

[15]   Campbell FC. Chapter 8 - Adhesive Bonding and Integrally Cocured Structure: A Way to Reduce Assembly Costs through Parts Integration. In: Campbell FC, editor. Manufacturing processes for advanced composites. Oxford: Elsevier, 2004. pp. 241–301.

[16]   Brockmann W. Klebtechnik: Klebstoffe, Anwendungen und Verfahren, 1st ed. Weinheim: Wiley-VCH, 2008.

[17]   Habenicht G. Kleben: Grundlagen, Technologien, Anwendungen mit 37 Tabellen, 5th ed. Berlin: Springer, 2006.

[18]   Hussey B, Wilson J. Structural Adhesives: Directory and Databook. Boston, MA: Springer US, 1996.

[19]   Bart JCJ. Additives in Polymers: Industrial Analysis and Applications: Wiley, 2005.

[20]   Rapra Technology Limited. Blowing Agents and Foaming Processes: Rapra Technology, 2004.

[21]   Altstädt V, Mantey A. Thermoplast-Schaumspritzgießen, 1st ed. s.l.: Carl Hanser Fachbuchverlag, 2010.

[22]   Ehrenstein G. Polymer-Werkstoffe: Struktur ; Eigenschaften ; Anwendung, 3rd ed. s.l.: Carl Hanser Fachbuchverlag, 2011.

[23]   Pausan N, Liu Y, Lu Y, Hutchinson AR. The Journal of Adhesion 2017;93(10):791–810.

[24]   Crutchley EB. Innovation Trends in Plastics Decoration and Surface Treatment: Smithers Information Limited, 2014.

[25]   Jonsson M. Thermally expandable microspheres prepared via suspension polymerization: Synthesis, characterization and application. Stockholm: Skolan för kemivetenskap, Kungliga Tekniska högskolan, 2010.

[26]   Blowing agents - Expancel Microspheres - Nouryon. [December 21, 2019]; Available from: https://expancel.nouryon.com/blowing-agents/.

[27]   Bardell R, Rapra Technology Limited. Addcon World: Venue: Crowne Plaza City Centre Hotel,Amsterdam,The Netherlands,28-29 September 2004: iSmithers Rapra Publishing, 2004.

[28]   Dai C, Gu C, Liu B, Lyu Y, Yao X, He H et al. Journal of Molecular Liquids 2019;293:111535.

[29]   Bayerl T, Schledjewski R, Mitschang P. Polymers and Polymer Composites 2012;20(4):333–42.

[30]   Suwanwatana W, Yarlagadda S, GILLESPIEJR J. Composites Science and Technology 2006;66(11-12):1713–23.

[31]   Suwanwatana W, Yarlagadda S, Gillespie JW. Composites Science and Technology 2006;66(15):2825–36.

[32]   Lucia O, Maussion P, Dede EJ, Burdio JM. IEEE Trans. Ind. Electron. 2014;61(5):2509–20.

[33]   Hergt R, Dutz S, Müller R, Zeisberger M. J. Phys.: Condens. Matter 2006;18(38):S2919-S2934.

[34]   George J. Tsamasphyros, Aggelos C. Christopoulos. Applied Mathermatics and Materials.

[35]   Wu W, Wu Z, Yu T, Jiang C, Kim W-S. Science and technology of advanced materials 2015;16(2):23501.

[36]   Sharafi Z, Bakhshi B, Javidi J, Adrangi S. Iran J Pharm Res 2018;17(1):386–95.

[37]   Jin Y, Yu C, Denman RJ, Zhang W. Chemical Society reviews 2013;42(16):6634–54.

[38]   McBride MK, Worrell BT, Brown T, Cox LM, Sowan N, Wang C et al. Annual review of chemical and biomolecular engineering 2019;10:175–98.

[39]   Denissen W, Winne JM, Du Prez FE. Chemical science 2016;7(1):30–8.

[40]   Zhang ZP, Rong MZ, Zhang MQ. Progress in Polymer Science 2018;80:39–93.

[41]   Aubert JH. The Journal of Adhesion 2003;79(6):609–16.

[42]   Kloetzel MC. The Diels-Alder Reaction with Maleic Anhydride. In: Organic Reactions, vol. 11. Hoboken, NJ, USA: John Wiley & Sons, Inc, 2004. pp. 1–59.

[43]   Ciaccia M, Di Stefano S. Organic & biomolecular chemistry 2015;13(3):646–54.

[44]   Becerra-Figueroa L, Ojeda-Porras A, Gamba-Sánchez D. The Journal of organic chemistry 2014;79(10):4544–52.

[45]   Liu Z, Yu C, Zhang C, Shi Z, Yin J. ACS Macro Lett. 2019;8(3):233–8.

[46]   Denissen W, Rivero G, Nicolaÿ R, Leibler L, Winne JM, Du Prez FE. Adv. Funct. Mater. 2015;25(16):2451–7.

[47]   Taynton P, Yu K, Shoemaker RK, Jin Y, Qi HJ, Zhang W. Advanced materials (Deerfield Beach, Fla.) 2014;26(23):3938–42.

[48]   Osthoff RC, Bueche AM, Grubb WT. J. Am. Chem. Soc. 1954;76(18):4659–63.

[49]   Zheng P, McCarthy TJ. Journal of the American Chemical Society 2012;134(4):2024–7.

[50]   Zou W, Dong J, Luo Y, Zhao Q, Xie T. Advanced materials (Deerfield Beach, Fla.) 2017;29(14).

[51]   Fortman DJ, Brutman JP, Cramer CJ, Hillmyer MA, Dichtel WR. Journal of the American Chemical Society 2015;137(44):14019–22.

[52]   Montarnal D, Capelot M, Tournilhac F, Leibler L. Science (New York, N.Y.) 2011;334(6058):965–8.

[53]   Li L, Chen X, Jin K, Torkelson JM. Macromolecules 2018;51(15):5537–46.

[54]   Motahari A, Omrani A, Rostami AA, Ehsani M. Thermochimica Acta 2013;574:38–46.

[55]   May C. Epoxy resins: chemistry and technology: Routledge, 2018.

[56]   Kolář F, Svitilova J. Acta Geodyn. Geomater 2007;4(3):85–92.

[57]   Sinturel C, Thomas R, Thomas S (eds.). Micro- and nanostructured epoxy/rubber blends. Weinheim, Germany: Wiley-VCH, 2014.

[58]   Capelot M, Montarnal D, Tournilhac F, Leibler L. Journal of the American Chemical Society 2012;134(18):7664–7.

[59]   Mauri AN, Riccardi CC. J. Appl. Polym. Sci. 2002;85(11):2342–9.

[60]   Pascault J-P, Williams RJJ. Epoxy polymers: New materials and innovations. Weinheim: Wiley-VCH Verlag GmbH, 2010.

[61]   Dyre JC. Thermochimica Acta 2006;78(3):953–72.

[62]   Liu T, Hao C, Zhang S, Yang X, Wang L, Han J et al. Macromolecules 2018;51(15):5577–85.

[63]   Capelot M, Unterlass MM, Tournilhac F, Leibler L. ACS Macro Lett. 2012;1(7):789–92.

[64]   Yang Y, Zhang S, Zhang X, Gao L, Wei Y, Ji Y. Nature communications 2019;10(1):3165.

[65]   Han J, Liu T, Hao C, Zhang S, Guo B, Zhang J. Macromolecules 2018;51(17):6789–99.

[66]   Liu T, Zhang S, Hao C, Verdi C, Liu W, Liu H et al. Macromolecular rapid communications 2019;40(7):1800889.

[67]   Demongeot A, Mougnier SJ, Okada S, Soulié-Ziakovic C, Tournilhac F. Polym. Chem. 2016;7(27):4486–93.

[68]   Pham, My-Phuong. Theoretical studies of mechanisms of epoxy curing systems. Dissertation. Salt Lake City.

[69]   Paramarta A, Webster DC. J Therm Anal Calorim 2017;130(3):2133–44.

[70]   Matějka L, Lövy J, Pokorný S, Bouchal K, Dušek K. J. Polym. Sci. Polym. Chem. Ed. 1983;21(10):2873–85.

[71] Blank WJ, He ZA, Picci M. J. Coatings Tech. 2002;74(3):33–41.

[72] Tang Z, Wang L, Yang J. Eur. J. Lipid Sci. Technol. 2008;110(8):747–53.

[73] Altuna FI, Hoppe CE, Williams RJJ. European Polymer Journal 2019;113:297–304.

[74] Hassel C. Dielektrische Polarisationsfluktuationen und Permittivität bei der Polymerisation von DGEBA: Über Gültigkeit des Fluktuations-Dissipations-Theorems bei Nichtgleichgewichtsystemen. Bachelor thesis. Heidelberg.

[75] Mohamed MA, Jaafar J, Ismail AF, Othman MHD, Rahman MA. Fourier Transform Infrared (FTIR) Spectroscopy. In: Membrane Characterization: Elsevier, 2017. pp. 3–29.

[76] Günzler H, Gremlich H-U. IR-Spektroskopie: Eine Einführung, 4th ed. Weinheim, Co. KGaA: Wiley-VCH GmbH & amp, 2003.

[77] Atta-ur-Rahman, Choudhary MI. The Basics of Modern NMR Spectroscopy. In: Solving Problems with NMR Spectroscopy: Elsevier, 1996. pp. 1–89.

[78] Dean JR. Extraction Techniques in Analytical Sciences: Wiley, 2010.

[79] File:Soxhlet extractor.svg - Wikimedia Commons. [February 04, 2020]; Available from: https://commons.wikimedia.org/wiki/File:Soxhlet_extractor.svg.

[80] Höhne G, Hemminger WF, Flammersheim HJ. Differential Scanning Calorimetry: Springer Berlin Heidelberg, 2013.

[81] GROENEWOUD WM. DIFFERENTIAL SCANNING CALORIMETRY. In: Characterisation of Polymers by Thermal Analysis: Elsevier, 2001. pp. 10–60.

[82] DIN 53504 S2 - Q-tec GmbH. [January 07, 2020]; Available from: https://q-tec-gmbh.de/produkte/stanzmesser/din-53504/din-53504-s2/.

[83] Bayerl T, Duhovic M, Mitschang P, Bhattacharyya D. Composites Part A: Applied Science and Manufacturing 2014;57:27–40.

[84] Zhao D-L, Zeng X-W, Xia Q-S, Tang J-T. Journal of Alloys and Compounds 2009;469(1-2):215–8.

[85]   Nikolic G, Zlatkovic S, Cakic M, Cakic S, Lacnjevac C, Rajic Z. Sensors (Basel, Switzerland) 2010;10(1):684–96.

[86]   González MG, Cabanelas JC, Baselga J. Applications of FTIR on Epoxy Resins - Identification, Monitoring the Curing Process, Phase Separation and Water Uptake. In: Theophanides T, editor. Infrared Spectroscopy - Materials Science, Engineering and Technology: InTech, 2012.

[87]   Juchnovski I, Veltcheva E, Kolev T. Spectroscopy Letters 1993;26(1):17–30.

[88]   Smith BC. Infrared Spectral Interpretation: A Systematic Approach, 1st ed. Bosa Roca: CRC Press, 1998.

[89]   Johnson LM, Gao L, Shields IV CW, Smith M, Efimenko K, Cushing K et al. Journal of nanobiotechnology 2013;11:22.

[90]   Zhang H, Cai C, Liu W, Li D, Zhang J, Zhao N et al. Scientific reports 2017;7(1):11833.

[91]   Hexahydromethylphthalic anhydride - Liste der für eine Zulassung in Frage kommenden besonders besorgniserregenden Stoffe - ECHA. [January 31, 2020]; Available from: https://echa.europa.eu/de/candidate-list-table/-/dislist/details/0b0236e1807de9d4.

[92]   Chandrasekaran VC. Rubbers, Chemicals and Compounding for 'O' Rings and Seals. In: Chandrasekaran VC, editor. Rubber seals for fluid and hydraulic systems, 1st ed. Oxford, Burlington, MA, Amsterdam: William Andrew; Elsevier Science, 2010. pp. 57–69.

10 APPENDIX

Fig. i: Expansion of NS-DU.

Fig. ii: Expansion of NS-D.
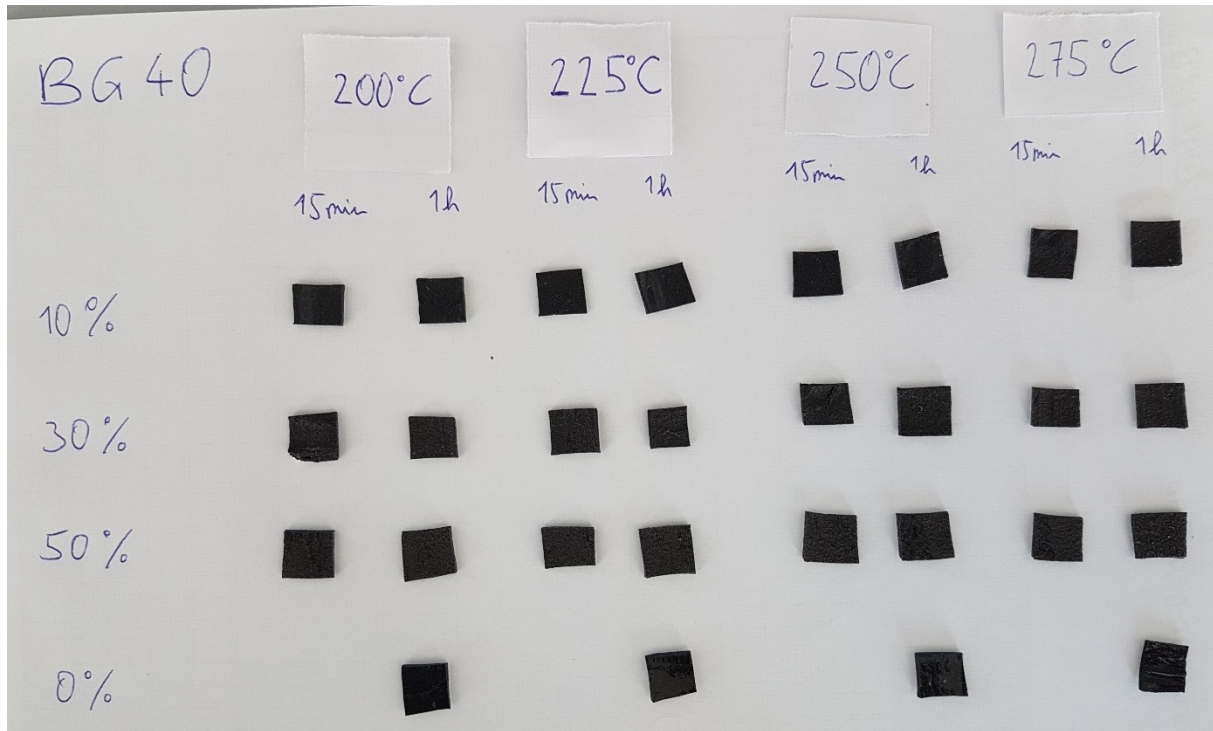
Fig. iii: Expansion of EG40.

Tab. i: Expansion of functional filler depending on temperature, time and filler content

Temperature, °C	Time, min	Calculated volumetric expansion, %				
		EXP	NS-DU	NS-D	EG300	EG40
10 wt.% functional filler						
125	15	173	98	96		
	60	277	108	97		
150	15	182	105	97		
	60	149	103	137		
175	15	121	237	199	105	
	60	125	122	173	98	
200	15	118	171	146	109	99
	60	91	210	202	93	91

Tab. i (continued)

225	15				120	83
	60				218	113
250	15				211	81
	60				200	114
275	15					96
	60					98
30 wt.% functional filler						
125	15	838	151	107		
	60	987	78	115		
150	15	1157	280	387		
	60	688	274	522		
175	15	524	578	676	107	
	60	198	334	754	113	
200	15	438	345	755	495	111
	60	155	329	672	90	59
225	15				328	135
	60				327	73
250	15				413	76
	60				597	136
275	15					85
	60					119

Tab. i (continued)

50 wt.% functional filler						
125	15	1459	94	329		
	60	2077	160	196		
150	15	2108	566	622		
	60	1601	469	1006		
175	15	1197	644	1217	101	
	60	395	742	1111	107	
200	15	386	790	1099	634	92
	60	228	367	733	165	97
225	15				565	82
	60				752	120
250	15				797	94
	60				908	107
275	15					98
	60					107

Tab. ii: Force and elongation at break results from lap shear test

Sample	Force at break, N	Standard deviation, N	Elongation at break, mm	Standard deviation, mm
NS_Ref_RT	526.5	51.0	3.6	0.5
NS_TC_RT	518.4	17.3	3.8	0.2
NS_DH_RT	200.7	10.0	3.2	0.1
EXP_low_Ref_RT	605.0	12.0	2.8	0.2

Tab. ii (continued)

EXP_high_Ref _RT	574.4	29.8	1.8	0.4
EXP_low_TC_R T	578.7	37.8	2.9	0.2
EXP_high_TC_ RT	599.9	40.4	2.5	0.2
EXP_high_DH_ RT	178.1	15.7	1.1	0.1
EG300_low_Re f_RT	242.0	16.8	1.4	0.1
EG300_high_R ef_RT	241.2	16.7	1.2	0.1
EG300_low_T C_RT	237.9	8.9	1.5	0.1
EG300_high_T C_RT	235.2	11.1	1.2	0.0
EG300_high_D H_RT	141.9	3.4	1.6	0.0
Vit_Ref_RT	32.4	5.9	0.5	0.1
Vit_TC_RT	107.2	13.5	1.1	0.1
Vit_TS_RT	84.4	2.6	0.4	0.0
Vit_Healed_RT	75.1	13.9	0.8	0.1
EXP_high_TC_ trig	402.2	33.9	3.5	0.1
EXP_high_DH_ trig	166.3	8.9	1.0	0.1

Tab. ii (continued)

EXP_low_TC_t rig	522.5	29.0	3.6	0.1
EXP_low_Ref_t rig	500.3	12.1	3.5	0.2
EXP_high_Ref _trig	273.7	44.8	2.6	0.3
NS_Ref_trig-EXP	546.4	42.8	4.3	0.1
NS_DH_trig-EXP	194.8	12.7	3.2	0.1
NS_TC_trig-EG	332.5	34.7	3.7	0.2
NS_Ref_trig-EG	297.3	26.5	3.5	0.1
NS_DH_trig-EG	68.8	6.6	2.9	0.1
NS_TC_160°C	309.9	8.7	2.6	0.6
NS_Ref_160°C	279.3	13.6	2.3	0.1
Vit_TC_160°C	44.6	23.2	0.3	0.1
Vit_Ref_160°C	30.6	6.4	0.5	0.1